

A novel detection system using  
neutron/gamma pulse shape  
discrimination, for use in active  
interrogation environments



Ashley Richard Jones

MEng. Nuclear Engineering (Hons)

This thesis is submitted in accordance with the requirements of the  
University of Lancaster for the degree of Doctor of Philosophy

October 2016

© British Crown Owned Copyright 2017/AWE

For Suzie.

# Acknowledgements

This research would not have been possible without the support and guidance of many people.

First, I would like to show my appreciation to my provider of financial assistance AWE plc. Aldermaston for supporting the research carried out, as well as the wider collaboration of Surrey University and UCL and the respective students and supervisors from them. I would like to thank my supervisor, Prof. Malcolm Joyce, not only for his knowledge and guidance but for his support, which without such enthusiasm and encouragement this research would have been impossible.

Second, I would like to thank my research colleagues; Sarah Jackson, Matthew Balmer, Helen Parker, Ioannis Tsitsimpelis, Jonathan Beaumont and Alex Grievson for not only making working life more enjoyable but for invaluable input at different periods throughout this research. Separate thanks must go to Peter Jones for his guidance with idea developments and expertise in manufacture and Dr Michael Aspinall for his guidance and knowledge with the Hybrid Instruments equipment. Separate thanks are also set aside to Peter Tovee for his time and effort in proof reading.

Huge gratitude and thanks go to my parents and family who have always supported me throughout all of life but especially in my academic pursuits. Finally I would like to thank my partner, Suzie, you not only support but encourage my obsessions and determination. This research and thesis would not have been possible without your help and encouragement.

# Declaration

I, Ashley Richard Jones, hereby certify that this thesis and the research described in it is all my own work unless otherwise indicated and has not been submitted in any previous application for a higher degree. The work presented here was carried out at Lancaster University between August 2012 and August 2015.

Date..... Signature of candidate.....

Ashley Richard Jones

I, Professor Malcolm John Joyce, hereby certify that the candidate has fulfilled the conditions of the resolution and regulations appropriate for the degree of Doctor of Philosophy at Lancaster University and that the candidate is qualified to submit this thesis in application for that degree.

Date..... Signature of supervisor.....

Professor Malcolm John Joyce

# Abstract

Continuous improvements are being sought to identify special nuclear material more accurately. Active interrogation is a current field of research for this application, capable of penetrating shielding materials but which can feature a complex and challenging radiation field for detectors to operate in. This research was aimed at improving active interrogation techniques further by optimising experimental setups and procedures and reducing undesirable dead periods of acquisition which may be observed.

The important outcomes from this research are listed below:

- The creation of a new empirical fit to better represent the rising edge of pulses from both neutrons and gamma rays than the currently used Marrone fit (suited to the decay tail of pulses).
- The ability to clearly distinguish a selection of gamma rays using this rise time technique post-processing previously acquired data consisting of a mixed radiation field.
- The effect of angular orientation of liquid scintillators on FoM values after performing PSD techniques has been identified as well as sensitivity issues associated with the position of the nitrogen void within these detectors.
- A novel gated organic plastic scintillator detector has been operated and controlled using a trigger circuit devised in this research. This circuit controlled whether the gated detector was active through the presence of light.
- A radiation based detector was integrated with this trigger circuit controlling the gated detector by making the device inactive whenever a radiation count was observed.

During this PhD, research has been presented at the ANIMMA conference (Advancements in Nuclear Instrumentation Measurement Methods and their Applications) 2013; this consisting of a short five minute oral presentation with associated poster session with the conference paper appearing in the conference proceedings shown in Appendix A. Contributions were also made to the following paper, this paper is not discussed further in this thesis.

K. Mitton, A.R. Jones, M. Joyce “Digital fast neutron radiography of rebar in concrete”  
*Journal of Instrumentation* 2014

Two more papers are currently in preparation, these being:

A.R. Jones, M.J. Joyce “The angular dependence of pulse shape discrimination and detection sensitivity in cylindrical and cubic EJ-309 organic liquid scintillators”

A.R. Jones, M.J. Joyce “A remote triggering system for fast neutron detection in plastic organic scintillators”

# Contents

<b>ACKNOWLEDGEMENTS.....</b>	<b>III</b>
<b>DECLARATION.....</b>	<b>IV</b>
<b>ABSTRACT.....</b>	<b>V</b>
<b>CONTENTS.....</b>	<b>VII</b>
<b>LIST OF TABLES .....</b>	<b>X</b>
<b>LIST OF FIGURES .....</b>	<b>XII</b>
<b>LIST OF ABBREVIATIONS AND ACRONYMS.....</b>	<b>XIX</b>
<b>1 INTRODUCTION.....</b>	<b>1</b>
1.1 RESEARCH AIMS .....	2
1.2 NOVELTIES OF THIS RESEARCH .....	3
1.3 REFERENCES.....	4
<b>2 BACKGROUND &amp; THEORY .....</b>	<b>5</b>
2.1 RADIOACTIVITY.....	5
2.1.1 Activity .....	6
2.2 IONISING RADIATION .....	6
2.2.1 Photons.....	8
2.2.2 Neutrons .....	11
2.2.2.1 Scattering.....	12
2.3 FISSILE MATERIAL .....	13
2.4 NON-DESTRUCTIVE INTERROGATION.....	16
2.4.1 Passive Detection .....	17
2.4.2 Active Interrogation .....	18
2.5 RADIATION DETECTION .....	21
2.5.1 Scintillation .....	21

2.5.2.1 Pulse shape discrimination .....	22
2.5.2.2 Inorganic scintillators .....	26
2.5.2.3 Organic scintillators.....	27
2.5.2.4 Detector modes of operation.....	30
2.6 PHOTOMULTIPLIER TUBES (PMT).....	31
2.6.1 MCP-PMT.....	35
2.6.2 Triggered PMT.....	36
2.7 REFERENCES.....	39
<b>3 EXPERIMENTAL METHODS .....</b>	<b>43</b>
3.1 SOURCES .....	43
3.2 WORKING WITH RADIATION.....	45
3.2.1 Radiation Protection .....	46
3.2.2 Dose definitions.....	48
Absorbed dose .....	48
Equivalent dose .....	48
Effective dose.....	49
3.2.3 Dosimetry .....	50
Thermoluminescent dosimeters .....	51
Mini Instruments dosimeter.....	52
Survey Meters .....	52
3.3 INSTRUMENTS.....	53
3.3.1 Detectors .....	53
3.3.2 Data Acquisition (DAQ).....	57
3.4 PULSE HEIGHT DISTRIBUTION .....	60
3.4.1 Figure-of-Merit .....	63
3.9 REFERENCES.....	64
<b>4 RISING EDGE DISCRIMINATION .....</b>	<b>66</b>
4.1 CONCLUSION .....	79
4.2 REFERENCES.....	80

<b>5</b>	<b>ANGULAR ORIENTATION OF LIQUID SCINTILLATORS .....</b>	<b>82</b>
	5.1 ANALYSIS .....	95
	5.1.1 <i>Figure-of-Merit calculations</i> .....	98
	5.2 CONCLUSION .....	106
	5.3 REFERENCES.....	110
<b>6</b>	<b>RADIATION HARDNESS TESTS &amp; TRIGGER TESTS .....</b>	<b>111</b>
	6.1 EJ-301 RADIATION HARDNESS.....	111
	6.2 TRIGGER TESTS.....	115
	6.3 ANALYSIS .....	130
	6.4 CONCLUSION .....	134
	6.4 REFERENCES.....	135
<b>7</b>	<b>PLASTIC SCINTILLATOR PERFORMANCE IMPROVEMENTS.....</b>	<b>138</b>
	7.1 ANALYSIS .....	142
	7.2 CONCLUSION .....	145
	7.2 REFERENCES.....	146
<b>8</b>	<b>CHOPPED GAMMA TRIGGERING SYSTEM.....</b>	<b>147</b>
	8.1 CONCLUSION .....	153
	8.2 REFERENCES.....	153
<b>9</b>	<b>CONCLUSIONS &amp; RECOMMENDATION .....</b>	<b>154</b>
	9.1 OVERALL CONCLUSIONS .....	154
	9.2 RECOMMENDATIONS .....	158
	9.2.1 <i>Autonomous Detector</i> .....	159
	9.2.2 <i>Gated Detector</i> .....	160
	9.2.3 <i>New Algorithms</i> .....	161
	9.3 REFERENCES.....	163
	<b>APPENDIX A .....</b>	<b>164</b>

# List of Tables

Table I. Comparison of detector properties.....	30
Table II. Weighting factors for different types and energies of radiation [4]. .....	49
Table III. Weighting factors for different organs [5]. .....	50
Table IV. $\gamma$ -ray and neutron composition of 100100 events with $^{252}\text{Cf}$ as a function of angle for the cubic cell. ....	90
Table V. $\gamma$ -ray and neutron composition for 2 minutes exposure with $^{252}\text{Cf}$ as a function of angle for the cubic cell.....	90
Table VI. $\gamma$ -ray and neutron composition with $^{252}\text{Cf}$ as a function of angle for 100100 counts for the cylindrical cell. ....	93
Table VII. $\gamma$ -ray and neutron composition with $^{252}\text{Cf}$ at $-90^{\circ}$ for 100100 counts for the cylindrical cell. ....	93
Table VIII. $\gamma$ -ray and neutron composition with $^{252}\text{Cf}$ as a function of angle for 2-minute exposure for the cylindrical cell. ....	95
Table IX. FoM as a function of angle exposed to $^{252}\text{Cf}$ for 100100 counts with the cubic and cylindrical detectors. ....	100
Table X. $\gamma$ -ray and neutron composition with $^{252}\text{Cf}$ as a function of angle for 2-minute exposure for the cubic cell rotating away from the source. ....	103
Table XI. $\gamma$ -ray and neutron composition with $^{252}\text{Cf}$ as a function of angle for 2-minute exposure for the cylindrical cell rotating away from the source. ....	104
Table XII. $\gamma$ -ray count on different faces of the cubic EJ-309 with $^{137}\text{Cs}$ source 50mm away. ....	106
Table XIII. $\gamma$ -ray count on different faces of the cubic EJ-309 with $^{137}\text{Cs}$ source against detector.....	106

Table XIV. The Average Number of Total Counts During 20-minute Exposure to $^{137}\text{Cs}$ . .....	127
Table XV. The Average Number of Total Counts During 20-minute Exposure to $^{137}\text{Cs}$ with Closer Proximity. ....	127
Table XVI. The Average Number of Total Counts During 20-minute Exposure to $^{252}\text{Cf}$ . .....	128
Table XVII. Total number of counts for each run (relating to Figure 65). ....	132
Table XVIII. FoM values for different 2nd integral delay times. ....	143
Table XIX. Count data and FoM values for un-triggered and triggered cases for 1 minute Am-Be exposures and 5 minute $^{252}\text{Cf}$ exposures. ....	145
Table XX. Count rates for chopped gamma field tests. ....	150
Table XXI. Background count rates for chopped gamma tests. ....	150
Table XXII. Count rates using the gamma source with background counts deducted for chopped gamma tests. ....	151
Table XXIII. Count rates using the gamma source with background counts deducted for chopped gamma tests. ....	152

# List of Figures

Figure 1. Image showing the different penetrative strengths of different radiations. ....	8
Figure 2. Illustration of different paths and interaction mechanisms for gamma rays, 'author's own' reproduced from [2].....	9
Figure 3. Jablonski diagram showing different absorption and fluorescence mechanisms, 'author's own' reproduced from [2].....	11
Figure 4. Example situation of the elastic scattering of a nucleus. ....	13
Figure 5. Sketch of a possible photofission active interrogation rig [7] Copyright © 2009, IEEE. ....	14
Figure 6. Component sketch of a neutron interrogation system [8] Copyright © 2005, IEEE. ....	15
Figure 7. Neutron-induced fission producing prompt neutron and gamma rays. ....	19
Figure 8. Light output for gamma, neutrons and alpha particles [24]. "Reprinted from "Measurement of the time dependence of scintillation intensity by a delayed-coincidence method", L.M. Bollinger and G.E. Thomas, <i>Rev. Sci. Instrum.</i> 32 (1961) with the permission of AIP Publishing" .....	23
Figure 9. Scatter plot of first vs second integral for EJ-301 liquid scintillator exposed to <sup>252</sup> Cf taken in this work. Two distinct regions are evident, the red plume (upper) associated with gamma rays and the blue plume (lower) associated with neutrons. ....	26
Figure 10. Gamma ray detection using a NaI(Tl) scintillator and a photomultiplier tube [45], courtesy of Hamamatsu Photonics K.K.....	32
Figure 11. Four of the most common types of electron multipliers [45], courtesy of Hamamatsu Photonics K.K. ....	34

Figure 12. Cross section of a typical MCP-PMT [45], courtesy of Hamamatsu Photonics K.K. ....	35
Figure 13. Block diagram of the electronics and a timing chart for the gated voltage divider between the gate pulse and the TFA output of the LaBr <sub>3</sub> (Ce) detector [49]. Reprinted from Nuclear Instruments and Methods in Physics Research Section A: Accelerators, Spectrometers, Detectors and Associated Equipment, 723. K.Y. Hara, et al., ‘γ-Flash suppression using a gated photomultiplier assembled with an LaBr <sub>3</sub> (Ce) detector to measure fast neutron capture reactions’, 121-127, 2013, with permission from Elsevier. ....	38
Figure 14. Steel enclosed tank housing <sup>252</sup> Cf. ....	44
Figure 15. All four detectors, upper two containing EJ-309 the upper left being of type V94A94/3MEJ309E1XNEG, and the upper right being of type 127A76/3M-EJ309X-NEG, bottom left containing EJ-301 of type 19A15/0.75-E1-LS-X-N and bottom right containing EJ-299-33 being of type 51A51/2ME1EJ299XN, all detectors supplied by Scionix, Netherlands. ....	54
Figure 16. A schematic of the VS1173-30 detector unit, containing the plastic scintillator EJ299-33, used in this research shown in a vertical orientation with the scintillator cell at the bottom of the diagram [10]. ....	56
Figure 17. MCA plot for cylindrical EJ-309 exposed to a <sup>137</sup> Cs sources for 2 minutes. .	58
Figure 18. Scatter plot from EJ-301 liquid scintillator exposed to <sup>252</sup> Cf. Two distinct regions are evident, the red plume (upper) associated with gamma rays and the blue plume (lower) associated with neutrons. ....	59
Figure 19. Normalised plot showing the cubic EJ-309 at 0° exposed to <sup>252</sup> Cf. ....	61
Figure 20. Example PHD histogram from Figure 19. ....	62

Figure 21. Averaged data for $\gamma$ -ray (solid) & neutron (dashed) pulses of voltage versus time arising from previous measurements. ....	67
Figure 22. Neutron (dashed) and $\gamma$ -ray (solid) pulses from the fit reported by Marrone et al. [6] as a function of voltage against time, normalised to each other for clarity. ....	69
Figure 23. The rising edge of the neutron and $\gamma$ -ray pulses based on the Marrone fit [6] normalised to the peak amplitude. ....	69
Figure 24. New $\gamma$ -ray fit (solid) and averaged experimental data (dots). ....	70
Figure 25. New neutron fit (solid) and averaged experimental data (dots). ....	71
Figure 26. PGA scatter plot (top), with individual radiation plots (below) using the falling edge. ....	73
Figure 27. Different plots of peak against normalised discrimination amplitude for $\gamma$ rays on the left and neutrons on the right for varying rise time discrimination sample points as stated as denoted at the top in between the plots. ....	74
Figure 28. Different plots of peak against normalised discrimination amplitude for $\gamma$ rays on the left and neutrons on the right for varying rise time discrimination sample points as denoted at the top in between the plots. ....	75
Figure 29. Joint $\gamma$ -ray (red) and neutron (blue) distributions for varying rise time discrimination sample points. ....	76
Figure 30. Joint $\gamma$ -ray (red) and neutron (blue) distributions for varying rise time discrimination sample points. ....	78
Figure 31. The different arrangements of the detector explored in this work relative to the position of the source situated at $0^0$ , shown in the vertical plane. ....	84
Figure 32. Detector set up at (a) $45^0$ , (b) $67.5^0$ and (c) the 4-channel MFA used to process the data. ....	86

Figure 33. MCA plots for cubic EJ-309 exposed to a gamma sources at 0 degrees (upper), and +45 degrees (lower).....	87
Figure 34. Scatter plot obtained from the cubic detector exposed to the $^{252}\text{Cf}$ source at $0^\circ$ for 100100 counts. The upper plume is attributed to $\gamma$ rays and the lower plume to neutrons. ....	88
Figure 35. Scatter plots obtained from the cubic detector at a variety of angles during exposure to the $^{252}\text{Cf}$ source for 100100 counts, angles denoted bottom right corners. ...	89
Figure 36. Scatter plot obtained from the cylindrical detector exposed to the $^{252}\text{Cf}$ source at $0^\circ$ for 100100 counts. The upper plume is attributed to $\gamma$ rays and the lower plume to neutrons. ....	91
Figure 37. Scatter plots obtained from the cylindrical detector at a variety of angles during exposure to the $^{252}\text{Cf}$ source for 100100 counts, angles denoted bottom right corners. ....	92
Figure 38. Scatter plots for the cylindrical cell (a) $0^\circ$ , (b) $-90^\circ$ , (c) $-90^\circ$ with revised PSD threshold, red points (upper) corresponds to gammas, blue points (lower) to neutrons. .	94
Figure 39. Example normalised plot for the cubic EJ-309 exposed to $^{252}\text{Cf}$ . ....	96
Figure 40. Four normalised plots corresponding to Figure 35 obtained using the cubic detector at a variety of angles during exposure to the $^{252}\text{Cf}$ as denoted in the lower right. ....	97
Figure 41. Four normalised plots corresponding to Figure 37 obtained using the cylindrical detector at a variety of angles during exposure to the $^{252}\text{Cf}$ .....	98
Figure 42. A histogram of the number of counts for the cubic detector for the full energy range exposed for 100100 counts at $0^\circ$ , with the model fit over the top. ....	99
Figure 43 Double Gaussian fits for each angle tested using the cubic detector exposed to $^{252}\text{Cf}$ .....	99

Figure 44 Double Gaussian fits for each angle tested using the cylindrical detector exposed to $^{252}\text{Cf}$ .	100
Figure 45. Total counts recorded for the 2-minute exposures of the cubic (black squares) and the cylindrical (grey circles) detector as a function of angle (uncertainties smaller than the size of the symbols in each case).	101
Figure 46. Pictorial representation of the uniform radiation field bisecting the detector cell.	102
Figure 47. Total counts recorded for the 2-minute exposures of the cubic (black squares) and the cylindrical (grey circles) detector as a function of angle on the horizontal plane.	104
Figure 48 Cubic detector setup for surface of attack experiments.	105
Figure 49. $^{60}\text{Co}$ gamma irradiator, Foss Therapy Service, Inc.	112
Figure 50. EJ-301 organic liquid scintillator inside the $^{60}\text{Co}$ irradiator.	113
Figure 51. EJ-301 organic liquid scintillator inside the $^{60}\text{Co}$ irradiator.	114
Figure 52. The circuit diagram of the trigger-signal circuit utilizing a silicon PIN diode developed in this work.	119
Figure 53. Oscilloscope traces of the PIN photodiode response under exposure to the strobed light (20 Hz) green trace (top) and the output from the trigger circuit (with voltage offset for clarity), yellow trace (bottom). Each square represents 50ms in the x axis and 1 V in the y axis.	121
Figure 54. Switching time for the trigger circuit from a high signal (PMT off), to a low signal (PMT on), the PIN photodiode response under exposure to the strobe light (20 Hz) green trace (top) and the output from the trigger circuit (with voltage offset for clarity) yellow trace (bottom). Each square represents 20ms in the x axis and 1 V in the y axis.	122

Figure 55. Low signal output from the trigger circuit, meaning gated detector is active, the PIN photodiode response under exposure to the strobed light (20 Hz) green trace (top) and the output from the trigger circuit (with voltage offset for clarity) yellow trace (bottom). Each square represents 50ms in the x axis and 1 V in the y axis..... 123

Figure 56. A schematic diagram of the experimental setup prepared for the trigger experiments described in this research..... 124

Figure 57. Pulse-height spectra (PHS) from the MFA operating in MCA mode of counts versus channel number with the VS1173-30 system exposed to  $^{137}\text{Cs}$ , without triggered (top), with triggering (bottom). Data were acquired to ensure qualitative consistency of PHS shape only; hence the acquisition periods were not the same for both plots..... 125

Figure 58. Scatter plots of first integral versus second integral for the system developed in this research exposed to  $^{137}\text{Cs}$  for 20 minutes, without triggering (top) and whilst being triggered by a strobe light source at 20 Hz, 50% duty cycle (bottom)..... 126

Figure 59. PSD scatter plots of first integral versus second integral for the system developed in this research exposed to  $^{252}\text{Cf}$  for 20 minutes, without triggering (top) and whilst being triggered by a strobe light source at 20 Hz, 50% duty cycle (bottom). Aside from triggering all other aspects of the measurements were unchanged.  $\gamma$ -ray events are denoted in red (upper) and neutrons in blue (lower)..... 129

Figure 60. Individual runs of 5 minutes, A. Background run in-situ, B.  $^{252}\text{Cf}$  exposed with no shielding, C.  $^{252}\text{Cf}$  exposed with lead shielding, D.  $^{252}\text{Cf}$  exposed with polyethylene shielding. .... 132

Figure 61. Detector and source arrangement. .... 139

Figure 62. Three different second integral settings using the EJ-299-33 exposed to an Am-Be source, sample position denoted lower right. .... 140

Figure 63. Scatter plots of EJ-299-33 exposed to  $^{252}\text{Cf}$  (left), and Am-Be (right). .... 141

Figure 64. Scatter plots using the EJ-299-33 detector, A. Un-triggered exposed to $^{252}\text{Cf}$ for 5 minutes, B. Triggered exposed to $^{252}\text{Cf}$ for 5 minutes, C. Un-triggered exposed to Am-Be for 1 minute, D. Triggered exposed to Am-Be for 1 minute.....	142
Figure 65. Normalised plots for the EJ-299-33 exposed to an Am-Be source with different second integral delays. ....	143
Figure 66. Normalised scatter plots for the EJ-299-33 A. Un-triggered exposed to $^{252}\text{Cf}$ for 5 minutes, B. Triggered exposed to $^{252}\text{Cf}$ for 5 minutes, C. Un-triggered exposed to Am-Be for 1 minute, D. Triggered exposed to Am-Be for 1 minute.....	144
Figure 67. Design for chopped gamma experiments. ....	149
Figure 68. Average measured pulse shapes for neutrons and gammas. Each shape is plotted twice, once showing the entire trace and again at a magnification factor of 10 (see right-hand scale) so as to show the pulse tail in detail. Reprinted from Nuclear Instruments and Methods in Physics Research Section A: Accelerators, Spectrometers, Detectors and Associated Equipment, 729. N.P. Hawkes, G.C. Taylor, ‘Analysis of the pulse shape mechanism in a plastic scintillator with efficient neutron/.gamma pulse shape discrimination’, 522-526, 2013, with permission from Elsevier [2].....	156

# List of Abbreviations and Acronyms

CC	Charge comparison
DAQ	Data Acquisition
DCF	Dalton Cumbria Facility
EM	Electromagnetic
EMC	Electromagnetic compatibility
FoM	Figure of Merit
GUI	Graphical User Interface
ICRU60	International Commission on Radiation Units & Measurements 60
IRR99	Ionising Radiation Regulations 1999
LINAC	Linear Accelerator
MCA	Mixed Channel Analysis
MCP-PMT	Micro-Channel Plate Photomultiplier Tube
MFA	Mixed Field Analyser
MSV	Mean Square Voltage
NDA	Non-destructive Assay
NPL	National Physical Laboratory
NRC	National Regulatory Commission
PGA	Pulse Gradient Analysis
PHD	Pulse Height Distribution
PMT	Photomultiplier Tube
PSD	Pulse Shape Discrimination
QE	Quantum Efficiency
SiPM	Silicon Photomultiplier
SNM	Special Nuclear Material
TLD	Thermoluminescent Dosimeter
ToF	Time of Flight
TTA	Triplet-triplet annihilation
TTL	Transistor-transistor logic

# 1 Introduction

Using radiation to examine objects non-destructively is becoming ever more prevalent with the planning of new civil nuclear sites that will result in an increase in fissionable material. Transportation is, as ever, a huge part of day-to-day life [1], with more material being transported as nuclear power is revitalised as a power source. This requires the supply of material for new build reactors and uprated power plants as well as the removal of waste and by-products from plants to storage facilities. There is a drive for research into recycling or repurposing of by-products for useful applications [2], however, these are the materials which pose a proliferation risk and security threat. Preventative measures are advancing to monitor and detect such materials [3].

An issue with detecting radiation has been caused by the need to protect ourselves from that which we wish to harness. This is the case in all aspects of radiation work and not just restricted to the civil nuclear power industry. For instance, in radiography medical practitioners carrying out X-ray examinations have procedures in place to protect themselves from receiving unnecessary doses. In any nuclear industry all attempts have to have been made to reduce the radiation received not only to workers but also to the wider public for obvious health concerns. Due to the advancements in protection from and shielding of radiation, this has caused the situation where material can be shielded. These advancements have made determination of objects for security purposes even more difficult [3].

Special Nuclear Material (SNM) by definition is material that is fissile: meaning that under stimulation it will undergo nuclear fission. This makes active

interrogation, where an object is stimulated to produce radiation, a feasible solution to its assessment. Active interrogation allows for the non-destructive identification of fissionable materials [4]. A limitation on the speed of identification is due to the processing of the information received about the object of interest. This speed limitation is dependent upon the detector system being used and the digital data acquisition (DAQ) that is available.

## 1.1 Research aims

The work presented in this thesis is focused on accessing signals at earlier times after an active interrogation pulse. Specifically one aspect is to gather information during/after the intense prompt gamma transients (also known as ‘the flash’) that occurs whilst using active interrogation techniques. This involves investigating a solution to protect photomultiplier tubes from being blinded during the intense prompt gamma transients. The key aims are listed below:

- Utilise the recently developed plastic scintillator, EJ-299-33.
- Find a solution to the dead time observed by the photomultiplier tube (PMT).
- Obtain radiation information as quickly as possible after the prompt gamma flash of radiation transients.

## 1.2 Novelties of this research

The aims of the research for this thesis are to acquire more information after the flash of radiation from an active interrogation pulse. The difficulties lie in the over-saturation of important components, none more so than the PMT whilst this prompt flash of intense radiation is present. This study reports on several different aspects of radiation detection:

- Increasing the throughput of information in the detector.
- Reducing the dead-time after high-intensity radiation fields
- The development of a novel trigger controlling the PMT that can determine and dictate when the PMT and subsequently when the detector is active.

Experiments with systems which could be used for active interrogation have shown dead-time issues associated with the prompt flash of radiation [4-6]; due to the intensity the PMT is unable to detect anything. The dead-time of the PMT is the time in which it takes for the tube to be evacuated by electrons, to allow for new signals to come in and be detected fully. The throughput of radiation entering the focusing electrode on the PMT and subsequently being amplified hits the limit on what can be passed through the tube, meaning that radiation is being missed. Before more information can be gathered the electrons within the tube have to be allowed to evacuate. The novel system that has been developed works on the principle of rendering the PMT to be inactive during this intense burst of radiation.

For the system to be autonomous in terms of when it will switch off, this research investigates using a trigger circuit that can switch the PMT off once radiation

## A novel detection system using neutron/gamma pulse shape discrimination, for use in active interrogation environments

levels go above a certain threshold. The trigger circuit will then allow the PMT to switch back on and become active when the threshold is back below this set limit. Key features that needed to be considered with the trigger circuit include the ability to be applied and not have a negative impact on the performance of the detector, PMT or DAQ system, the speed at which a signal can be sent to the PMT to be switched off.

The ability to trigger remotely the PMT using the radiation level is novel and is relatively unexplored, and one that may have uses in several applications.

### 1.3 References

1. S.Z. Kane & D.S. Koltick, "A neutron based interrogation system for SNM in cargo" *Application of Accelerators in Research and Industry conference proceedings* 1336, pp. 717-722 (2011)
2. R. Taylor, "Reprocessing and Recycling of Spent Nuclear Fuel" Woodhouse Publishing, 2015
3. J.M. Mueller, M.W. Ahmed, H.R. Weller, "A novel method to assay special nuclear materials by measuring prompt neutrons from polarized photofission", *Nucl Inst. Meth A* 754 (1) pp. 57-62 (2014)
4. R.C. Runkle, L.E. Smith, A.J. Peurrung, "The photon haystack and emerging radiation detection technology" *Journal of Applied Physics Reviews* 106, (2009)
5. C.D. Clemett et al., "Neutrons for active detection of special nuclear material: An intense pulsed  ${}^7\text{Li}(p,n){}^7\text{Be}$  source", Nuclear Science Symposium and Medical Imaging Conference, IEEE, NSS/MIC'12
6. C. Hill et al., "Photofission for active SNM detection I: intense pulse 8MeV Bremsstrahlung source" Nuclear Science Symposium Conference Record, IEEE, NSS'12
7. P. Mistry et al., "Photofission for active SNM detection II: intense pulsed  ${}^{19}\text{F}(p,\alpha\gamma){}^{16}\text{O}$  characteristic  $\gamma$  source" Nuclear Science Symposium Conference Record, IEEE, NSS'12

## 2 Background & Theory

This chapter discusses information relevant to the research described in this thesis as well as a brief overview of studies that have been carried out in the wider context of the field. The chapter starts by going through fundamental topics on radiation and radioactivity explaining the different radiation types, the classification of nuclear material, non-destructive interrogation, the detection of radiation and provides information on instruments that have been utilized in this work.

### 2.1 Radioactivity

Radioactive is the adjective used when an atomic nucleus is unstable and is prone to decay emitting radiation in order for it to reach a more stable state. Radioactive decay is a random process and the timing of when a specific decay will take place is impossible to predict. Radiation is present in everyday life due to its natural occurrence in our environment. In the context of experimental procedures, background radiation is defined by the International Atomic Energy Authority (IAEA) [1] as the dose rate associated to all sources other than the one specified, described more commonly as any radiation present in a location excluding the specific source in use. Typical procedures to negate the effect of background radiation from experiments include carrying out background calibration runs in-situ but without the presence of the source giving a baseline measurement of the background radiation. In certain cases this can simply be subtracted from the experimental results, or alternatively if equipment allows can be eliminated by thresholds being placed above the background levels.

### 2.1.1 Activity

To determine the activity of a source the rate of decay is used and this is given in units of becquerel (Bq) or curie (Ci). The activity is given by,

$$Activity = \lambda N = \frac{dN}{dt} \quad \text{[Equation 1]}$$

where  $\lambda$  is the radioactive decay constant and  $N$  is the number of radioactive nuclei present. The curie is  $3.7 \times 10^{10}$  disintegrations per second, the unit was derived from the specific activity of radium, known as the radium gram equivalent. The becquerel in comparison is 1 disintegration per second.

## 2.2 Ionising radiation

Ionising radiation has sufficient energy that upon interaction with an atom or molecule it results in the atom or molecule becoming ionised. Ionising radiation can occur both naturally or be man-made and can appear as either particles (with mass) or electromagnetic radiation. The four most common types of ionising radiation are: alpha & beta particles, gamma rays and neutrons. Gamma rays are a form of electromagnetic radiation while the other radiation types are all emitted particles.

To be able to identify ionising radiation it requires the observation of the effects that occur once it has interacted and ionised matter. Each type of radiation has its own set of interactions. Radiation can either be charged or uncharged, which is also a contributing factor in the way it will interact. Charged radiation will interact by the Coulomb interaction and will ionise matter, directly exciting electrons.

## A novel detection system using neutron/gamma pulse shape discrimination, for use in active interrogation environments

One result relevant to this work is that these electrons will enter a higher level of energy when excited and during the de-excitation process will emit a luminescence photon. These photons can be used in radiation detection with scintillators as the intensity at which the photon luminesces corresponds to the energy that had been imparted by the initial radiation.

Neutrons being uncharged interact in a different manner and their detection relies on secondary interactions. Initially they have to react to create charged particles that then go on to interact as described above. The charged particles can be created through a number of different mechanisms that are described below.

The neutrally-charged neutrons and gamma rays are types of indirectly ionising radiation in contrast to the alpha and beta particles which are both charged and directly ionising. These different radiation types interact differently allowing distinctions between them to be made. For example, the level of penetration is dependent on the type of radiation. Alpha particles can be blocked with a sheet of paper, whereas with gamma rays a sheet of lead is required and for neutrons hydrogenous substances are often best to stop them, as illustrated in Figure 1. The interactions of photons and neutrons which are specific to this research are described in the sections below.

## A novel detection system using neutron/gamma pulse shape discrimination, for use in active interrogation environments

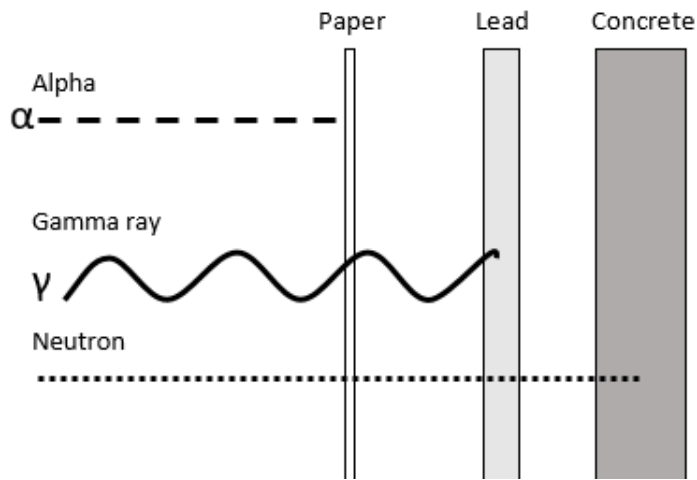


Figure 1. Image showing the different penetrative strengths of different radiations.

### 2.2.1 Photons

A photon is a form of electromagnetic radiation having zero mass and traveling at a speed of  $c$ , the speed of light. The energy of a photon is defined in equation 2 [2];

$$E_{\gamma} = h\nu \quad \text{[Equation 2]}$$

where  $h$  is Planck's constant and  $\nu$  is the frequency of the electromagnetic (EM) wave. Both gamma rays and X-rays are types of photons that can have sufficient energy to penetrate and interact in matter. Gamma rays are photons that appear from nuclear decay.

The ability to detect gamma rays is dependent on the gamma photon undergoing an interaction with which it imparts some or all of its energy to an electron in the material of interest. From these interactions it is only the electrons that can be used to identify information about the incident gamma radiation. The most common interaction mechanisms that a gamma ray can undergo are: pair production, Compton scattering and photoelectric absorption, these mechanisms are depicted schematically

in Figure 2. Depending on the energy that the gamma ray interacts with different mechanisms are observed.

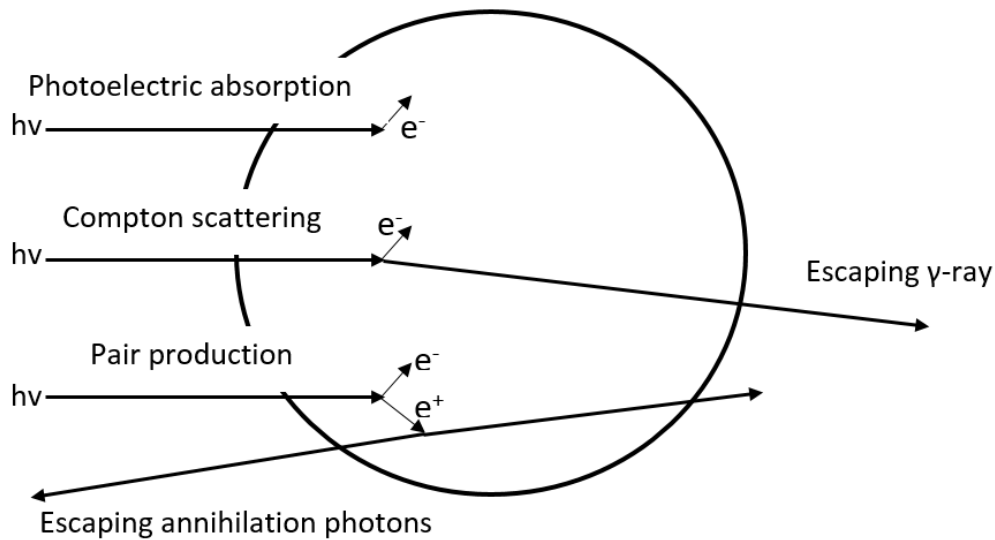


Figure 2. Illustration of different paths and interaction mechanisms for gamma rays, 'author's own' reproduced from [2].

- Pair production is the conversion of a photon into a positron-electron pair through the electric field. This positron will pair with an electron due to charge attraction, with both constituents of the pair sharing the incident energy. Pair production can occur when the incident radiation has energy more than double that of the electron rest mass. Once the positron has slowed down it will annihilate with the electron within the material causing the emission of photons. Pair production interactions dominate at higher photon energies.
- Compton scattering occurs when the photon only transfers part of its energy to an electron within the atom. This causes the photon to scatter from its original

trajectory with reduced energy. The amount of energy transferred is dependent on the scattering angle, which can be calculated via equation 3 [2];

$$h\nu' = \frac{h\nu}{1 + \frac{h\nu}{m_0c^2}(1 - \cos \theta)} \quad \text{[Equation 3]}$$

where  $m_0c^2$  is the rest mass of an electron,  $h\nu'$  is the energy of the gamma ray after interaction and  $\theta$  is the scattering angle of the photon.

- Photoelectric absorption is where all the energy from the incident radiation is absorbed by the electron. The excited atom then emits a photo-electron. There is a slight scatter of the atom on ejection of the photo-electron but this is negligible due to it being a low mass compared with the atom. The emitted photo-electron therefore has an energy given by equation 4 [2];

$$E_{e^-} = h\nu - E_b \quad \text{[Equation 4]}$$

where  $E_b$  is the binding energy of the electron in its atomic orbital and  $h\nu$  is the energy of the gamma ray. The photoelectric effect dominates at lower photon energies.

With these interactions an electron from the atom absorbs energy, resulting in the electron entering an excited state. In particular with regards to the photoelectric absorption the system has both an excited vibrational and electronical state. The system will relax vibrationally and then fluoresces, which can be shown in a Jablonski diagram, Figure 3. The fluorescence that occurs in organic scintillators is the basis for scintillation detection and the research in this thesis.

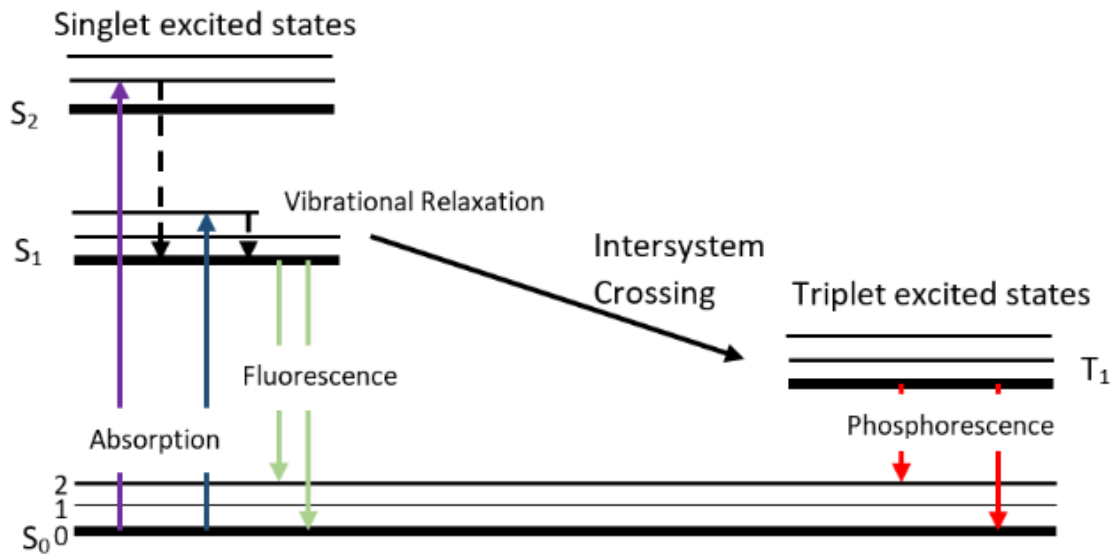


Figure 3. Jablonski diagram showing different absorption and fluorescence mechanisms, 'author's own' reproduced from [2].

The Jablonski diagram is an energy diagram of the transitions between electronic states. The diagram shows the different mechanisms that are associated with excited electrons and how they relax back to their normal state. Electrons will first relax either by vibrational relaxation or radiationless de-excitations as depicted, before undergoing fluorescence.

### 2.2.2 Neutrons

A neutron is a subatomic particle with zero electric charge and has a rest mass of  $1.675 \times 10^{-27}$  kg. Due to the lack of charge neutrons interact with atomic nuclei as they are able to pass the cloud of electrons surrounding the nucleus. As a result of their lack of charge neutrons have become a common component for the investigation of materials composition. Once a neutron comes into contact with the nucleus there are several

possible outcomes. The two major types of interactions are *scattering* and *absorption* [3]. Neutrons that are scattered exhibit changes in speed and direction. Under neutron absorption with the nucleus an array of different radiations can be emitted. The determining factor on the interaction the neutron undertakes is based on the kinetic energy of the neutron and the isotope of the nucleus.

#### 2.2.2.1 Scattering

There are two types of scattering the neutron can undergo with interactions both of which are informative in interrogation purposes. Elastic scattering is the process by which the neutron will collide with the nucleus and impart some of its kinetic energy with which both the trajectory of the neutron and the nucleus will change. In this instance the incident neutron will be emitted from the interaction with less kinetic energy than it started, with this lost kinetic energy being passed to the nucleus. This follows the laws of classical mechanics that the sum of the kinetic energy is the same before the reaction as the sum of the kinetic energy after the reaction. The neutron and nucleus can be considered analogous to two marbles colliding, Figure 4.

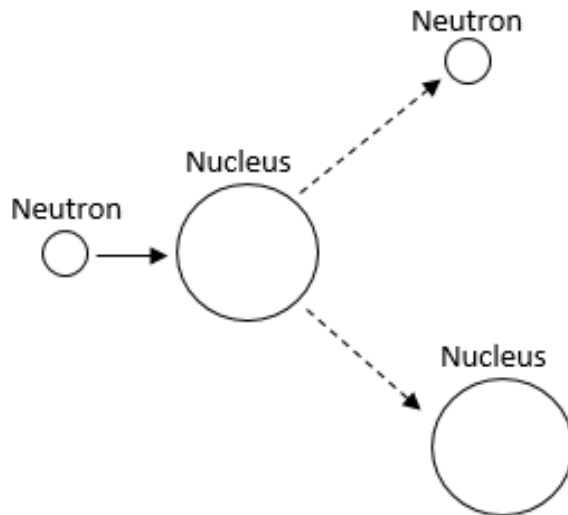


Figure 4. Example situation of the elastic scattering of a nucleus.

With inelastic scattering the nucleus after collision enters an excited state due to the energy that has been imparted upon it. To reach a stable state again the nucleus can emit several combinations of particles or photons. For inelastic scattering the emission from the excited nuclear state is a neutron, which looks identical to elastic scattering, the only distinction being that kinetic energy is not conserved with inelastic scattering. This apparent disappearance of energy is caused by emission of gamma rays, whilst the nucleus is returning to its stable state.

## 2.3 Fissile material

The research behind this thesis is focussed on security and safeguard protection with regards to nuclear material detection. Nuclear materials according to the IAEA refers to uranium, plutonium and thorium in any form, and special fissionable material

A novel detection system using neutron/gamma pulse shape discrimination, for use in active interrogation environments

comprising materials enriched in  $^{235}\text{U}$ ,  $^{233}\text{U}$  or  $^{239}\text{Pu}$  [1], whereas in the United States this is given the term of Special Nuclear Materials (SNM) by the National Regulatory Commission (NRC). With regard to this work fissile materials will be the term used to describe any special fissionable material or special nuclear materials of interest in border security applications. Extensive research activity has been carried out, especially in the United States, into active interrogation to find such fissile materials [4-6]. Detection modes for these materials tend to follow two paths: passive detection and active interrogation, both coming under the title *non-destructive interrogation* described in the next section. In either field of research some means of a detector system is required to identify the radiation, a sketch of a possibility for active interrogation using photofission techniques is given in Figure 5.

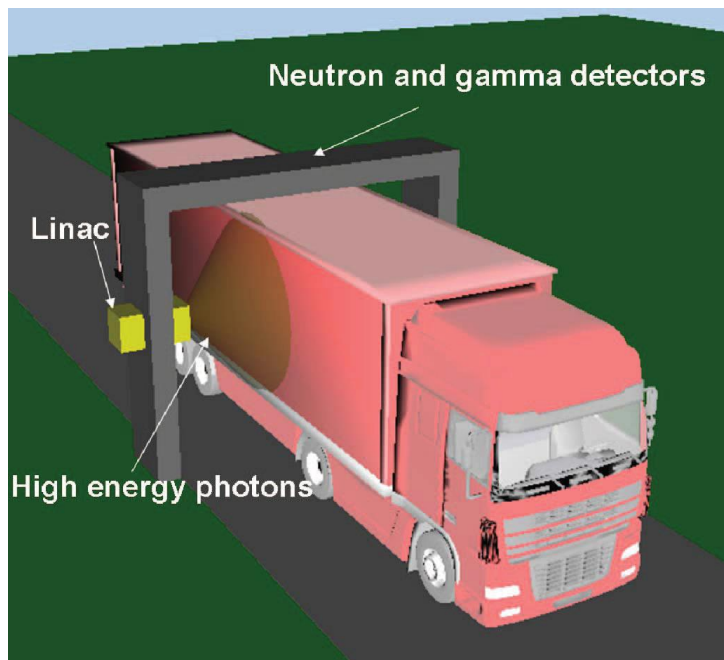


Figure 5. Sketch of a possible photofission active interrogation rig [7] Copyright © 2009, IEEE.

A novel detection system using neutron/gamma pulse shape discrimination, for use in active interrogation environments

The setup in Figure 5 is focussed on the use of photons from a LINAC to interrogate the container whereas an alternative form of active interrogation is neutron interrogation of which a component sketch is shown in Figure 6.

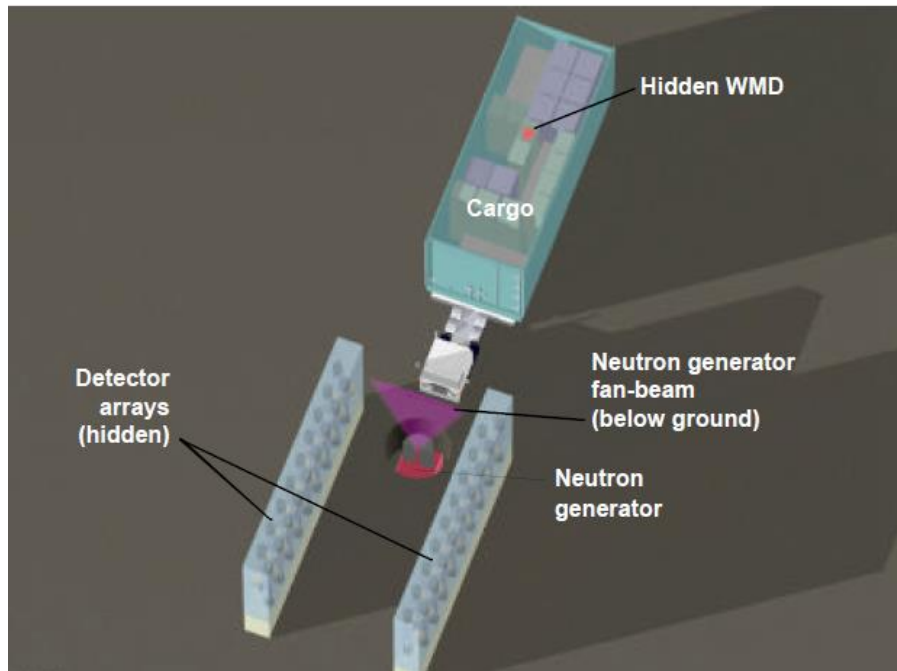


Figure 6. Component sketch of a neutron interrogation system [8] Copyright © 2005, IEEE.

Other research has focussed on the use of investigating objects in-situ with portable systems for maritime investigation [9]. It is worthy to note that this sort of investigation would require both prior suspicion of material on-board as well as a rough location because the range and penetration capability of such a portable device is expected to be very limited. Also due to the device having to be portable, able to fit within ship hatches and used by a search team, heavy accelerator-driven devices and radioactive sources requiring significant shielding are less suitable, the only currently viable option is a deuterium-tritium neutron generator. Due to these constraints

research is much more focused toward scanning cargo and containers at ports, border controls and entrance gates to sites as depicted in Figure 5 & 6.

## 2.4 Non-destructive Interrogation

Interrogation techniques enjoy an extensive history where non-destructive interrogation is the action of investigating objects without damaging them [10]. Radiation can be used in certain interrogation purposes due to its ability to penetrate through high-Z materials. It has been used extensively in radiography because of its non-destructive properties. Radiography uses electromagnetic radiation, usually X-rays, to view the composition and structure of materials. This technique has well known medical uses, but it has also been applied to the scanning of objects for protection and safeguarding. One use that has become commonplace is in airport security. High throughput of luggage can quickly and effectively be scanned with different densities in the image and potential threats identified, with ambiguous homogenous densities investigated further by visual inspection. In radiographic imaging as with other non-destructive interrogation methods the technique can locate and discern the contrast differences between high-Z and low-Z materials.

In the interest of this research the quantity of fissile material being transported is set to rise within the nuclear industry with the resurgence of new nuclear builds being set in motion and the uprating of power plant. The interrogation of fissile material has become a priority [11] and the increase and higher-profile international terrorist events over the past two decades has caused security to become a greater

concern. Non-destructive interrogation, also known as non-destructive assay (NDA) [10], involves observing the radiation from stimulated fission to identify the amount of nuclear material present in a sample. For detection there are two types; these being *passive* and *active* interrogation. Both types are described in the sections below. The research presented in this thesis is aimed at active interrogation inspection, but most of the research has been carried out in passive systems for calibrations and proof of principle due to the greater ease of carrying out tests within the laboratory.

#### 2.4.1 Passive Detection

Passive detection in the context of interrogating SNM is the process of detecting the radiation produced when radioactive materials decay naturally, such as for example by spontaneous fission or alpha decay. This requires no external stimulation meaning the target receives no radiation dose. The process of spontaneous fission of a nucleus only occurs in the transuranic elements and those with the higher the atomic mass numbers generally the more likely it is for the isotope to undergo spontaneous fission. Nuclei that undergo spontaneous fission decay into lower-mass fragments, until stable lighter isotopes are reached, freeing several neutrons in the process, both prompt and a delayed time after the fission event.

With passive systems the detection can be simpler to implement due to not needing stimulation for the material. In the area of non-proliferation passive measurements have been used successfully with the identification of  $^{240}\text{Pu}$  due to its spontaneous fission [12] although the downside can be the level of radiation that is spontaneously emitted limits detection compared to the relative intensity of the

background radiation sources. This means although passive detection is relatively simple and cheap, shielding can limit the effectiveness of detection and measurements can require long acquisition periods to obtain any statistically-relevant data.

As mentioned above passive detection was implemented in this research due to the ease of laboratory based experiments; both  $^{137}\text{Cs}$  and  $^{252}\text{Cf}$  were used. The caesium sources that were used produce a gamma-only field. The sources used were also relatively low activity in nature and used mainly for the calibration of detectors due to the characteristic peak produced from the  $^{137}\text{Cs}$  spectrum. The californium source was used due to the mixed field of radiation it provides, where the housing of this and activities of all the sources are described in section 3.1.

#### 2.4.2 Active Interrogation

The aim of active interrogation for non-destructive assay is to identify materials within containers or any transportation device, similar to radiography but by inducing fission in fissile materials that may be present. Active interrogation has been selected to be used as it has the potential to succeed in circumstances that involve shielded material by the process of induced fission [13-16]. After the induced fission, the excited material in its unstable state releases both prompt gamma and neutron radiation when the nuclei splits into two smaller isotopes. These daughter nuclei themselves are usually unstable and in excited states, causing a second stage of decay releasing delayed gamma and neutron radiation. Typical prompt emissions for the fission of  $^{235}\text{U}$  consist of 0-6 neutrons and 0-20 photons within  $10^{-14}\text{s}$  [17]. When this is compared to the background present and with the additional radiation that is caused by the source

of the interrogating media, distinguishing prompt fission neutrons from those created in the environment can be a significant task [18]. Figure 7 depicts a neutron-induced fission event producing prompt neutrons and gamma rays.

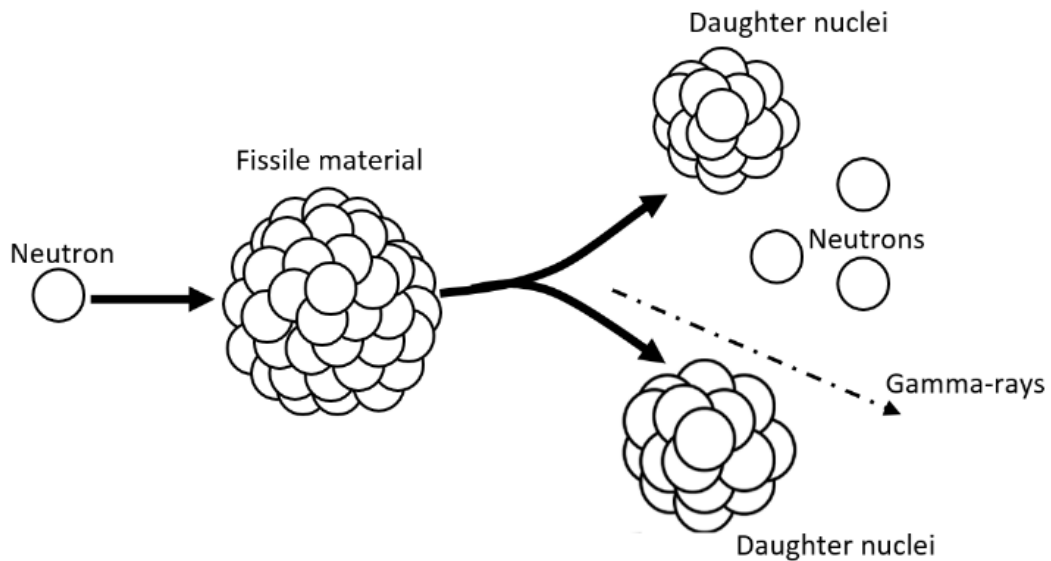


Figure 7. Neutron-induced fission producing prompt neutron and gamma rays.

The mixed field of radiation that is produced via induced fission contains information about the elemental composition of the object or material under interrogation. Due to radiation detection not requiring any direct contact it makes it ideal for a wide spectrum of uses including scanning containers.

There are different techniques of active interrogation; using neutrons or gamma rays as the interrogating media, and either looking at prompt or delayed signatures that are induced by the aforementioned radiation or any combination of these. Delayed neutron analysis is the earliest work carried out under active interrogation [19]. This is due to the delayed neutrons being emitted outside the instantaneous burst of radiation information and being more easily distinguishable without the background

## A novel detection system using neutron/gamma pulse shape discrimination, for use in active interrogation environments

radiation obscuring the readings. Delayed neutrons are a reliable indication of the presence of fissile material but they are not produced in great quantity and also have relatively low energies, 200-500 keV [20], meaning they can be attenuated by the presence of cargo making them harder to detect. Delayed gamma rays are released from short-lived fission fragments in larger numbers and of higher energy than the neutrons, often above 3000 keV, [21], giving a higher probability that they will be detected after escaping through any cargo and the container itself. Out of the prompt and delayed radiation emitted by the induced fission, the intensity of the prompt radiation is of an order of magnitude higher making it easier to be detected remotely. However when working with the prompt radiation this needs to be distinguished from the increased background noise levels produced from the radiation used to induce the fission which is a more difficult task.

Neutron interrogation usually involves a high intensity beam of neutrons being directed at the sample, so that some of these neutrons interact and induce the fission process, whereas photofission is the fission of the nucleus after absorbing a gamma ray. The material in question splits into fission fragments that decay until they are stable, releasing in the process energy in the form of a mix of radiation types. Active interrogation is being extensively researched due to the opportunity to detect and characterize fissile materials [19]. The main conclusions drawn from this review is there are several possible systems proposed but these were in the proof of principle stage at the time of this review. Any system that achieves the requirement of not just detecting but quantifying materials that are shielded still requires significant advancements to be implemented, especially on a resource and economical front.

## A novel detection system using neutron/gamma pulse shape discrimination, for use in active interrogation environments

Another point to consider with any active interrogation technique are the long-term effects whether the environment experiences a higher background radiation count than that which would be expected and whether the cargo becomes activated to an extent where it would affect the economic value of it, or have an effect on personnel who must handle it.

### 2.5 Radiation detection

Many types of detectors exist that can produce observable signals for either an individual quantum or collective quanta of radiation. With the interaction time of the radiation inside the detector usually being very short, the deposition of energy from radiation can usually be assumed to be instantaneous. Most detectors result in an output of electric charge from the radiation within them. In high-flux situations the irradiation of the substance could be high enough to cause a current being detected due to more than one interaction simultaneously as opposed to individual quanta.

#### 2.5.1 Scintillation

Scintillation is the process by which a flash of light is produced within a material when a particle or radiation interacts with it. In scintillation detection this light is usually converted into an electronic signal and then can be processed to allow the intensity and energy of the radiation to be inferred.

## A novel detection system using neutron/gamma pulse shape discrimination, for use in active interrogation environments

A scintillation material absorbs a quantum of radiation and subsequently fluoresces emitting photons with a characteristic spectrum. The light output of the scintillator can then be collected and amplified, the most common approach is using the focussing electrode of a photomultiplier tube (PMT), although photodiodes and other devices are also utilised. The light output of a scintillator is dependent on both the radiation type that is interacting and its energy, and is called the scintillation efficiency. There are 6 properties which the ideal scintillator should possess [2] relating to; high efficiency, linear conversion rate, transparency to its own emissions, short luminescence decay times, good optical qualities over larger sizes that can be manufactured and hold a refractive index close to glass for coupling to a PMT. There is no ideal material to match all these requirements so the selection process is usually based on a compromise between them for the application at hand. There are two commonly-used types of scintillators; inorganic crystals and organic scintillators. Generally the inorganics tend to have better linearity with regards to the PMT, but are slower in response time with no possibility for PSD as they are amplitude based. As opposed the organic scintillators are faster but the light yield is reduced.

### 2.5.2.1 Pulse shape discrimination

The techniques used to identify the different radiation outputs from a scintillator come under the category of Pulse Shape Discrimination (PSD). Light output pulses from excitation in the scintillator possess a very quick rise time, however this prompt response is followed by a slower decay tail. A long established technique involves the determination of neutron and gamma radiation by the shape of the pulses that are

produced within scintillator detectors using this decay tail [22]. Neutron-stimulated pulses take a longer time to decay than the gamma ray counterparts [23], this difference is more identifiable with certain scintillator materials than others. The ratio of neutrons to gamma photons can be manipulated with the setup of the interrogation exploiting the different penetrating strengths of the radiations by adding certain shielding to reduce one type of radiation over another. This can be an easy way of confirming that two different radiation types are present by adding a material that will decrease only one type of radiation in the readings giving confidence of the discrimination ability. Figure 8 shows the light output pulses for gamma rays, fast neutrons and alpha particles.

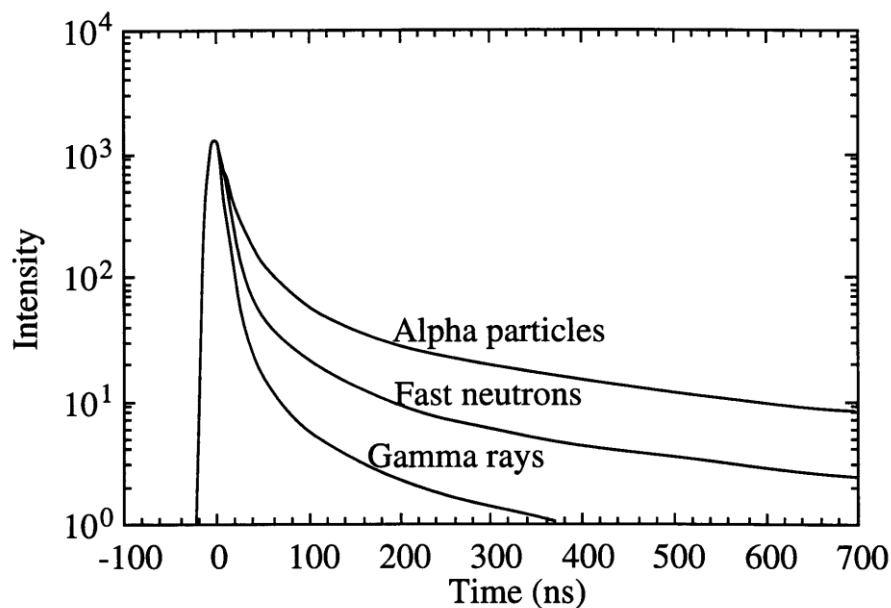


Figure 8. Light output for gamma, neutrons and alpha particles [24]. “Reprinted from “Measurement of the time dependence of scintillation intensity by a delayed-coincidence method”, L.M. Bollinger and G.E. Thomas, *Rev. Sci. Instrum.* 32 (1961) with the permission of AIP Publishing”

## A novel detection system using neutron/gamma pulse shape discrimination, for use in active interrogation environments

The pulses above can be described by the equation 5 [24];

$$L(t) = L_0 \left[ \exp\left(\frac{t}{\tau}\right) - \exp\left(\frac{t}{\tau^1}\right) \right] \quad \text{[Equation 5]}$$

where  $L(t)$  is the number of photons emitted at time  $t$ , following the energy deposition by the incident particle,  $L_0$  is the photons emitted at  $t=0$ ,  $\tau$  is the decay time constant of the scintillator, while  $\tau^1$  is the rise time. There are several types of pulse shape discrimination techniques and algorithms [25], a few of the most common are described below although there are many techniques being utilised. More are being developed to achieve the best possible results in separating mixed fields of radiation.

### Charge Comparison (CC)

This technique is well established [26, 27] and widely used [28, 29] it is based on taking two integrals during the light output pulse. These are known as the long and short integrals or gates. The long integral relates to the entire pulse from start to finish, with the short integral being set to part of the decay tail area. The selection of where the short integral begins is found from optimising the Figure of Merit (FoM) results, where the FoM is a value indicating how well the radiation types can be distinguished and is fully described later in section 3.4.1. Due to the slower decay of neutron pulses, they exhibit a larger short integral than a gamma ray, so in charge comparison plots of short integral against long integral two plumes are observed. On the resulting plots the upper of these plumes is produced by neutrons and the lower relates to gamma rays.

### Model pulse

## A novel detection system using neutron/gamma pulse shape discrimination, for use in active interrogation environments

The model pulse technique is based on constructing two models prior to any experiment, one model being for neutrons and one for gammas [30, 31]. Unknown pulses are then compared to the two constructed models and classified according to which model they best fit toward using a chi-squared criterion. The drawbacks of this technique is the requirement of these two models beforehand and the discrimination outcome is only as good as the information that has initially been input into the algorithm.

### Pulse Gradient Analysis (PGA)

PGA is the technique that has been used within this project and will be focussed on the most. This is a simple and fast method for classification of mixed field radiation into constituent events, the method is described fully [32-34]. The manner in which this is done is by taking a sample from the peak amplitude of the pulse, called the first integral, and comparing this to a sample amplitude from a point on the decay tail of the pulse, second integral, this is a user specified number of samples after the peak. The time at which this sample is to be taken is dependent on different factors, mainly the scintillator being used and the source or radiation that is being observed as these affect the length of the pulses and the energy of the radiation respectively. One drawback with this technique is if the start of the second integral is not selected at the correct place within the pulse, or the integrals are taken over too short a period of time, then the results from both gamma rays and neutrons will be identical. For the technique to compare different pulses the peak amplitudes are always normalised, giving each pulse a comparable gradient. The digitised pulses are put through a moving average

filter, this filter smooths the pulse shapes and allows the separation between radiation types to be observed. When selected in the correct place the second integral will be higher for that of neutrons than it will of gamma rays due to the slower decay tail as shown above. This means that when the first integral is plotted against the second integral in a scatter plot the upper plume of events corresponds to any  $\gamma$ -rays that are present, with the lower plot relating to neutrons. An example scatter plot is shown in Figure 9.

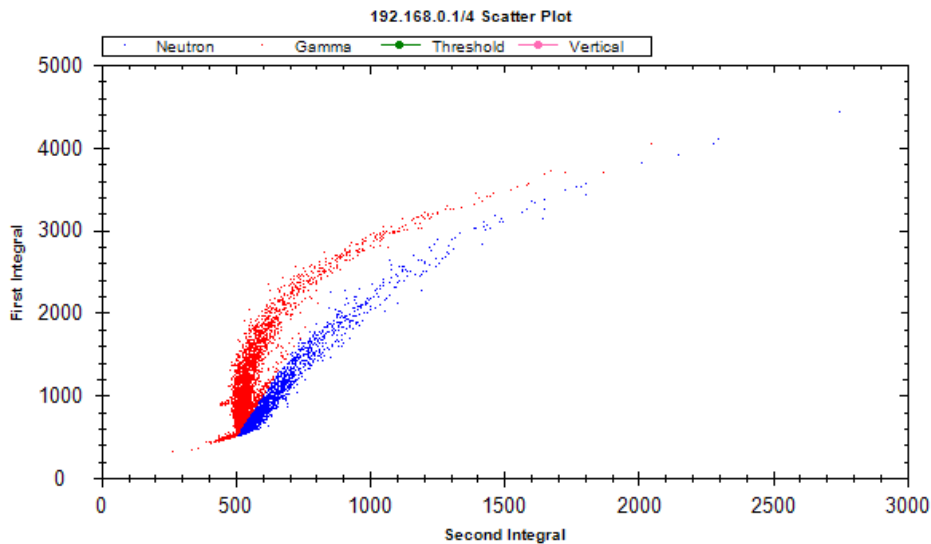


Figure 9. Scatter plot of first vs second integral for EJ-301 liquid scintillator exposed to  $^{252}\text{Cf}$  taken in this work. Two distinct regions are evident, the red plume (upper) associated with gamma rays and the blue plume (lower) associated with neutrons.

When the system is being run a three point threshold is positioned between the two plumes to separate the two regions. This threshold is used as the basis for assignment within the GUI system.

#### 2.5.2.2 Inorganic scintillators

The most commonly used inorganic scintillator material is sodium iodide. The mechanisms for scintillation depends on the structure of the crystal. In a purely

inorganic crystal lattice, electrons can only be at certain energies. The band gap is the energy range in which the electron is unable to occupy. In pure crystal structures when energy is absorbed into the scintillator, electrons from the valence band can move up to the conduction band. The electron will then return back down to the valence band with the emission of a photon. Due to this being an inefficient process few photons are released per decay, the energy is often dispersed in other ways. In pure crystals often the band gap width is too great for the emitted photon to be within the visible range, to try and change this impurities are added to pure crystal scintillators. These impurities create several excited states between the valence and conduction band of a pure crystal allowing the electron when dropping from the conduction band to go through several different states. As the drop to these intermediate states is lower, the photons emitted will have less energy. This can shift the wavelength of the emitted photon to within the visible range and maintain transparency to its own radiation.

#### 2.5.2.3 Organic scintillators

Organic scintillator materials fluoresce relatively independently of the physical state that the organic substance is in, allowing for a greater variety of materials to be used. Similarly to the inorganic scintillators, energy from an incident particle is absorbed and can raise the electron to one of a variety of states. Each of these states has different separation regions, and each separation state has sub levels which take into account the vibrational state of the molecule. If an electron is excited in an organic scintillator past the first excited state, then it will quickly drop down to this level through radiationless de-excitations. When the electron then drops from this first excited state

back to the ground state, scintillation light is observed also known as prompt fluorescence shown in the Jablonski diagram in section 2.2.1, Figure 3. The intensity of this prompt fluorescence can be calculated at a given time after the excitation using equation 6;

$$I = I_0 e^{-\frac{t}{\tau}} \quad \text{[Equation 6]}$$

where  $\tau$  is the fluorescence decay time from the first excited state to ground level.

As mentioned above organic scintillators can be used in both liquid and solid phases, but until recently only the liquid scintillators were available having pulse shape properties for discrimination. Liquid scintillators have long been the main type of organics that have been used for discrimination of mixed fields [22, 35]. This is due to the technique to separate these radiation types based on the decay tail of neutrons being longer than that for gamma rays. This longer decay tail arises from the possibility of triplet-triplet annihilation (TTA) in the de-excitation process for neutrons. This occurs when two triplet excited state molecules are within short enough distance that they annihilate, allowing one molecule to reach the ground state  $S_0$  and elevates the other molecule to the excited singlet state  $S_1$  [36]. This then allows the second molecule to de-excite through the normal fluorescence process, but at a delayed time to that which has already occurred creating a longer time for the neutron pulse to decay than that of a gamma pulse. This process of the TTA explains why liquid scintillators exhibit a more effective degree of discrimination than plastics, due to the mobility of the molecules giving a high probability that the two triplet states can be in close enough proximity. Conversely plastics do not allow for the mobility of molecules giving a low probability of TTA to occur.

## A novel detection system using neutron/gamma pulse shape discrimination, for use in active interrogation environments

Recent developments in plastic scintillators however have produced devices with mixed field discriminatory properties [37], thusly creating a flourish of developments [38-41], as well as sparking the particular ideas for this research. Different organic scintillators have various advantages where the push towards using the plastic scintillators is due to them being inherently safer and easier to use than the liquid counterparts. The safety concerns surrounding the liquids being deployed in systems are due to the flammability and toxicity that is associated with them. The new commercially-available plastic scintillator EJ-299-33 has been reported as having a lower efficiency and light output for neutrons compared to an EJ-309 liquid scintillator [38, 41, 42]. A comparison was also carried out for the FoM performance between the two devices. The plastic came out with a FoM of significantly lower value in both studies [38, 41] and the overriding conclusion was that the plastic will bring modest Pulse Shape Discrimination (PSD) capability at higher neutron energies and has potential for certain applications where the liquid systems are unsuitable.

Specific devices used in this work include EJ-301 and EJ-309 which are both organic liquid scintillators and EJ-299-33 which is a plastic scintillator. The EJ-301 scintillator has the best PSD qualities but has higher risks associated with it due to a relatively low flash point. Whereas in comparison the EJ-309 has much safer attributes at the cost of the quality of the PSD. The plastic scintillator has only recently been developed and is the first such plastic to show comparable PSD to the liquid scintillators but still carries a significant reduction in quality. The idea of using a plastic is highly appealing due to the safety and flexibility of manufacturing associated with it. Table I below compares some of the values of the scintillators.

Table I. Comparison of detector properties

	EJ-299-33 [43]	EJ-301 [44]	EJ-309 [44]
Light output (% Anthracene)	56%	78%	75%
Photons produced by a 1MeV Electron	8,600	12,000	11,500
Wavelength of Maximum Emission	420nm	425nm	424nm
Decay Time (short component)		~3.2ns	~3.5ns
Refractive Index		1.505	1.57
Flash Point ( <sup>0</sup> C)	N/A	26	144

#### 2.5.2.4 Detector modes of operation

There are three general modes of operation for radiation detectors that evolve an electrical charge as a response, these being: pulse, current and mean square voltage (MSV) mode. MSV will not be covered due to it having limited use in only some specialized applications. Pulse and current mode both are related to the current that is output from the detectors.

##### Pulse mode

Pulse mode operation is used in most applications as it retains information on the amplitude and timing of individual radiation quanta. In this mode the measurement equipment is set to take data for each individual piece of radiation that has interacted with the detector. The time integral for each burst of current, or quanta of radiation, is recorded. Any system that requires the energy of individual quanta must be operated in pulse mode, this is known as radiation spectroscopy [2]. Pulse counting is a simplified approach where, regardless of the current produced all quanta are registered

from the detector. This can be useful when only intensity, the gross number of events, is required. The main limitations to pulse mode operation is that during high flux rates the time between consecutive events is too short for the analysis to be carried out as events overlap one another giving piled-up readings. In these situations current mode is often preferred.

#### Current mode

When operated in current mode the measurement equipment will give a steady signal current proportional to the total light yield, which has contributions from all the decay components. However whilst in current mode if the intensity of the radiation changes rapidly there will be a residual effect from any long-lived components remaining on the current detected. The average current,  $I_o$ , is given by the product of the average event rate  $r$  and the charge produced per event  $Q$  [2];

$$I_o = rQ = r \frac{E}{W} q \quad \text{[Equation 7]}$$

where  $E$  is the average energy deposited per event,  $W$  is the average energy required to produce a unit of charge and  $q$  is the unit charge  $1.6 \times 10^{-19}$  C.

## 2.6 Photomultiplier tubes (PMT)

The light that is produced due to the scintillation process then needs to be turned into an electrical signal for processing. There are several available devices for converting light signals, but the most common device is the PMT. PMTs are very good at producing electrical signals from light; the first component within a PMT is a semi-

A novel detection system using neutron/gamma pulse shape discrimination, for use in active interrogation environments

transparent photocathode at one end, followed by a vacuum tube. This photocathode absorbs incident light and converts it into low energy electrons that are ejected into the tube. Light guides can be used to transfer the photons from the scintillator cell to the photocathode of the PMT. When a photon is absorbed by the photocathode it must have enough energy to survive any electron-electron collisions as the electron moves to the surface. Once it gets to the surface the potential barrier, called the work function, must be overcome for the electron to be emitted. The sensitivity or quantum efficiency of the photocathode is defined as the chance that one photon produces one electron, [45];

$$QE = \frac{\text{number of photoelectrons emitted}}{\text{number of incident photons}} \quad \text{[Equation 8]}$$

quantum efficiency is an important parameter when choosing a PMT, and can range from 15 up to 30%.

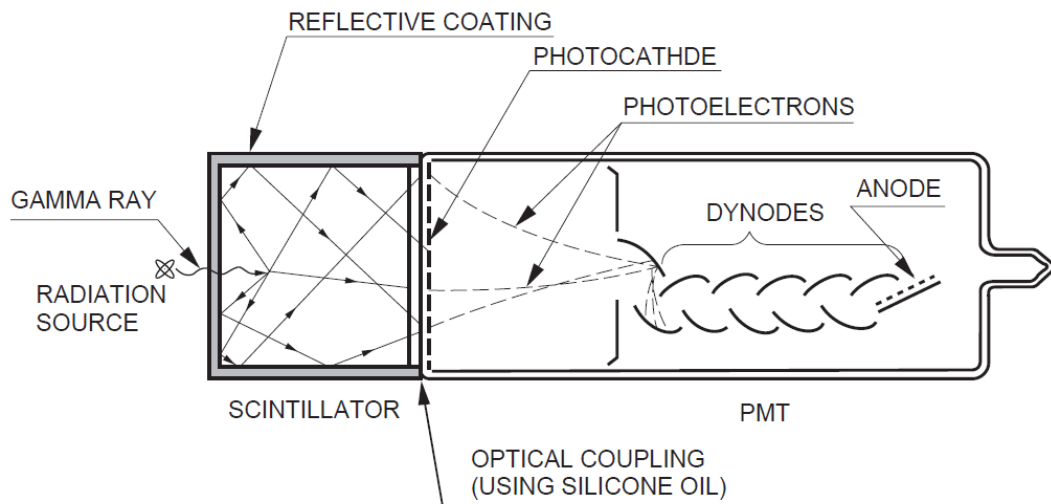


Figure 10. Gamma ray detection using a NaI(Tl) scintillator and a photomultiplier tube [45], courtesy of Hamamatsu Photonics K.K.

A novel detection system using neutron/gamma pulse shape discrimination, for use  
in active interrogation environments

The tube has a vacuum enclosure that houses dynodes, which are electrodes set out in a chain formation between the photocathode and the anode as shown in Figure 10. An electrical signal that is emitted from the photocathode into the tube is amplified by the process of electron multiplication along the dynode chain. The electrons are accelerated toward the first dynode by an electric field which is applied across the whole tube. When the electron comes into contact with the electrode it deposits the kinetic energy it has gained, which results in re-emission of multiple secondary electrons. Again the alleviation of electrons from a dynode has the same constraints and losses as the photocathode. The overall multiplication factor for one dynode is given in equation 9 [45];

$$\delta = \frac{\text{number of secondary electrons emitted}}{\text{number of primary incident electron}} \quad \text{[Equation 9]}$$

typical PMTs have dynode chains in the region of 7-15 dynodes long, even with the losses this creates a huge gain in number of electrons. The overall gain for the PMT can be calculated using equation 10 [45];

$$\text{Gain} = \delta^N \quad \text{[Equation 10]}$$

where  $N$  is the number of multiplication stages within the dynode. This equation however assumes all the secondary electrons from one dynode reach the next dynode. This increase in the number of electrons and their energy, increases the amplitude of the electrical signal whilst still keeping the same pulse shape. The dynodes within the tube can be made up in several different structures and arrangements to suit requirements as shown in Figure 11.

A novel detection system using neutron/gamma pulse shape discrimination, for use in active interrogation environments

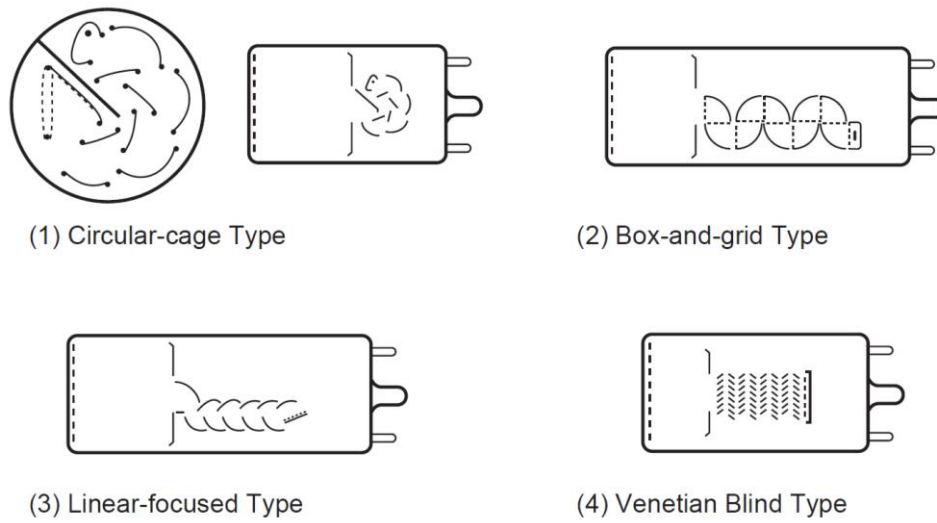


Figure 11. Four of the most common types of electron multipliers [45], courtesy of Hamamatsu Photonics K.K.

Each configuration of dynode structure exhibits different gain, time response, uniformity and secondary-electron collection efficiency. For example the circular-cage structure is compact and can be used in all side-on devices. Due to the small structure it has a fast time response. The linear-focussed structure also exhibits a fast time response, but has excellent pulse linearity as well as good time resolution. This is mostly used in head-on PMTs.

Part of the inspiration behind this research arose from the situation that PMTs in certain set ups and environments were becoming saturated with information [46]. A tube is saturated with events when the output signal is no longer proportional to the incoming light intensity, therefore it will be missing information until it undergoes its ‘dead time’. The dead time is the period it takes for a PMT to go from saturation to a state that allows for normal operation again. In high-flux environments the dead time of detectors has always been limiting to the speed at which information can be gained, meaning lots of prompt information is lost by the PMT being blind. One of the main

aims from this research was to try and extract more information from these high-flux periods.

### 2.6.1 MCP-PMT

Traditional PMTs have been around for a long time but developments have led to new types for example the micro-channel plate PMT (MCP-PMT). These devices use a 1 millimetre thick plate, as the base for the dynode structure, as shown in Figure 12. The size of this structure results in dramatically improved time resolution and assures high stable gain in high EM fields. These types of PMTs can possess multiple micro channel plates as required.

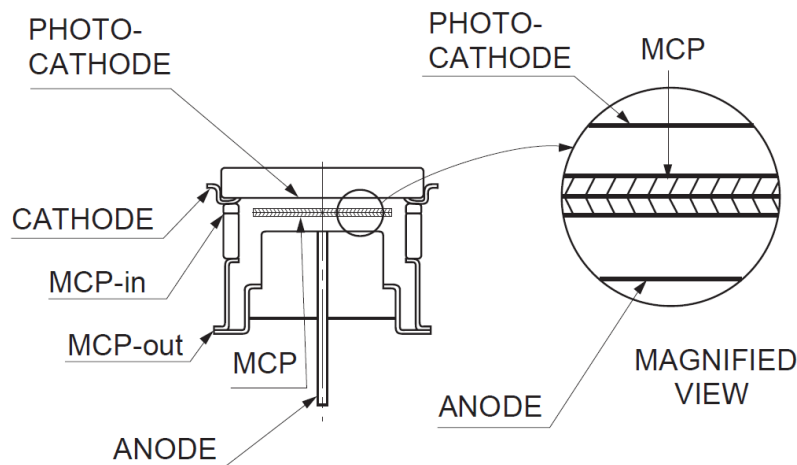


Figure 12. Cross section of a typical MCP-PMT [45], courtesy of Hamamatsu Photonics K.K.

With a MCP-PMT the photoelectrons emitted from the photocathode enter the channels of the MCP and bombard the inner wall which then creates the multiplication of the secondary electron emissions [45]. Each end of the walls is covered with a thin

## A novel detection system using neutron/gamma pulse shape discrimination, for use in active interrogation environments

metal film which acts as an electrode. This is repeated along the channel and is finally collected conventionally via the anode. The gain of an MCP-PMT is a function of the length to diameter ratio [45];

$$\mu = \exp(G \times \alpha) \quad \text{[Equation 11]}$$

where  $G$  is the secondary emission characteristics called the gain factor and  $\alpha$  is the ratio between the length and diameter [45];

$$\alpha = \frac{L}{d} \quad \text{[Equation 12]}$$

where  $L$  is the length of the channel and  $d$  is the diameter of the channel. The constraint with the MCP-PMT is the limiting small size in which they are available.

### 2.6.2 Triggered PMT

Specific to this work is the use of a triggered PMT with the objective to try and negate the saturation that occurs during the intense gamma flash associated with active interrogation with photons. This currently is a relatively unexplored area to the application of radiation detection, with only limited previous research carried out for different applications. Some of the first research carried out with the idea of gating a photomultiplier was for use in neutron time-of-flight (ToF) measurements using a LINAC [47]. This study introduced a new gating circuit to avoid saturation of the PMT among other reasons, which works by switching the PMT off during the gamma flash and having it reliably recovered within less than 1  $\mu$ s. Whilst this proved the possibility of the technique it was at a relatively slow speed for what is currently required.

## A novel detection system using neutron/gamma pulse shape discrimination, for use in active interrogation environments

More recently due to developments in electronics it has been possible to trigger a PMT on a much quicker timescale than the previous work described. One example, [48], takes advantage of the development in recent electronics to gate a MCP-PMT in the nanosecond range. This work is aimed at fusion diagnostics and ultra-fast optical pulses, which allows the use of MCP-PMTs as described above. This research presents the fastest PMTs recorded at the time with transitions as fast as 2ns. The work presented in this thesis would not be able to take advantage of MCP-PMTs due to the limited sizes they are available in as well as the proximity they need to be used being impractical for the application.

One successful study in the suppression of the gamma flash using a gated photomultiplier was investigated for nuclear astrophysics applications [49]. This study involved the use of a gated PMT coupled to a  $\text{LaBr}_3(\text{Ce})$  detector looking at measuring fast neutron capture reactions, due to the normal scattering of the gamma flash causing overloading of the detector and the circuitry used. The gating technique used in this study was to control the reverse bias between the cathode and the dynodes using a gate pulse, the device will turn the reverse bias off during the intense gamma flash.

The system in this study works by switching off the bias on the photocathode making the PMT dormant for a set time period. This requires knowledge of the starting time for the interrogating neutron pulses as well as knowledge of the time period required for the interrogating pulse to interact and the gamma flash to both appear and then die away in order to start the PMT back up at a suitable time to capture data. The gating technique used here successfully avoids the PMT becoming overloaded and manages to start obtaining radiation pulses and information a lot sooner than

previously possible [49]. The timing chart for the operation of the device described in this research is shown in Figure 13.

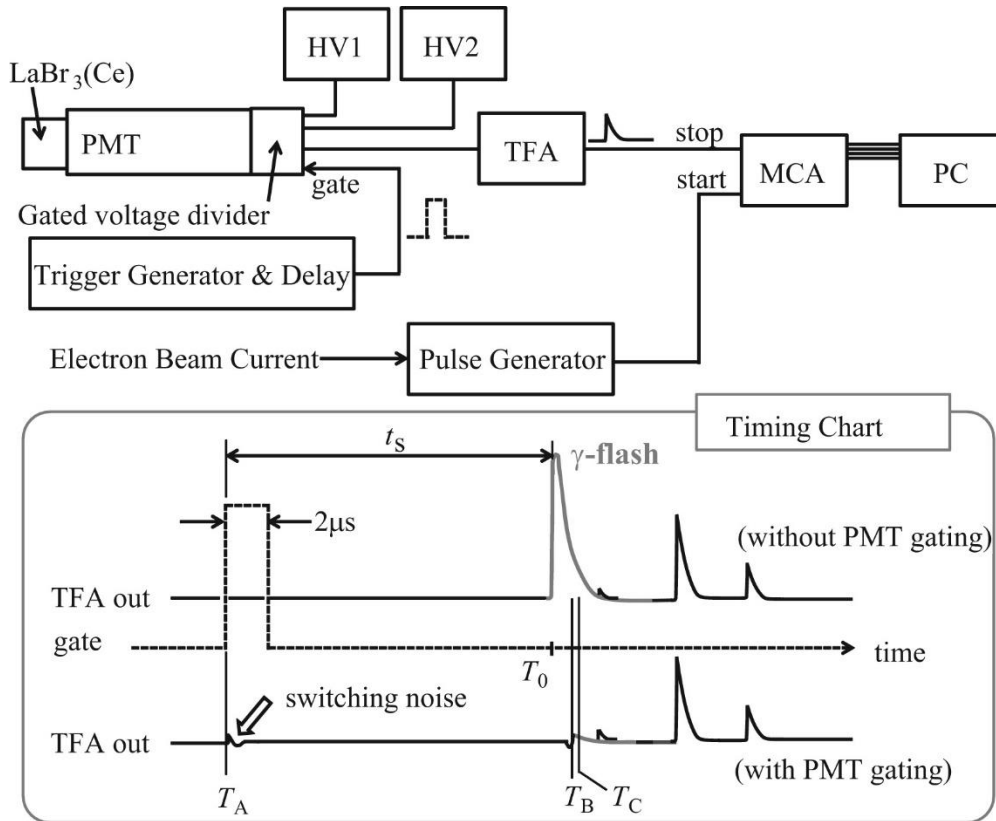


Figure 13. Block diagram of the electronics and a timing chart for the gated voltage divider between the gate pulse and the TFA output of the LaBr<sub>3</sub> (Ce) detector [49]. Reprinted from Nuclear Instruments and Methods in Physics Research Section A: Accelerators, Spectrometers, Detectors and Associated Equipment, 723. K.Y. Hara, et al., ‘γ-Flash suppression using a gated photomultiplier assembled with an LaBr<sub>3</sub>(Ce) detector to measure fast neutron capture reactions’, 121-127, 2013, with permission from Elsevier.

This thesis describes the use of a similar construct to [49] in terms of the gating of the PMT during the gamma flash period, but using organic scintillators, mainly the plastic EJ-299-33.

## 2.7 References

1. IAEA safety glossary, “Terminology used in nuclear safety and radiation protection”, 2007 Edition
2. G.F. Knoll, “Radiation Detection and Measurements” Third Edition ed2000, USA: John Wiley & Sons, Inc.
3. P. Rinard, “Neutron Interactions with Matter” *Passive Nondestructive Assay of Nuclear Materials* pp.357-377 (1991)
4. C.E. Moss, et al., “Portable active interrogation system” *Nucl Inst. Meth B* 241, pp. 793-797 (2005)
5. D. Dietrich, et al., “A kinematically beamed, low energy pulsed neutron source for active interrogation” *Nucl Inst. Meth B* 241, pp.826-830 (2005)
6. P.A. Hausladen et al., “An alpha particle detector for a portable neutron generator for the Nuclear Materials Identification System (NMIS)” *Nucl Inst. Meth B* 241, pp. 835-838 (2005)
7. M. Agelou, et al., “Detecting special nuclear materials inside cargo containers using photofission” Nuclear Science Symposium Conference Record, IEEE, NSS’09, Copyright © 2009, IEEE
8. D.R. Slaughter, et al., “The “nuclear car wash”: a scanner to detect illicit special nuclear material in cargo containers” *IEEE Sensors Journal* pp. 560-564 (2005), Copyright © 2005, IEEE
9. B.R. Grogan, et al. “Investigating of active interrogation techniques to detect special nuclear material in maritime environments: Boarded search of a cargo container”, *Nucl Inst. Meth B* 316, pp. 62-70 (2013)
10. T. Gozani, “Active non-destructive assay of nuclear materials” (1981)
11. D. Slaughter, et al., “Detection of special nuclear material in cargo containers using neutron interrogation” UCRL-ID-155315 (2003)
12. J.L. Dolan, et al., “Passive measurements of mixed-oxide fuels for nuclear nonproliferation” *Nucl Inst. Meth A* 703, pp. 102-108 (2013)
13. R.C. Runkle, L.E. Smith, A.J. Peurrung, “The photon haystack and emerging radiation detection technology” *Journal of Applied Physics Reviews* 106, (2009)

14. J.L. Jones, et al., “High-energy photon interrogation for non-proliferation applications”, *Nucl Inst. Meth B* 261, pp. 326-330 (2007)
15. D.R. Slaughter, et al., “The “nuclear car wash”: a scanner to detect illicit special nuclear material in cargo containers” *IEEE Sensors Journal* pp. 560-564 (2005)
16. E. Padovani, S.D. Clarke, S.A. Pozzi, “Feasibility of prompt correlated counting from photon interrogation of concealed nuclear materials” *Nucl Inst. Meth A* 583, pp. 412-420 (2007)
17. J.T. Mihalczo, “Radiation detection for active interrogation of HEU”, Nuclear Science and Technology Division, (2004)
18. B. Blackburn, et al., “Detection of special nuclear material by means of promptly emitted radiation following photonuclear stimulation” Nuclear Science Symposium Conference Record, IEEE, NSS’07
19. R.C. Runkle, D.L. Chichester, S.J. Thompson, “Rattling nucleons: new developments in active interrogation of special nuclear material” *Nucl Inst. Meth A* 663, pp. 75-95 (2012)
20. H. Franz, et al., “Delayed neutron spectroscopy with  $^3\text{He}$  spectrometers” *Nucl Inst. Meth* 144, pp. 253-261 (1977)
21. E.B. Norman, et al. “Signatures of special nuclear material: high-energy  $\gamma$  rays following fission”, *Nucl Inst. Meth A* 521, (2003)
22. F.D. Brooks, “A scintillation counter with neutron and  $\gamma$ -ray discriminators” *Nucl. Inst. Meth.* 4 pp. 151-163 (1959)
23. F.D. Brooks, “Development of organic scintillators” *Nucl Inst. Meth* 162, pp. 477-506 (1979)
24. L.M. Bollinger and G.E. Thomas, “Measurement of the time dependence of scintillation intensity by a delayed-coincidence method” *Rev. Sci. Instrum.* 32 (1961)
25. K.A.A. Gamage, M.J. Joyce, N.P. Hawkes, “A comparison of four different digital algorithms for pulse-shape discrimination in fast scintillators” *Nucl Inst. Meth A* 642, pp. 78-83 (2011)

26. J.M. Adams, G. White, "A versatile pulse shape discriminator for charged particle separation and its application to fast neutron time-of-flight spectroscopy" *Nucl Inst. Meth* 156, pp. 459-476 (1978)
27. J.H. Heltsley, et al., "Particle identification via pulse-shape discrimination with a charge-integrating ADC" *Nucl Inst. Meth A* 263, pp. 441-445 (1988)
28. Y. Kaschuck, B. Esposito "Neutron/gamma-ray digital pulse shape discrimination with organic scintillators" *Nucl Inst. Meth A* 551, pp. 420-428 (2005)
29. M. Flaska, S.A. Pozzi, "Identification of shielded neutron sources with the liquid scintillator BC-501A using a digital pulse shape discrimination method" *Nucl Inst. Meth A* 577, pp. 654-663 (2007)
30. S. Marrone, et al., "Pulse shape analysis of liquid scintillators for neutron studies" *Nucl Inst. Meth A* 490, pp. 299-307 (2002)
31. C. Guerrero, et al., "Analysis of the BC501A neutron detector signals using the true pulse shape" *Nucl Inst. Meth A* 597, pp. 212-218 (2008)
32. B. D'Mellow, et al., "Digital discrimination of neutrons and  $\gamma$ -rays in liquid scintillators using pulse gradient analysis" *Nucl Inst. Meth A* 578, pp. 191-197 (2007)
33. M.D. Aspinall, et al., "The empirical characterization of organic liquid scintillation detectors by the normalized average of digitized pulse shapes" *Nucl Inst. Meth A* 578, pp. 261-266 (2007)
34. M.D. Aspinall, et al., "Verification of the digital discrimination of neutrons and gamma rays using pulse gradient analysis by digital measurement of time of flight" *Nucl Inst. Meth A* 583, pp. 432-438 (2007)
35. F.D. Brooks, "Liquid Scintillation Counting", *Nuclear Physics* 284 pp. 268 (1958)
36. G.H.V. Bertrand, et al., "Pulse shape discrimination between (fast or thermal) neutrons and gamma rays with plastic scintillators: State of the art", *Nucl Inst. Meth A* 776, pp. 114-128 (2015)
37. N. Zaitseva, et al., "Plastic scintillators with efficient neutron/gamma pulse shape discrimination" *Nucl Inst. Meth A* 668, pp. 88-93, (2012)

38. S.A. Pozzi, M.M. Bourne, S.D. Clarke, "Pulse shape discrimination in the plastic scintillator EJ-399-33", *Nucl Inst. Meth A* 723, pp. 19-23, (2013)
39. S. Nyibule, et al., "Radioluminescent characteristics of the EJ 299-33 plastic scintillator", *Nucl Inst. Meth A* 728, pp. 36-39, (2013)
40. D. Cester, et al., "Experimental tests of the new plastic scintillator with pulse shape discrimination capabilities EJ-299-33", *Nucl Inst, Meth A* 735, pp. 202-206, (2014)
41. C.C. Lawrence, et al., "Neutron response characterization for an EJ299-33 plastic scintillation detector", *Nucl Instr. Meth A* 759, pp. 16-22, (2014)
42. R.S. Woolf, et al., "Comparing the response of the PSD-capable plastic scintillator to standard liquid scintillator", *Nucl Inst. Meth A* 784, pp. 80-87, (2015)
43. Eljen Technologies, Accessed 29/06/2016  
<http://www.eljentechnology.com/index.php/products/plastic-scintillators/ej-299-33a-ej-299-34>
44. Eljen Technologies, Accessed 29/06/2016  
<http://www.eljentechnology.com/index.php/products/liquid-scintillators/ej-301-ej-309>
45. Hamamatsu "Photomultiplier Tubes" Third Edition (2007)
46. B.W. Blackburn, et al., "Utilization of actively-induced, prompt radiation emission for non-proliferation applications" *Conference on Accelerator Applications in Research and Industry*, (2006)
47. M.R. Sené, "A simple gating system for the Hamamatsu R1250 photomultiplier", *Nucl Inst. Meth A* 278, pp. 503-506 (1989)
48. J. Milnes, et al., "Ultra-high speed photomultiplier tubes with nanosecond gating for fusion diagnostics" *The review of scientific instruments* 83 (2012)
49. K.Y. Hara, et al., "γ-Flash suppression using a gated photomultiplier assembled with an LaBr<sub>3</sub>(Ce) detector to measure fast neutron capture reactions" *Nucl Inst. Meth A* 723, pp. 121-127, (2013)

## 3 Experimental Methods

The following chapter explains the methods behind all the experiments carried out and the different setups that have been implemented. The first sections describe the radioactive sources that have been used and the principles of radiation safety. Following this, the instruments and their operation that have been used in this research will be described, with specifications for these, before moving onto each individual experiment and set-up.

### 3.1 Sources

The majority of experiments carried out for this research were based in the Engineering department at Lancaster University, largely due to the variety of available sources and ease of access. The main source used for the majority of these experiments was a water based  $^{252}\text{Cf}$  source which undergoes spontaneous fission emitting neutrons in the process.  $^{252}\text{Cf}$  has an overall half-life of 2.645 years, with a spontaneous fission half-life of 85.5 years. The source has a neutron emission rate of  $2.3 \times 10^6$  neutrons per microgram per second, with an average neutron energy of 2.1 MeV and a most probable energy of 0.7 MeV [1]. The source in February 2014 had an activity of 74.8 MBq and sits in the center of a double hull  $1 \text{ m}^3$  tank filled with water. This tank is then shielded on all sides by 33 mm of steel. The source is located at the center of the tank during non-exposure. For exposure it can be brought forward to one face of the tank to reduce the effect of water moderation. When in the exposed position, the shielding & moderation effect on the source to the exposed face is significantly

A novel detection system using neutron/gamma pulse shape discrimination, for use in active interrogation environments

reduced having only the 33mm of steel plates and the double hull tank giving any effect. On the exposed face of the source there is 1m of space before the brick outer wall and the floor is concrete. These materials will both have an effect on the counts monitored, for example adding back-scattered events. A picture of the steel enclosure is shown in Figure 14.



Figure 14. Steel enclosed tank housing  $^{252}\text{Cf}$ .

Other sources at the university that were utilised in this project include 3 different sealed  $^{137}\text{Cs}$  gamma sources each  $\sim 395$  kBq. These sources were used for calibration purposes for detectors due to the known photopeak that is produced at 662 keV when  $^{137}\text{Cs}$  decays to  $^{137}\text{Ba}$ . The sources were also used to test that prototype circuits were operating correctly due to the lower radiation dose and easier accessibility to expose a source in situ.

Outside of the department the main experiments carried out took place at Sheffield University and utilised both a bare  $^{252}\text{Cf}$  and a bare Am-Be source. These

## A novel detection system using neutron/gamma pulse shape discrimination, for use in active interrogation environments

sources were used for direct comparisons between the two sources in the same environment without the moderation caused by the water-based  $^{252}\text{Cf}$ , as is the case at Lancaster. The bare Am-Be source had an activity of 37 GBq, emitting between  $2 \times 10^6$  and  $2.4 \times 10^6$  neutrons per second, and the  $^{252}\text{Cf}$  source had an activity of 4.38 MBq emitting  $5.3 \times 10^5$  neutrons per second. The Am-Be source however emits higher energy neutrons than the  $^{252}\text{Cf}$  source with an average neutron energy of 4 MeV going up to a maximum of 11 MeV [2].

### 3.2 Working with radiation

Working with radiation requires adherence to safety procedures and regulations [3]. Due to radiation having ionizing effects this can affect biological matter including body tissue, breaking molecular bonds that can control different functions within the body. Most of the damage caused by radiation can be repaired by the body's own natural mechanisms but this process can also cause abnormalities in the repairing process, this leads to the rapid multiplication of these faulty repairs. Naturally the body will try to attack these through its own immune system but they can grow into cancers. Different legislator dose rates are in place with respect to a person's involvement with radiation, all of which are well below the limit at which the exposure to biological tissue is unrepairable. Any work carried out with radiation must be done so with the principles of radiation safety in mind and kept As Low As Reasonable Practicable (ALARP).

## A novel detection system using neutron/gamma pulse shape discrimination, for use in active interrogation environments

With regard to working with radiation there should always be a justification to carry out any work which should outline a benefit from carrying out the work that outweighs the associated risk with the exposure of the radiation. Non-radioactive alternatives should be considered wherever possible. In all cases of radiation work, procedures should be in place to protect those using it, limit exposure and keep it ALARP. Regulatory authorities state that the risk should be kept as low as reasonable achievable (ALARA) in the UK. The ALARA code of practice has been produced to state enforceable legal limits for individuals. The ALARP principle is used to make sure that every practical effort should be made to minimize both risk and exposure as there is no limit known at below which potential harm will not occur

### 3.2.1 Radiation Protection

There are four main considerations to take into account to keep radiation exposure ALARP:

1. Exposure time - The accumulated dose to a worker is dependent on the exposure time to the individual. This is always considered prior to experiments being carried out, to ensure the exposure is limited to as short a period as possible. This is achieved by planning experiments and setups ahead of time, and having everything in place before a radiation source is exposed or introduced.
2. Source activity - The activity of any source to be used should be the smallest possible to achieve the desired results. The absorbed dose is linearly dependent on both the exposure time and the activity of the source.

A novel detection system using neutron/gamma pulse shape discrimination, for use in active interrogation environments

3. Shielding - All sources have materials that can be used to shield them during storage and use, depending on the radiation type that is emitted. For example the gamma sources held within the department are stored in a lead-lined safe, whereas the  $^{252}\text{Cf}$  source is held within the centre of a metre-cubed water tank that in addition is shielded by 33 mm of steel on every side. Shielding should also be taken into account whilst using sources, to ensure exposure is ALARP. For example a source and detector setup can be isolated from the controlling equipment, computer, meaning that the user only has exposure during the placement of the source and is then protected by the shielding in place.

4. Distance from the source - When all other factors have been considered, keeping maximum distance from the source can often be the easiest way to reduce exposure to radiation. As radiation from a point source is released isotropically in all directions, (not taking into account scattering effects from the surroundings), then the intensity is inversely proportional to the square of the distance from the source. For non-point sources, they can often be perceived as a point source at very large distances.

As well as keeping exposure ALARA there are also regulations limiting the effective whole body dose a person can receive in a year. These are outlined from the Ionising Radiation Regulations 1999 (IRR99), and state that the legal limit is 20 millisieverts a year for an employee over 18, 6 millisieverts a year for a trainee and 1 millisievert a year for any other person or member of the public [3].

### 3.2.2 Dose definitions

#### Absorbed dose

Absorbed dose,  $D$ , is a measurement of the concentration of energy that is imparted per unit mass and is given by the following equation;

$$D = \frac{d\varepsilon}{dm} \quad \text{[Equation 13]}$$

where  $\varepsilon$  is the mean energy that has been absorbed by the material with a mass of  $m$ . Absorbed dose by definition does not take account of the type of radiation that is imparting the energy or the material that absorbs it. This means that the absorbed dose on its own is not an accurate indicator of the relative risk because it is known that different radiations impart energy differently to one another and different materials absorb it differently.

#### Equivalent dose

Equivalent dose takes into account the radiation type and addresses the influence that the specific radiation has upon the absorbed dose. The equivalent dose can be calculated from the absorbed dose using the following equation;

$$H = W_R D \quad \text{[Equation 14]}$$

where  $W_R$  is the radiation weighting factor, and  $D$  is the absorbed dose by radiation type  $R$ . Example weighting factors for different types of radiation are shown in Table II [4].

Table II. Weighting factors for different types and energies of radiation [4].

Radiation Type and Energy Range	Radiation Weighting Factor, $W_R$
X and $\gamma$ rays	1
Electrons, positrons and muons	1
Neutrons:	
<10 KeV	5
10 KeV to 100 KeV	10
>100 KeV to 2 MeV	20
>2 MeV to 20 MeV	10
>20MeV	5
Protons >2MeV	2-5
$\alpha$ particles, fissions fragments, heavy nuclei	20

Equation 14 is used to work out the equivalent dose by one type of radiation in turn. If more radiation types are involved these would be summed. The equivalent dose does not take account of the specific tissue type exposed.

#### Effective dose

As different body tissues have different sensitivities to radiation the effective dose takes these into account. This dose quantity takes into account both the type of radiation and the tissue/organ at risk of being exposed. The effective dose can be calculated by taking the equivalent dose and adding in a tissue weighting factor  $W_T$  using the following equation

$$E = W_T H \quad \text{[Equation 15]}$$

where  $H$  is the equivalent dose being imparted on the particular type of tissue. From the effective dose the *total dose* can be calculated by summing all the effective doses

for different tissues. Example tissue weighting factors for different organs are shown in Table III [5].

Table III. Weighting factors for different organs [5].

Organ	Tissue weighting factor $\tau$
Bone-marrow (red), colon, lung, stomach, breast, remainder tissues	0.12
Gonads	0.08
Bladder, oesophagus, liver, thyroid	0.04
Bone surface, brain, salivary glands, skin	0.01

### 3.2.3 Dosimetry

To ensure that radiation regulations are being followed and that procedures are sufficient, the law requires that exposure to radiation is monitored where it is considered possible. Measures include the use of personal dosimeter badges, which are required to be processed regularly to inform a record of the dose received by an individual. From the values obtained practises can be further intensified and classified workers can be withdrawn from carrying out radiation work all together if their recorded individual exposure were a cause for concern. Methods of dosimetry monitoring related to this research have included thermoluminescent dosimeters (TLD's), film badges, Mini Instruments dosimeter and survey meters.

## A novel detection system using neutron/gamma pulse shape discrimination, for use in active interrogation environments

### Thermoluminescent dosimeters

TLDs consist of inorganic crystals which, when hit by ionizing radiation, liberate electrons from atoms and subsequently move them to other parts of the material. This leaves voids of positive charge from where the electron was freed. When the TL material is heated, the electrons and the voids realign and release the stored up energy in the form of visible light. The intensity of this emitted light is dependent upon the incident radiation exposure, making it a useful device for monitoring.

TLDs comprise of a foil sheet to filter the radiation in addition to the TL sheet which is locked within a plastic casing. After the set time period for the dosimeters use the TLD is sent back for reading. The light emissions are used to calculate the radiation exposure to the person who has been using the TLD. The dosimetry period is usually between 1 and 3 months, after which time a new dosimeter will be issued while the previous one is used to take the dose reading. During this research gamma sensitive badges have been used.

### Film badge

Film badges are comprised of two parts the first being a film with an emulsion coating with the second being a housing for the film. A film badge can be constructed of a single film with multiple layers of emulsion or multiple films with different emulsion sensitivities. The holder is made of different materials depending on the radiation type the badge is to be sensitive towards. To calculate the dose the badge consists of multiple radiation-filtering materials to attenuate the radiation at different sections of the film. The level of radiation is a comparison of the darkening of the film at different

## A novel detection system using neutron/gamma pulse shape discrimination, for use in active interrogation environments

rates behind the filter materials. During this research neutron sensitive film badges have been used.

### Mini Instruments dosimeter

The Mini Instruments monitor, a Geiger counter, has been used as laboratory safety equipment. In the sealed source laboratory the worktops and areas of experiments are scanned both before and after use to make sure no contamination remains. The immediate audio feedback when radiation is present makes it ideal for quickly scanning areas as required for this purpose.

### Survey Meters

Survey meters are portable devices that are used to show immediate feedback on the spatial intensity of neutrons. A survey meter consists of a detector and a readout unit. There are several different types usually comprising a moderated gas-filled detector. Survey meters are calibrated devices with the capabilities of either audio or visual feedback or both. This research has utilised a neutron survey meter NMS017 from John Caunt Scientific Ltd. [6] which features a Bonner sphere (a polyethylene sphere) which is used as the moderator to ensure as linear a response as possible. This can be used as a dose rate meter, for dose measurements and neutron counting. During the experiments carried out a survey meter was left running every time the  $^{252}\text{Cf}$  source was exposed to give a constant readout of the dose level present and to confirm that the source had fully returned to its stored position.

### 3.3 Instruments

#### 3.3.1 Detectors

This research was to utilise the new developments being made in organic scintillators, namely the low-hazard liquids available and the solid state plastics with discrimination properties. As described in the previous chapter in section 2.5.2.2, research has been carried out using three different types of scintillator detectors, one of which has two different cell shapes. Photographs of all 4 are given in Figure 15. The main scintillator for investigation is the low-hazard plastic EJ-299-33 [7, 8] (Eljen Technology, Sweetwater, TX). The other two scintillator types are EJ-301 and EJ-309, both of these being liquids. EJ-309 is a more recently developed low hazard version of the EJ-301 due to having a much higher flash point and reduced toxicity. All of these detectors are optically coupled to a PMT for signal gain purposes which outputs charge signal pulses for each interaction of radiation.

A novel detection system using neutron/gamma pulse shape discrimination, for use in active interrogation environments



Figure 15. All four detectors, upper two containing EJ-309 the upper left being of type V94A94/3MEJ309E1XNEG, and the upper right being of type 127A76/3M-EJ309X-NEG, bottom left containing EJ-301 of type 19A15/0.75-E1-LS-X-N and bottom right containing EJ-299-33 being of type 51A51/2ME1EJ299XN, all detectors supplied by Scionix, Netherlands.

The EJ-309 detectors consist of two different cell shapes, one of these detectors being cylindrical with a diameter of 127 mm and depth of 76 mm. The other detector is cubic with sides of 94 mm, also including a light guide within the cell containing the scintillator.

The EJ-299 plastic detector used also consists of an integrated gating board attached to the end of the PMT, the location of which can be seen in the schematic diagram shown in Figure 16. The gated system utilised in this research is based upon the combination of a PMT of type 9214 [9] with a GB1A/DC gating unit [10] (both ET Enterprises Ltd., UK). When active the gating board provides a reverse bias with respect to the focusing electrode to the photocathode [10]. This reverse bias prevents any photoelectrons from entering the dynode section of the PMT, making the PMT inactive and holding the system in a quiescent state. This reverse bias is provided and

## A novel detection system using neutron/gamma pulse shape discrimination, for use in active interrogation environments

held whilst the gating board is receiving an external input signal. A similar device has previously been described and used in gamma ray experiments with an inorganic  $\text{LaBr}_3(\text{Ce})$  detector [11], but at the time of writing, this is not believed to have been previously implemented with organic scintillators, or in mixed field tests as is presented in this research. As the use of a gating board has never been implemented with any organic scintillator before, the performance of the plastic would need to be compared to the system relatively without the gating unit active. This is to verify that when it is in operation, it does not have any negative effect on the performance quality of the scintillator or PMT other than desired. This has not gone as far as to compare a standard EJ-299-33 plastic scintillator without a gating unit with the system used in these experiments.

The convention of operation is that the GB1A/DC unit renders the PMT inactive when a negative bias signal is fed to it. The system as assembled is a type VS1173-30 unit (Scionix, Netherlands) and is shown in Figure 16 [12]. This system is the first use of the Scionix gated-PMT detector system with an organic scintillator and the detector specifications were defined in this research for investigation and use in active interrogation systems.

A novel detection system using neutron/gamma pulse shape discrimination, for use in active interrogation environments

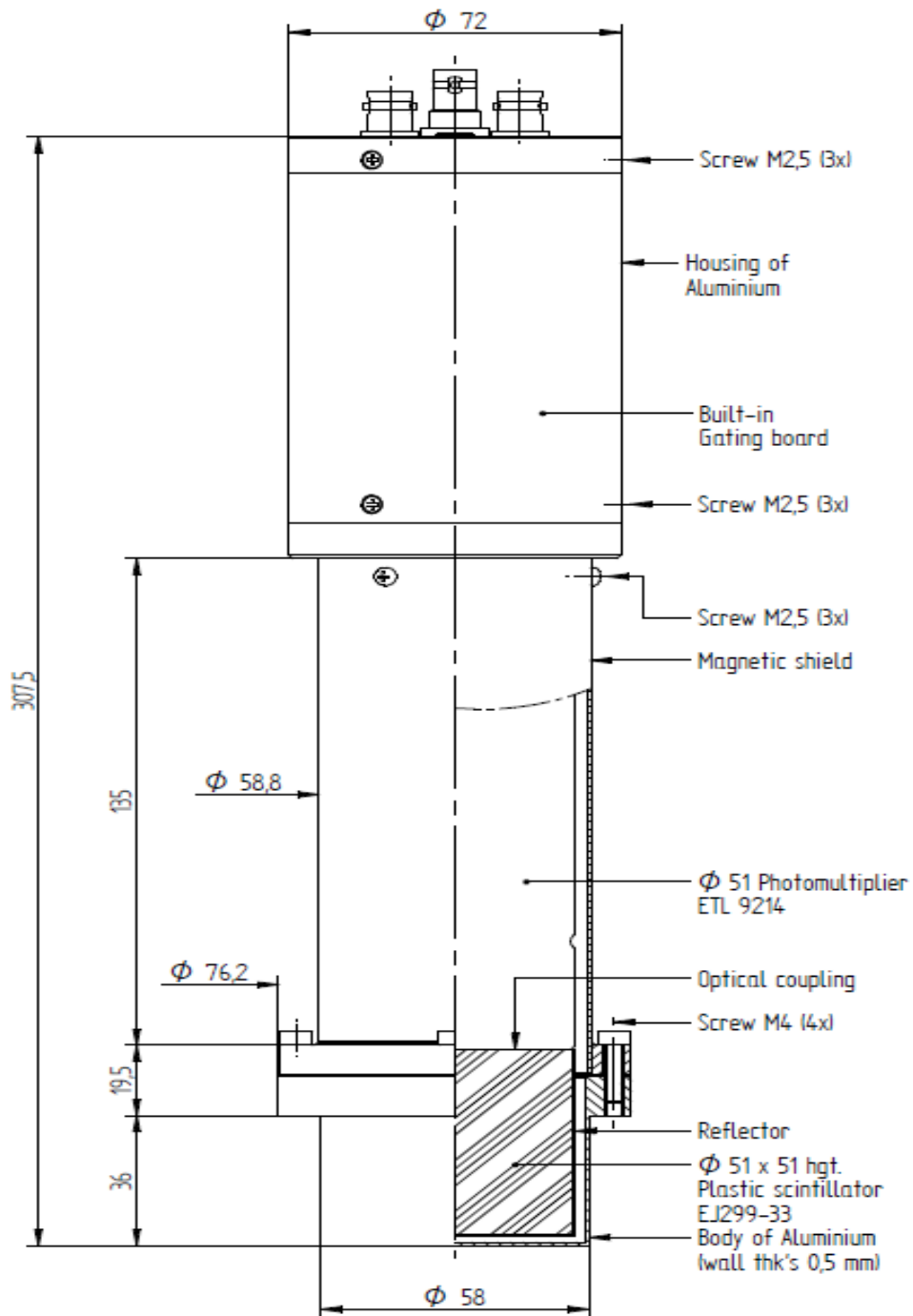


Figure 16. A schematic of the VS1173-30 detector unit, containing the plastic scintillator EJ299-33, used in this research shown in a vertical orientation with the scintillator cell at the bottom of the diagram [10].

### 3.3.2 Data Acquisition (DAQ)

There are several different data acquisition (DAQ) units that are commercially available and used within the nuclear instrumentation research discipline. A Hybrid Instruments mixed field analyser (MFA) [13] was chosen for use in this research, due to the real time aspect of the device which is unique in the field. The device implements the pulse gradient analysis (PGA) algorithm to perform pulse shape discrimination [14] and produces real time scatter or pulse height distribution (PHD) plots whilst in operation [15]. These are described further in the previous chapter in section 2.5.2.1.3. This real-time feedback, allows for adjustments to be made easily to parameter setups. In this research both a single and 4-channel analyser were used, with the single channel being the main system employed due to the fact that only one detector is required at a time. The premise of this research however will eventually be expanded into a full imaging system, requiring multiple detectors in varying positions and thus the use of several sets of 4-channel analysers [16]. As well as the real time visual feedback provided by the graphical user interface (GUI) system with the MFA, there is also a higher throughput option using the transistor-transistor logic (TTL) lines connected directly to a counter or oscilloscope. In order to use the TTL lines the system needs to have previously been set up and the discrimination thresholds placed prior to counting.

Every detector required initial calibration before each experiment and this was carried out using the known pulse height spectrum produced by a  $^{137}\text{Cs}$  source that exhibits a characteristic emission due to the 662 keV gamma ray transition line. An example MCA plot produced from the DAQ is shown in Figure 17. This particular plot was acquired with the liquid scintillator EJ-309, with a cylindrical scintillator cell,

exposed to a 400 kBq  $^{137}\text{Cs}$  gamma source for a period of 2 minutes with the source placed on the front face of the detector.

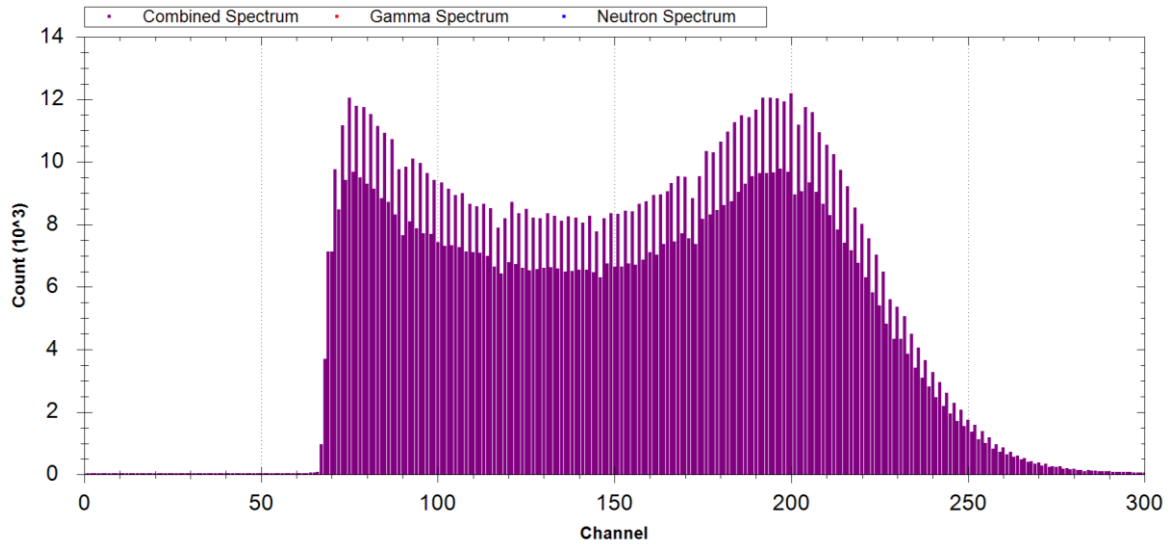


Figure 17. MCA plot for cylindrical EJ-309 exposed to a  $^{137}\text{Cs}$  sources for 2 minutes.

The spectrum for  $^{137}\text{Cs}$  as shown should have a clear Compton edge associated with the 662 keV gamma ray transition as shown in Figure 17. The lack of a photo peak that would normally be associated with gamma spectroscopy of a  $^{137}\text{Cs}$  source is due to the lower atomic number of the absorber (the liquid or plastic scintillators) making the cross-section for photoelectric reaction almost zero [17]. For consistency throughout tests this was always positioned at the 200 channel mark allowing simple fine tuning of the high voltage supply to the detectors in order for gain matching. In all tests every adjustment in high voltage needs a short period of time to stabilise before a new run is started. Also, as information is delivered in packets to the GUI, there may be packets left from the previous run depending on when the system was stopped. Therefore, once new settings are selected, the system is run for a short time period to allow the left over packet of information to be processed through the system and the

new setup to be delivering information before any experiments are started. After calibration of the Compton edges the MFA software is then switched into PSD mode. This is where the system produces scatter plots of the first vs second integrals associated with the peaks versus the discrimination amplitudes as explained later in the analysis section. An example scatter plot for the mixed radiation field produced by the  $^{252}\text{Cf}$  source is shown in Figure 18.

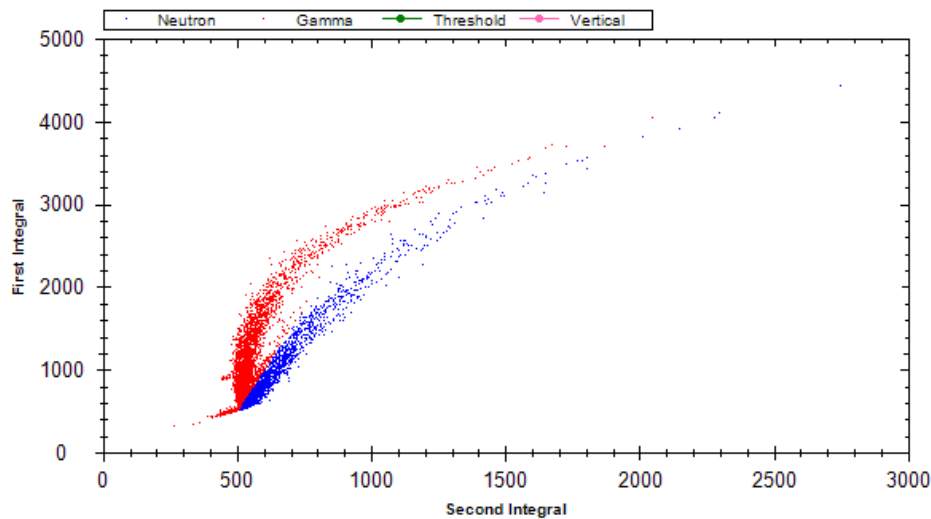


Figure 18. Scatter plot from EJ-301 liquid scintillator exposed to  $^{252}\text{Cf}$ . Two distinct regions are evident, the red plume (upper) associated with gamma rays and the blue plume (lower) associated with neutrons.

The time period over which the first and second integrals can be taken can be adjusted manually, as can the placement of the second integral with respect to the first. The settings are manually adjusted to optimise the separation of the two plumes and when applied the new settings are uploaded. Next time the system is set to run it will use these new values. The software identifies the two radiation types by a manually placed threshold line that consists of 2 straight lines between 3 points which are placed between the two plumes. Applying these thresholds allows for a quick real-time response from the system in the GUI. Offline techniques can be implemented to

completely satisfy the correct positioning of the thresholds for further analysis. Once satisfactory thresholds have been set online, the system is then set to record data for either a required count rate or time period as specified for each experiment.

### 3.4 Pulse Height Distribution

For post-processing applications, the Hybrid Instruments MFA obtains data sets wherein the information is captured as three numbers per channel. The first of these numbers is the radiation classification that has been assigned to it by the digitiser itself and takes a value of; either 1 or 2 for a gamma ray or a neutron respectively. This radiation classification is assigned in accordance with the user-defined thresholds. The second number is the peak amplitude, or first integral, of the pulse and the final number is the discrimination amplitude, or second integral the latter is a user-defined point after the peak amplitude and set up through the GUI. The peak and discrimination amplitude are used to work out the gradient of the decay. A scatter plot can then be created by plotting the first and second integral, which is the same as is populated in the GUI readout from the digitiser during operation.

When PSD techniques are implemented, these scatter plots are analysed using a standard Pulse Height Distribution (PHD) plot. The PHD is a histogram used to show the number of pulses at different pulse amplitudes of the scatter plots. It displays the peak amplitude information by showing the ratio of discrimination/peak amplitude against number of pulses per pulse height, the horizontal axis displays this in increments or 'bins'. If a PHD plot produced for a mixed field has good pulse shape

discrimination properties, it will present two peaks: one peak representing the gamma ray plume and one peak representing the neutron plume.

For PGA techniques an intermediate step is required to produce a PHD plot. This intermediate step involves removing the baseline from the scatter plots and normalising, thus linearising the plumes as shown below in Figure 19.

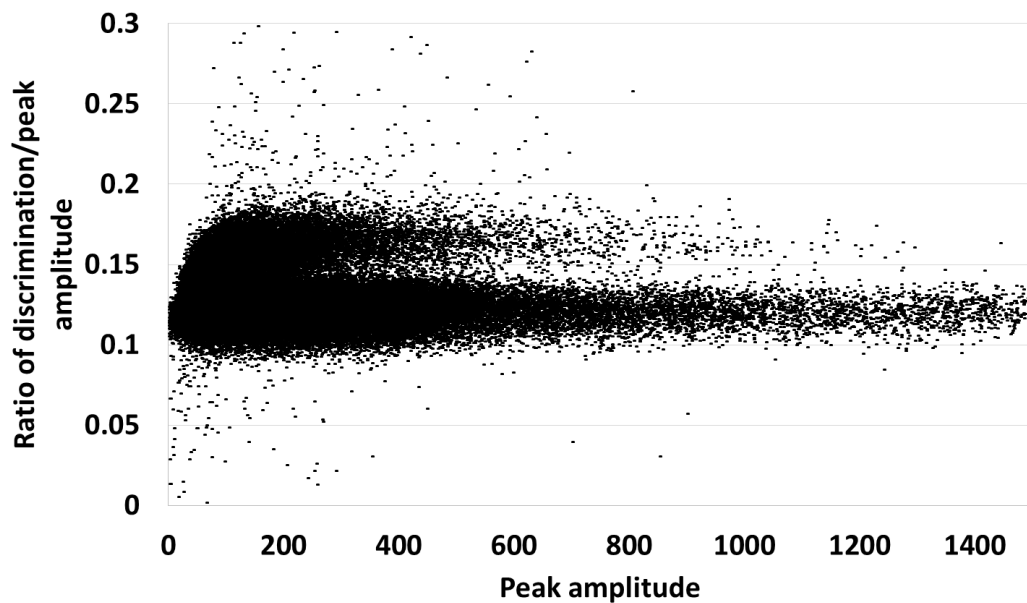


Figure 19. Normalised plot showing the cubic EJ-309 at 0° exposed to  $^{252}\text{Cf}$ .

This allows a PHD plot to be produced by taking different ‘bins’ or individual sample ranges along the Y axis, and producing a number of counts which lies within that region. The more ‘bins’ that are taken, or similarly, the smaller the sample ranges, the more precise the PHD plot will be in following the outline of the plumes although the number of counts in each range still needs to be statistically significant. An example PHD histogram is shown in Figure 20.

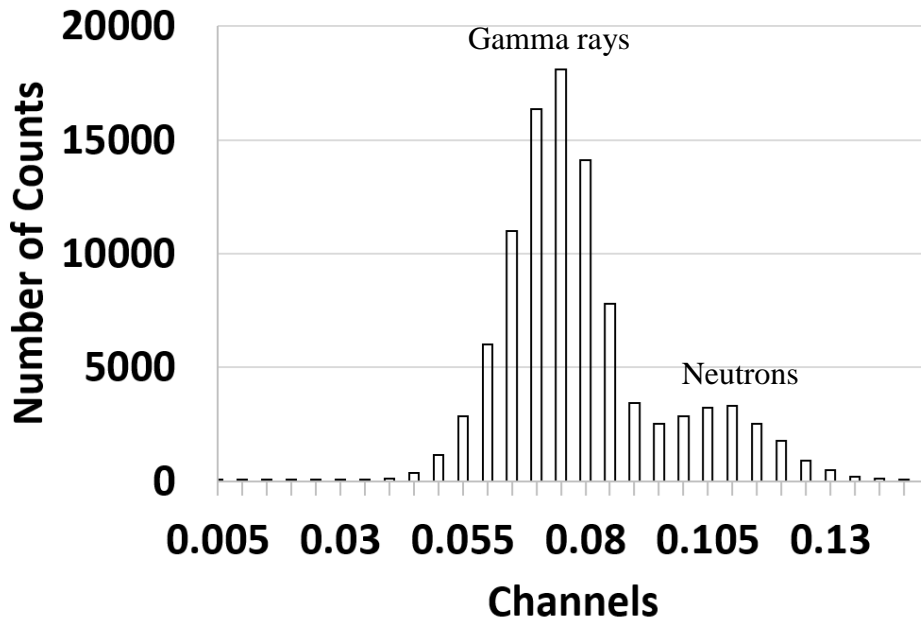


Figure 20. Example PHD histogram from Figure 19.

To give an exact value as to the quality of the discrimination between these two plumes the histogram can be fitting with a double Gaussian distribution to it. The double Gaussian takes the form of the equation below:

$$f(x) = Ae^{\left[-\frac{(x-\mu_\gamma)^2}{2\sigma_\gamma^2}\right]} + Be^{\left[-\frac{(x-\mu_n)^2}{2\sigma_n^2}\right]} \quad \text{[Equation 16]}$$

where  $\mu_\gamma$  and  $\mu_n$  are the means for each distribution, and  $\sigma_\gamma$  and  $\sigma_n$  are the standard deviations for each distribution, with  $A$  and  $B$  the constants for each radiation type.

Once a fit is produced, an assessment for how well it fits the data is desirable, which is done using the reduced chi-squared value [18]. The reduced chi-squared test is used to give a value that compares a fit to a set of described statistics, thus showing how well they match giving confidence in the fit. The chi-squared value is worked out by taking each point on the fitted plot and comparing it to the actual data points from the histogram. The reduced chi-squared works by taking the normal chi-squared value

and dividing by the number of data points minus the number of parameters used in the fit. This value ideally should be as close to 1 as possible; if the value is below 1 then the errors are too large. Once confidence is obtained in the fit's ability to fit with the data set then the Figure-of-Merit (FoM) can be calculated.

### 3.4.1 Figure-of-Merit

The Figure-of-Merit (FoM) is used to give a value that indicates the degree of separation of an event into either the neutron or gamma plume. The FoM is calculated below.

$$FoM = \frac{S}{FWHM_n + FWHM_\gamma} \quad \text{[Equation 17]}$$

where  $S$  is the separation between the two peaks of the histogram and,  $FWHM_n$  and  $FWHM_\gamma$  are the full-width-at-half-maximum of the neutron and gamma ray peaks respectively [19]. This value is a standard measure of how well the detector and analysis cope with distinguishing between two different radiation types. A figure close to 1 is accepted as distinguishing nearly all the events into one category or another, whilst a figure close to 0 will compound to only one distinct plume and it would be impossible to distinguish the different radiation types. The liquid scintillator EJ-301 is the benchmark for PSD, (formally NE213 & BC501) and therefore has been shown to exhibit a much higher FoM, sometimes as high as 2. FoM values higher than this can be observed when thresholds are added to data sets in order to look at specific energy ranges.

### 3.9 References

1. R.C. Martin, J.B. Knauer, P.A. Balo, "Production, Distribution, and Applications of Californium-252 Neutron Sources." (1999)
2. E.A. Lorch, "Neutron spectra of  $^{241}\text{Am-B}$ ,  $^{241}\text{Am-Be}$ ,  $^{241}\text{Am-F}$ ,  $^{242}\text{Cm-Be}$ ,  $^{238}\text{Pu-13C}$  and  $^{252}\text{Cf}$  isotopic neutron sources." *Int. J. Applied Radiation and Isotopes* 24 pp. 585-591 (1973)
3. The Ionising Radiations Regulations (1999)
4. International Commission on Radiation Units & Measurements "Fundamental Quantities and Units for Ionizing Radiation (Report 60)" (1991)
5. International Commission on Radiological Protection "The 2007 Recommendations of the International Commission on Radiological Protection", ICRP Publication 103 (2007)
6. NMS John Caunt Scientific, Accessed 29/06/2016  
(<http://johncaunt.com/products/neutron-monitor/>)
7. N Zaitseva, et al., "Plastic scintillators with efficient neutron/gamma pulse shape discrimination" *Nucl. Instr. and Meth. A* 668 pp. 88-93 (2012).
8. S.A. Pozzi, M. M. Bourne and S. D. Clarke, "Pulse shape discrimination in the plastic scintillator EJ-299-33" *Nucl. Instr. and Meth. A* 723 pp. 19-23 (2013).
9. ET Enterprises 9214 PMT Datasheet, Accessed 29/06/2016  
(<http://my.et-enterprises.com/pdf/9214B.pdf>)
10. ET Enterprises GB1B Datasheet, Accessed 29/06/2016  
(<http://my.et-enterprises.com/pdf/gating%20boards.pdf>)
11. K.Y. Hara, et al., " $\gamma$ -Flash suppression using a gated photomultiplier assembled with an  $\text{LaBr}_3(\text{Ce})$  detector to measure fast neutron capture reactions" *Nucl. Instr. and Meth. A* 723 pp. 121-127 (2013).
12. Scionix VS-1171-30 Datasheet, personal communications with Paul Schotanus at Scionix
13. Hybrid Instruments 4 Channel MFA Datasheet, Accessed 29/06/2016  
(<http://hybridinstruments.com/products/mfax4.3.html>)

14. M.J. Joyce, et al., "The design, build and test of a digital analyzer for mixed radiation fields", *IEEE Trans. Nuc. Sci.* 57 (5 pt. 2) 5603496 pp. 2625-2630 (2010).
15. M.J. Joyce, et al., "Real-time, pulse-shape discrimination in non-hazardous fast liquid scintillators: prospects for safety and security", *IEEE Trans. Nuc. Sci.* 59 (4 pt. 2) 6133314 pp. 1245-1251 (2012).
16. M.J. Joyce, et al., "A 16-channel real-time digital processor for pulse-shape discrimination in multiplicity assay", *IEEE Trans. Nuc. Sci.* 61 (4) pp. 2222-2227 (2014).
17. G. Choppin, J-O. Liljenzin, J. Rydberg & C. Ekberg, "Radiochemistry and Nuclear Chemistry" Fourth Edition, 2013.
18. P.R. Bevington & D.K. Robinson "Data reduction and error analysis for the physical sciences", Second edition, McGraw-Hill, 328
19. R.A. Winyard, J.E. Lutkin, G.W. McBeth, "Pulse shape discrimination in inorganic and organic scintillators. I", *Nucl Inst. Meth* 95, pp. 141-153, (1971)

## 4 Rising Edge Discrimination

It has long been known that radiation type can be discerned on the basis of subtle differences in pulse shape from a variety of detection materials [1], but discrimination in fast organic scintillators has long been reliant on the separation in the decay tail of the pulses [2]. This can constrain pulse shape discrimination techniques to follow after the peak amplitude of the event and they can thus be susceptible to the effects of pile up. Furthermore, discrimination in the decay tail can place a fundamental limit on the time relative to the evolution of the event when discrimination can be performed and thus this can be a significant constraint on the event processing rate for high pulse-rate applications. In this section correspondence between established mathematical fits of organic pulse shapes and real events in the rising edge part of the event is investigated, and the potential for rise time based pulse-shape discrimination in mixed-field data from organic scintillators is explored. An increased data throughput and ease on computation could be beneficial to applications such as active interrogation where PSD is required and the high flux fields, described previously, could lead to significant pile up.

The most commonly-used method for pulse-shape discrimination with organic scintillators in a mixed field is based on the trailing edge of an acquired pulse due to a distinct difference between the pulses of  $\gamma$  rays and neutrons [2]. The problems that arise from this are that it can be susceptible to pulse pile-up resulting in reduced detection rates and spurious pulse assignments, whilst pile-up recovery can be a lengthy and data-intensive process.

## A novel detection system using neutron/gamma pulse shape discrimination, for use in active interrogation environments

An ability to discriminate on the rising edge could reduce the processing intensity and the time required to carry out investigations on objects. Discrimination has previously been suggested based on the time it takes each pulse to reach its peak [3], but the advancement of technology has previously prevented practical application of this.

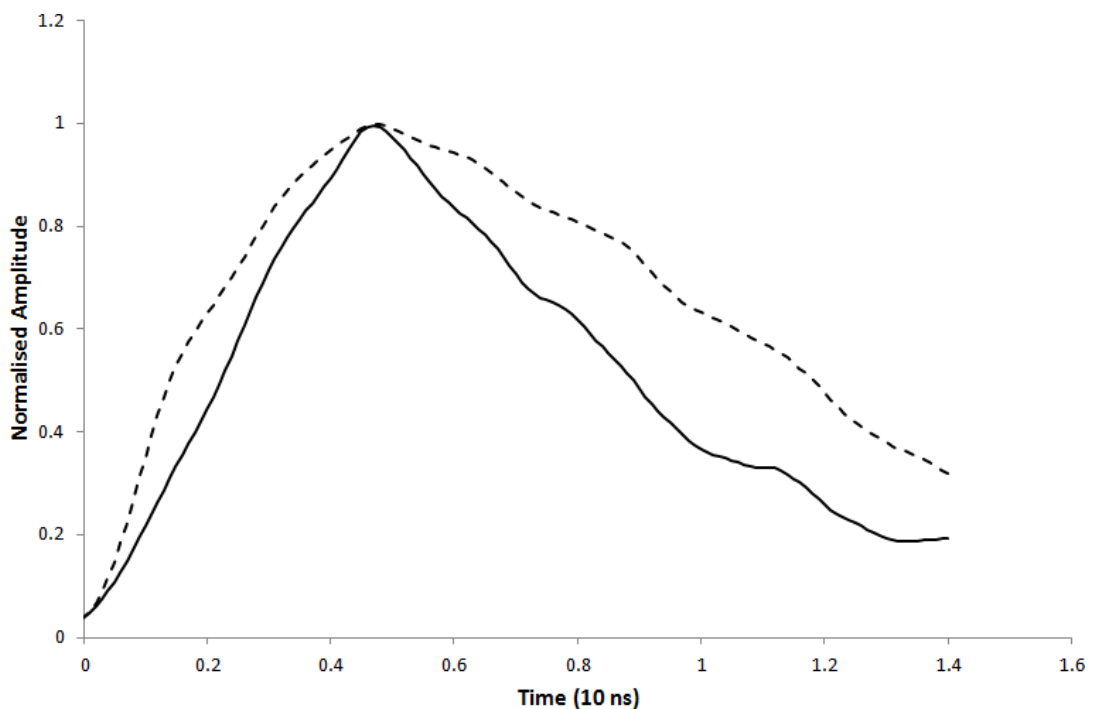


Figure 21. Averaged data for  $\gamma$ -ray (solid) & neutron (dashed) pulses of voltage versus time arising from previous measurements.

To investigate the possibility of rising-edge discrimination, experimental data have been analyzed for this purpose from a data set collected as described in a previous publication [4]. The data was obtained from an experiment using the Van de Graaff accelerator at the National Physical Laboratory (NPL, Teddington, UK) to produce a 2.924 MeV proton beam that was incident on a lithium fluoride target. The data consists of events arising from the  ${}^7\text{Li}(p,n){}^7\text{Be}$  reaction consisting of two different neutron energies, these being 0.745 and 1.225 MeV. The data set consisted of over

20,000 pulses, which was truncated to a workable number of 250 for the purposes of this research. The reduced number of pulses was selected due to the average pulse shapes and new fit that has been developed being carried out in Microsoft Excel. These were then separated into  $\gamma$ -ray and neutron events using ToF data and then averaged to give an average  $\gamma$ -ray pulse shape and an average neutron pulse shape from the mixture of 250 events as described in earlier work [5]. The resulting average pulses shapes are shown in Figure 21, indicating the potential for separation on the rising edge. With separation evident on the rising edge, the next stage was to determine if this was consistent with numerical fits, particularly that reported by Marrone *et al.* [6]. This fit has long been used for fitting the pulse shape analysis in organic scintillators but was produced to fit the decay tails accurately and not focused on the rising edge, as given in the following equation,

$$L(t) = A(e^{-\theta(t-t_0)} - e^{-\lambda_s(t-t_0)}) + B(e^{-\theta(t-t_0)} - e^{-\lambda_l(t-t_0)}) \quad [\text{Equation 18}]$$

the usual application of the fit for amplitude as a function of time  $L(t)$  in the equation above is focused on the trailing edge, where  $\theta$ ,  $\lambda_s$  and  $\lambda_l$  are exponential decay constants,  $t_0$  is the time reference and  $A$  and  $B$  are normalization parameters. By plotting the fits it can be determined if they show if any discrimination was feasible between the rising edges of a neutron and  $\gamma$ -ray pulse, or whether the fit was not sufficiently robust. The resulting pulses, shown in Figure 22, demonstrate there are differences between the trailing edges as is well known. Furthermore, however, a focus on the start of the pulses indicates that there is some separation on the rising edge within the first couple of nanoseconds also, as highlighted in the expanded portion of the fit in Figure 23.

A novel detection system using neutron/gamma pulse shape discrimination, for use in active interrogation environments

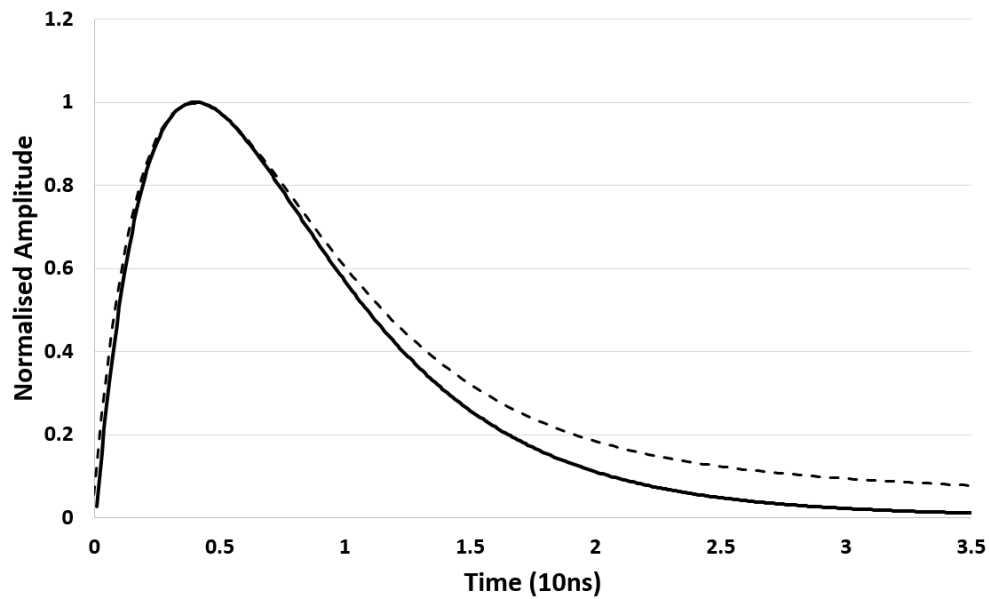


Figure 22. Neutron (dashed) and  $\gamma$ -ray (solid) pulses from the fit reported by Marrone et al. [6] as a function of voltage against time, normalised to each other for clarity.

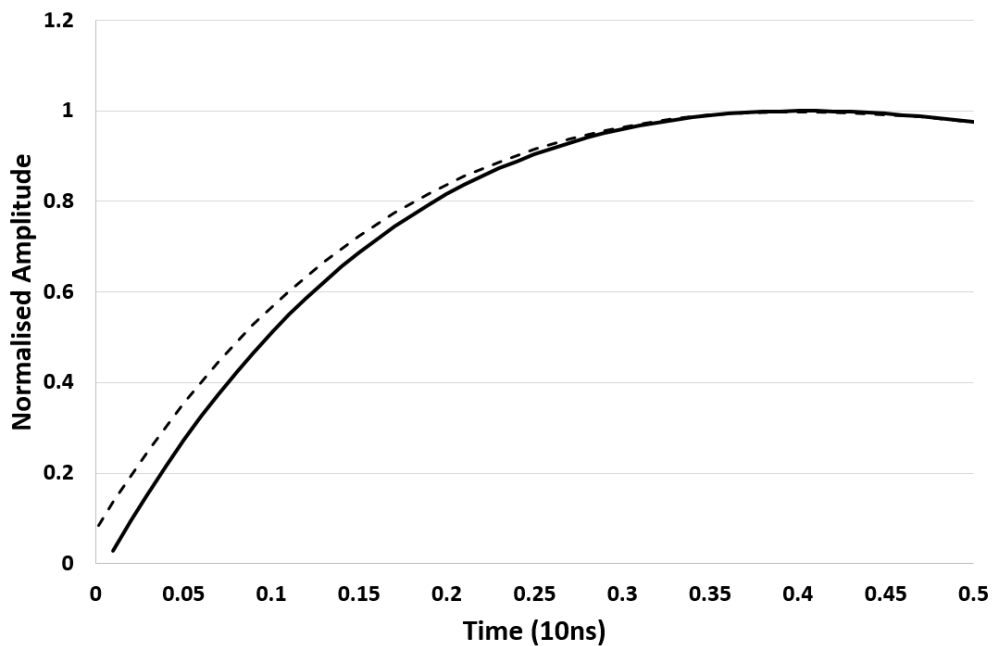


Figure 23. The rising edge of the neutron and  $\gamma$ -ray pulses based on the Marrone fit [6] normalised to the peak amplitude.

The data infer a degree of separation between the rising edges of the pulses. This suggests the possibility that a development of the Marrone formalism might

describe a generalized form of early-stage, pre-peak amplitude PSD, and from these new fits work towards a practical solution of rising-edge separation.

To obtain a better understanding for the rising edge, an entirely new fit has been developed as part of this research. This fit was initially based on a combination of several exponent terms and is entirely empirical. This empirical fit was then tuned to fit the averaged pulse shapes compared previously to the Marrone fit as effectively as possible. The resulting fit is given as,

$$M(t) = ae^{(t^3-x)} + \beta e^{\frac{(t-y)}{\epsilon}} + \gamma e^{(-t^2-z)} - \eta \quad [\text{Equation 19}]$$

the resulting fit tracks the data analyzed in this work very accurately, as shown in Figures 24 & 25. However, this fit still needs to be tested against a variety of organic scintillation compounds to determine how widely applicable it is.

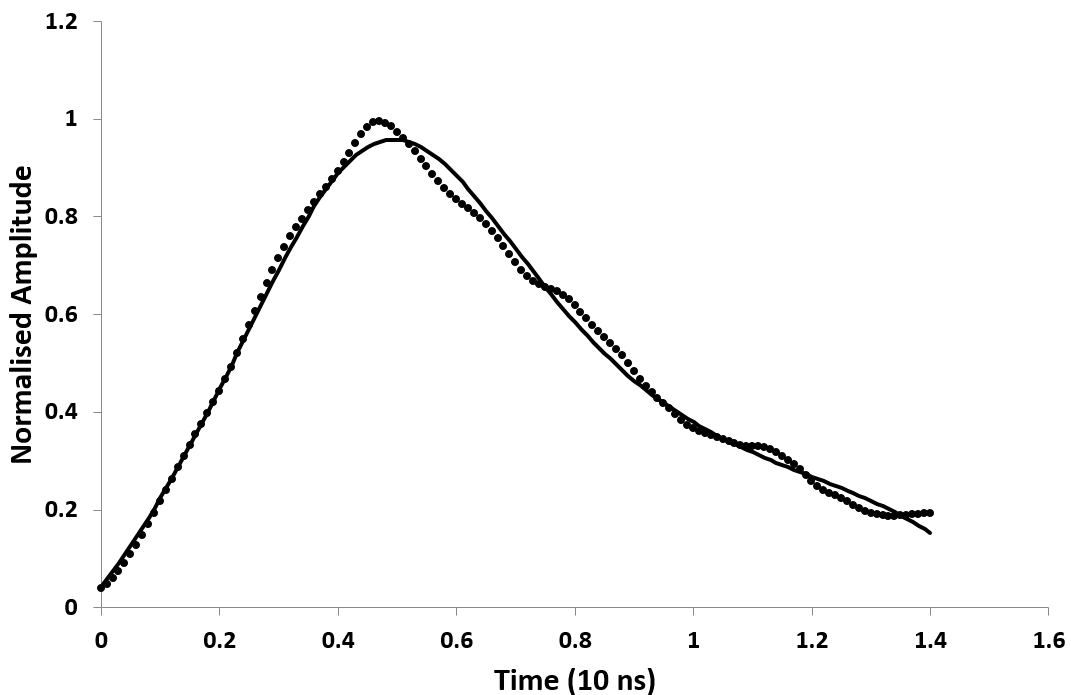


Figure 24. New  $\gamma$ -ray fit (solid) and averaged experimental data (dots).

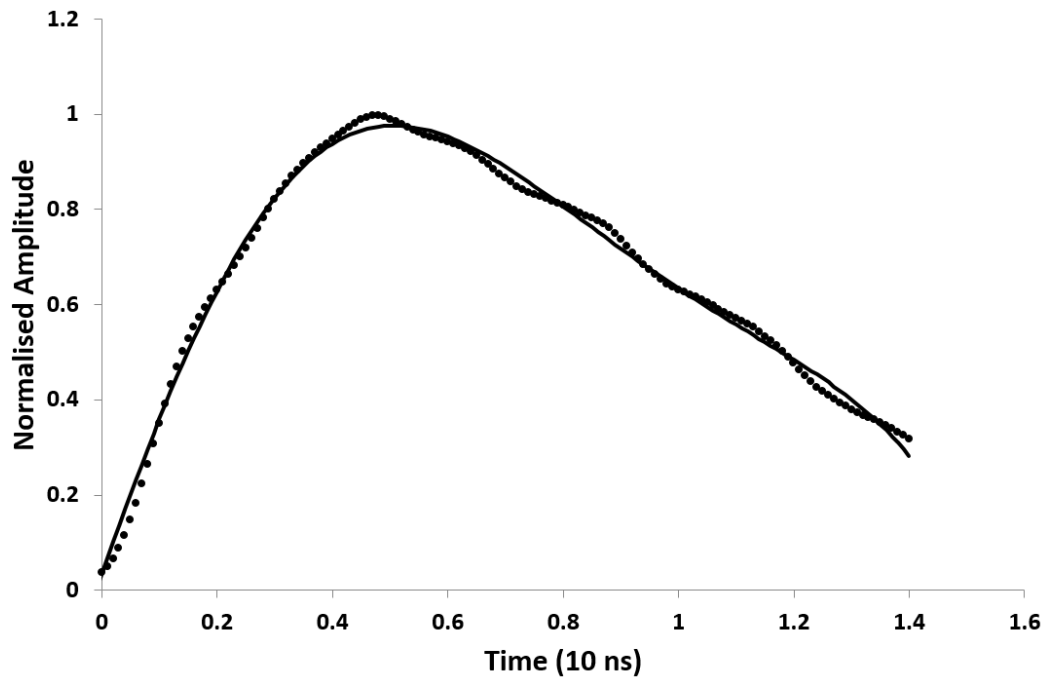


Figure 25. New neutron fit (solid) and averaged experimental data (dots).

As the above results show that there is separation between the two radiation types on the rising edge of the pulses. The PGA algorithm codes were altered to investigate the ability of a pre-peak amplitude to be taken as the discrimination sample point and compare the gradients between the two points to allow for rise time discrimination. The research carried out relied upon previously written MATLAB scripts for PGA [7] and incorporated a new script for rise time discrimination of the data previously discussed from the  ${}^7\text{Li}(p,n){}^7\text{Be}$  reaction. These codes assign pulses as different radiation types of different energies based upon ToF data [4]. Once the pulses have been assigned they were plotted both using the usual PGA method taking a discrimination sample of 16 ns after the peak amplitude, Figure 26, and using the new rise time concept looking at a discrimination sample from 0.125 – 3 ns before the peak amplitude Figure 27, 28 & 29. Figures 27 & 28 show the gamma (left) and neutron (right) pulses that have been assigned using the ToF data then plotted in these graphs

A novel detection system using neutron/gamma pulse shape discrimination, for use  
in active interrogation environments

using the rise time sample against the peak amplitude. Each plot states the starting point of the rise time sample at the top middle of the plots, for example the first plots, -0.125 ns, corresponds to a rise time sample that started 0.125 ns before the peak amplitude. The first three plots are equal due to the lower sampling rate used for the initial plots, this means that the rise time samples were all using the same sample points. For these plots 4000 pulses were taken from the data set to shorten the computational time required.

A novel detection system using neutron/gamma pulse shape discrimination, for use in active interrogation environments

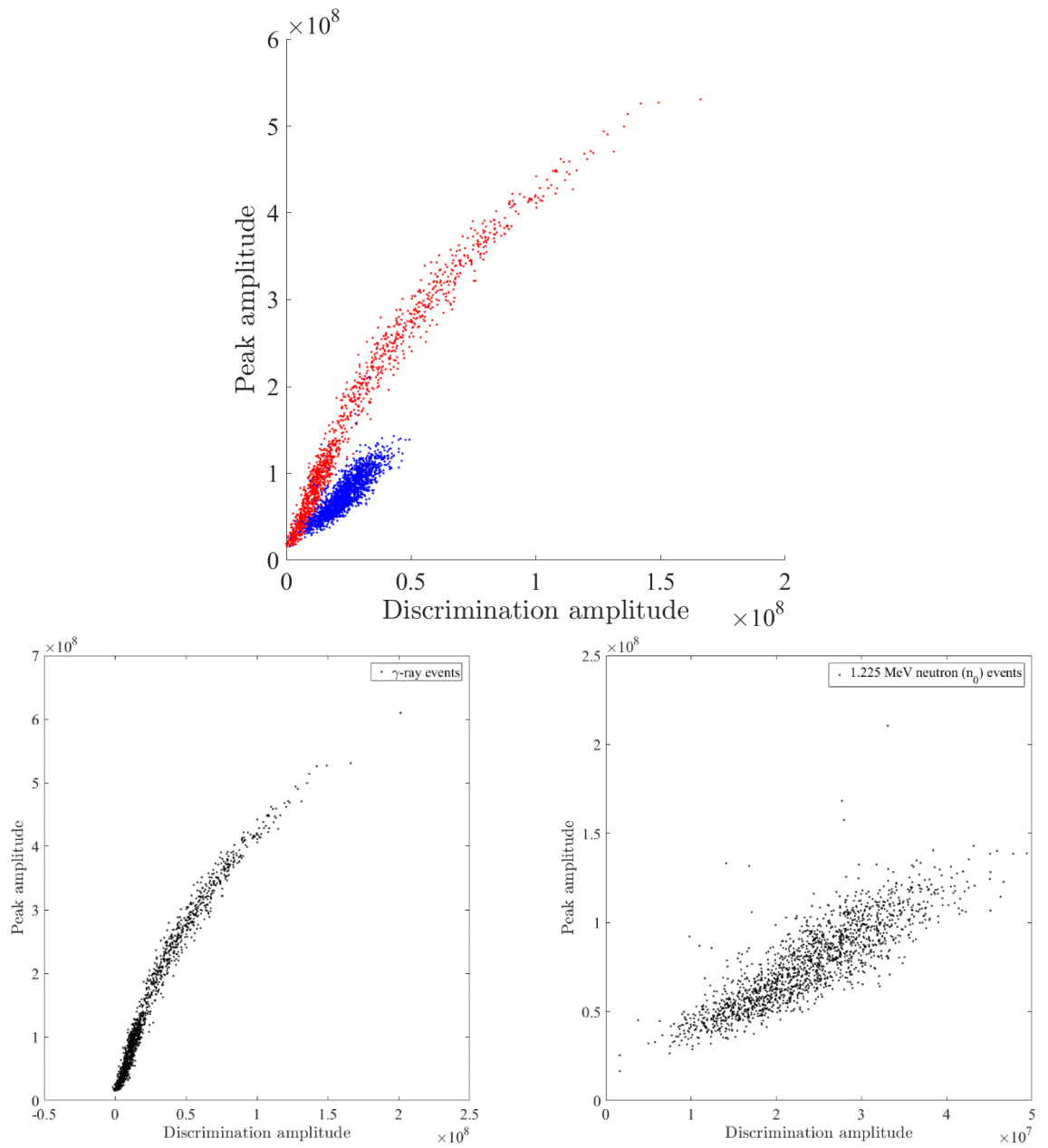


Figure 26. PGA scatter plot (top), with individual radiation plots (below) using the falling edge.

A novel detection system using neutron/gamma pulse shape discrimination, for use in active interrogation environments

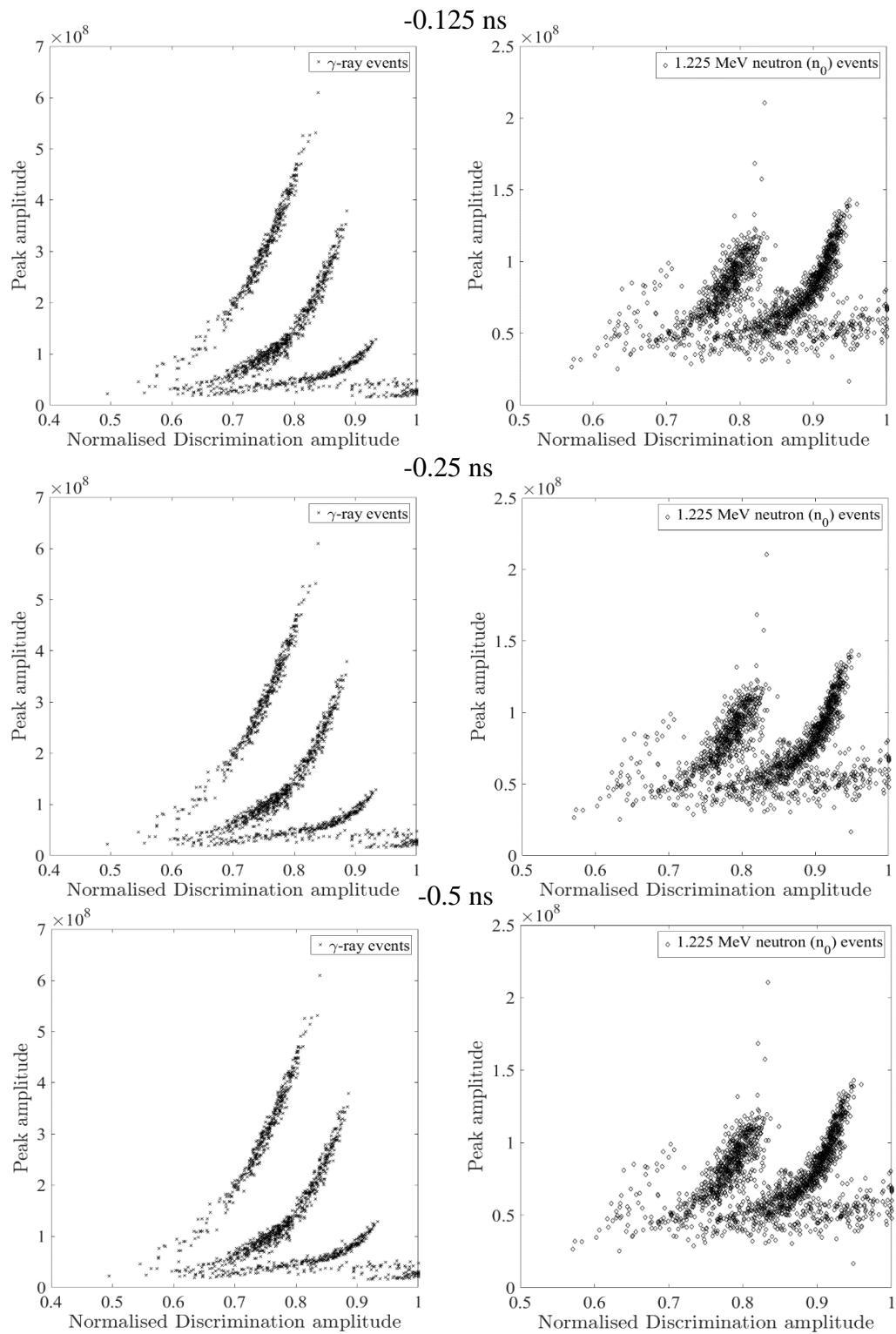


Figure 27. Different plots of peak against normalised discrimination amplitude for  $\gamma$  rays on the left and neutrons on the right for varying rise time discrimination sample points as stated as denoted at the top in between the plots.

# A novel detection system using neutron/gamma pulse shape discrimination, for use in active interrogation environments

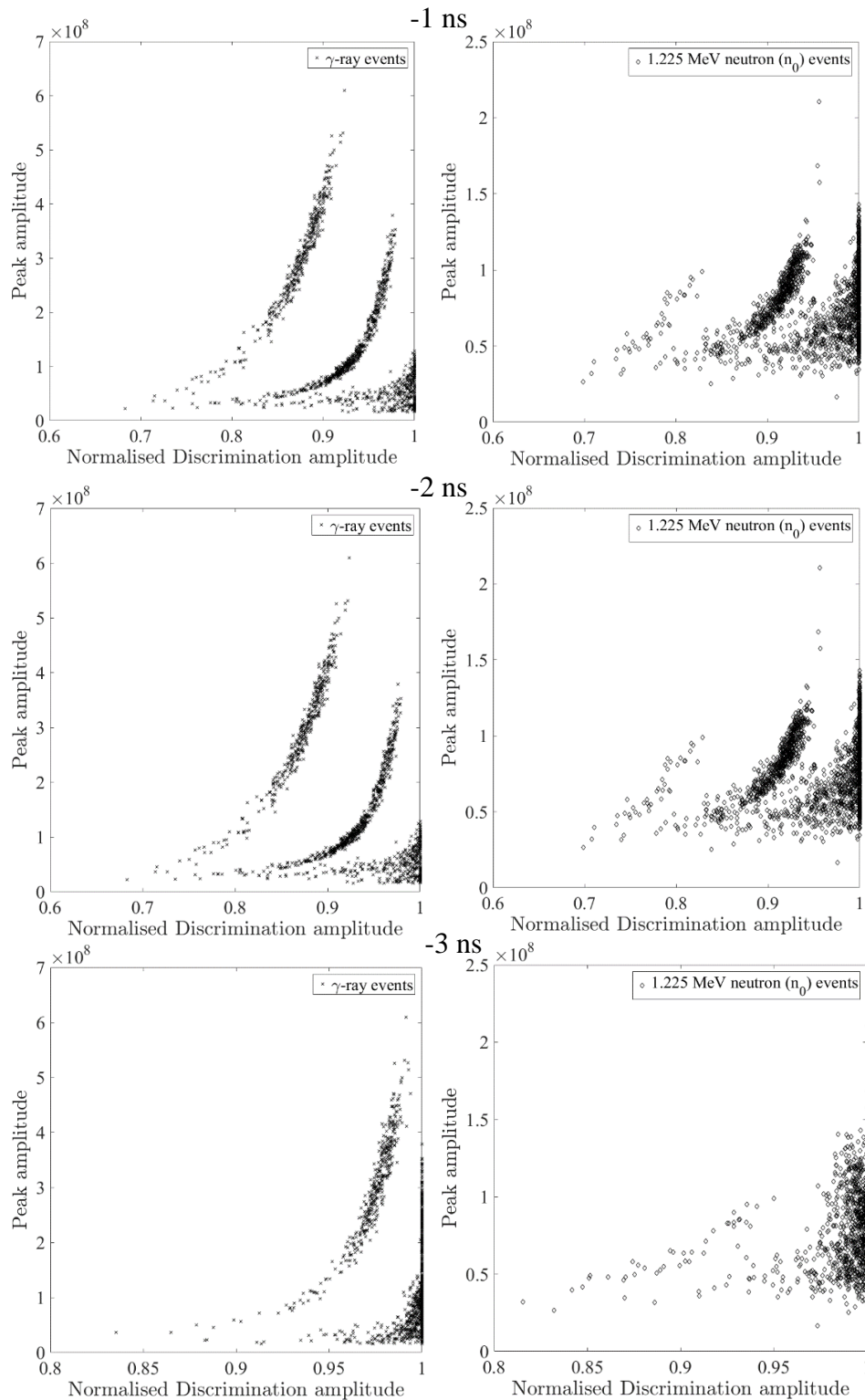


Figure 28. Different plots of peak against normalised discrimination amplitude for  $\gamma$  rays on the left and neutrons on the right for varying rise time discrimination sample points as denoted at the top in between the plots.

A novel detection system using neutron/gamma pulse shape discrimination, for use in active interrogation environments

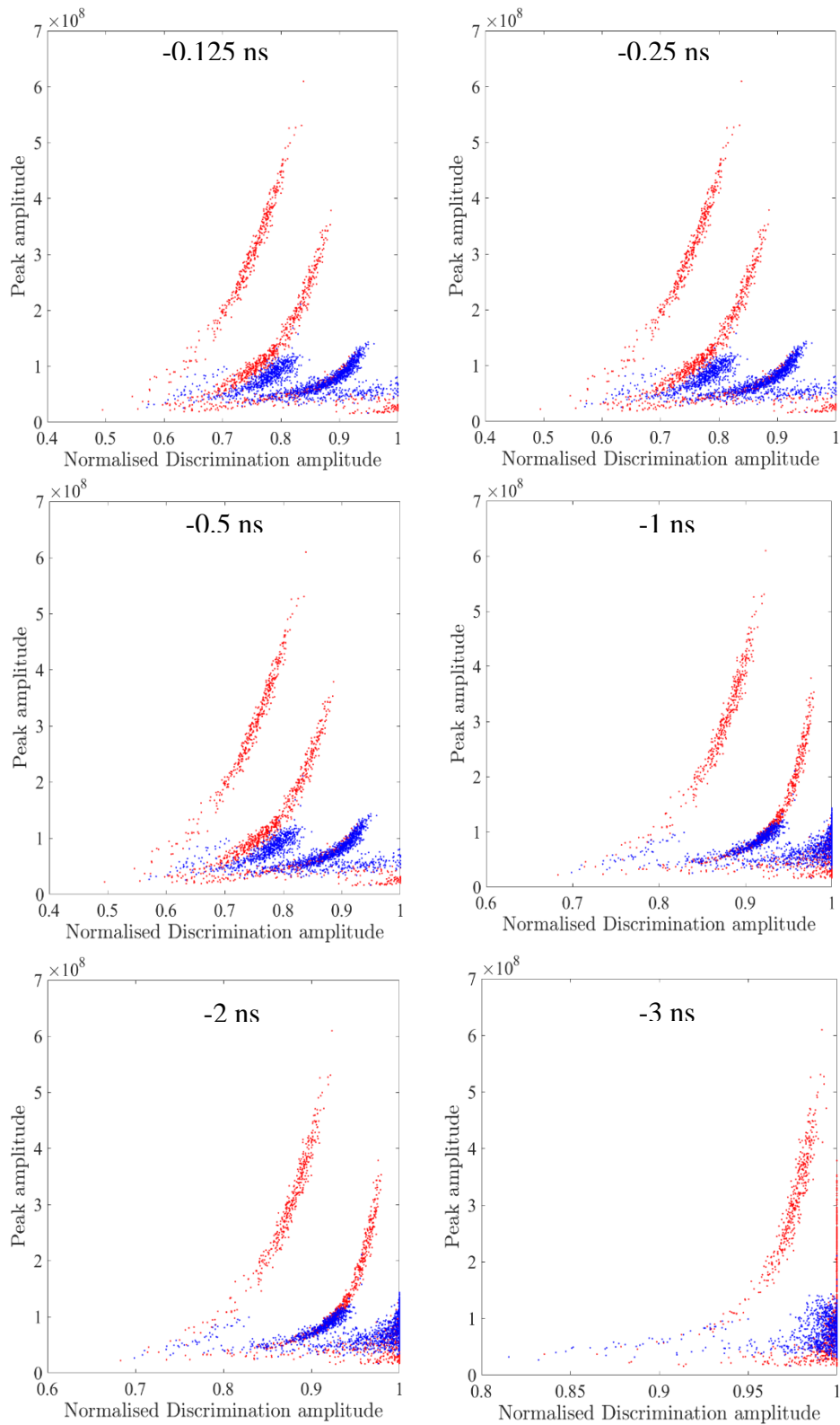


Figure 29. Joint  $\gamma$ -ray (red) and neutron (blue) distributions for varying rise time discrimination sample points.

## A novel detection system using neutron/gamma pulse shape discrimination, for use in active interrogation environments

The results of several different discrimination samples taken on the rising edge are shown in Figure 29 ranging from 0.125ns to 3ns before the peak amplitude. The rise time discrimination shows distinct groupings within the radiation types. The data that have been used here is that from measurements carried out in 2007 [4]. As can be seen, the shorter time period that the rise time discrimination sample is taken away from the peak amplitude sample the better defined the plumes are. There are still some sporadic pulses that are in the incorrect regions for their classification. The research that collected this data used an Infiniium digitally configurable oscilloscope from Agilent Technologies, with data recorded at a sampling rate of 8 GSa s<sup>-1</sup>, however the codes used for these plots reduced this sampling rate to 0.6 GSa s<sup>-1</sup> to reduce the computation time, which was attributed to the reason for the different groupings within each radiation type. The reduced sampling rate was taken out leaving the full data set at 8 GSa s<sup>-1</sup>, this produced the plots shown in Figure 30.

# A novel detection system using neutron/gamma pulse shape discrimination, for use in active interrogation environments

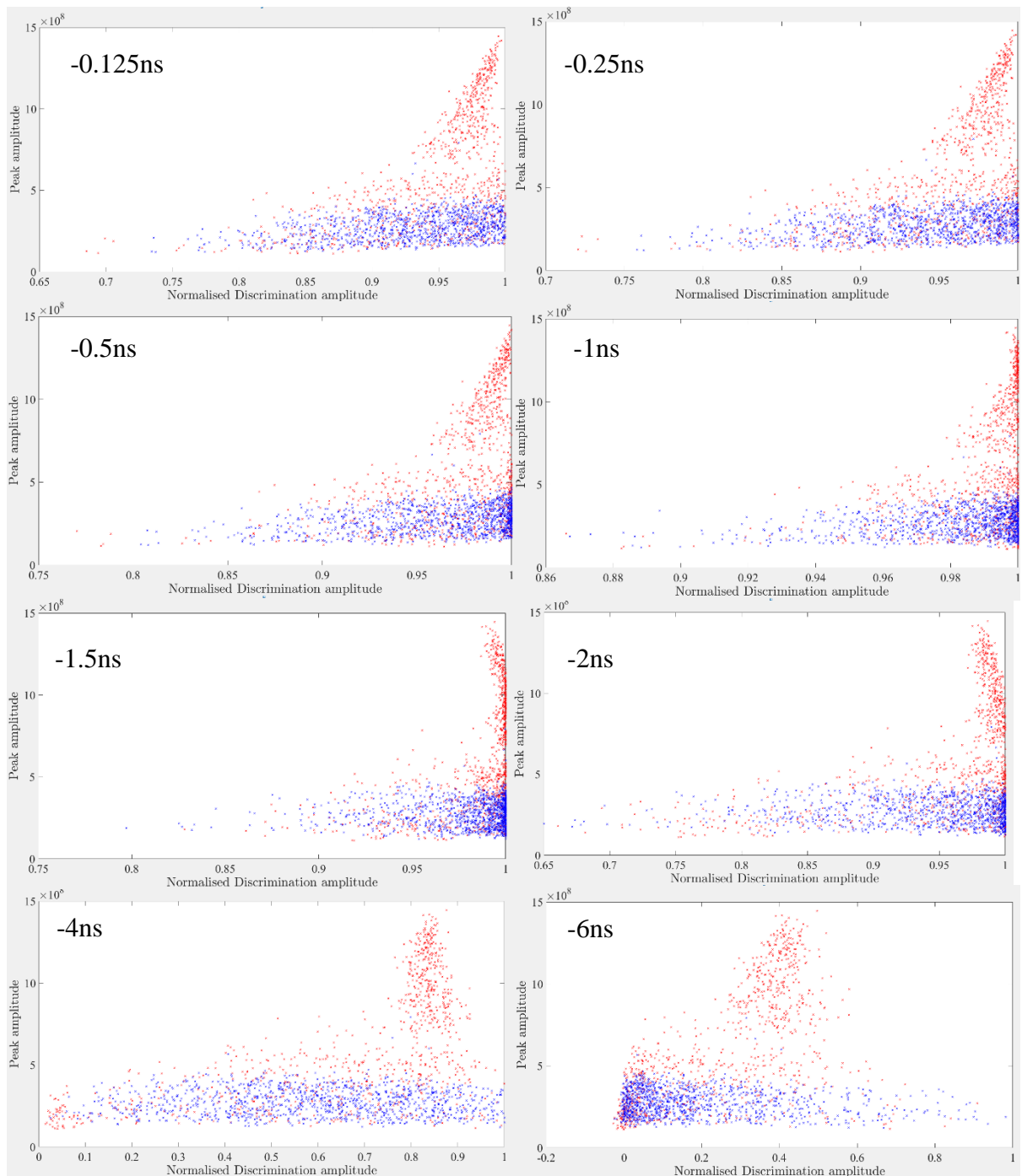


Figure 30. Joint  $\gamma$ -ray (red) and neutron (blue) distributions for varying rise time discrimination sample points.

The plots above had radiation types assigned through the ToF data similar to before. These show that there is a mix of radiation types in a cluster along a horizontal

line, but there is also some clearly separated gamma plumes above the rest. These outlying gamma pulses would have been enough to shift the average fit produced prior to these tests to show a different rise edge characteristic, when in reality it is only a selection of the  $\gamma$ -ray pulses that have an outlying characteristic and could be discriminated.

## 4.1 Conclusion

This aspect of the research discussed in this thesis has investigated the possibility of a solution to detector saturation to increase the speed of PSD. The feasibility to look at the rising edge means that each pulse would only have to be processed up until the peak amplitude itself, increasing the speed of acquisition for each pulse and consequently the speed of discrimination also making the system more resistant to pulse pile up. The research started by considering the current fit used for pulse shapes, although the fit was specifically tailored for matching the decay tail of pulses this showed slight separation prior to the peak amplitude of gamma and neutron pulses. This led to a new empirical fit to be created during this research with the focus on the rising edge of the pulses which was presented at ANIMMA 2013 and is included in Appendix A.

From the positive separation seen in the average fits a new code was developed to take a discrimination sample on the rising edge. The radiation in these plots was tagged using ToF data and then the rising edge discrimination samples were plotted. When analysing the rising edge separation at the 8 GSa  $s^{-1}$  there is a mix of radiation in one horizontal plume, with the  $\gamma$ -ray plume extending in the vertical direction. This

extension of the gamma plume will be the cause of the slight separation on the averaged fits previously presented. The concept of rise time discrimination is very desirable and from the results presented here it may be feasible to state that certain pulses are gamma signatures by looking at the rising edge although the results have suggested the classifications of pulses as neutrons using the rising edge is not possible at present. However, this development is the first look into the use of rise time discrimination and has been implemented with old data with a single scintillator. Further research and investigations into other types of scintillators and better fits could bear fruitful as well as the use of a faster oscilloscope for data capture.

## 4.2 References

1. G.F. Knoll, "Radiation Detection and Measurements" Third Edition ed2000, USA: John Wiley & Sons, Inc.
2. F.D. Brooks, "Development of organic scintillators" *Nucl Inst. Meth* 162, pp. 477-506 (1979)
3. A.J. Peurrung et al. "Direct Fast-Neutron Detection: A Status Report", Pacific Northwest National Laboratory Richland, Washington, 1997
4. M.D. Aspinall et al. "Verification of the digital discrimination of neutrons and gamma rays using pulse gradient analysis by digital measurement of time-of-flight" *Nuclear Instruments and Methods in Physics Research*, vol A583 432-438, 2007.
5. M.D. Aspinall, B. D'Mellow and M.J. Joyce, "The empirical characterisation of organic liquid scintillation detectors by the normalized average of digitized pulse shapes", *Nuclear Instruments and Methods* vol. 578 261-266, 2007.
6. S. Marrone, et al., "Pulse shape analysis of liquid scintillator for neutron studies" *Nuclear Instruments and Methods in Physics Research Section A: Accelerators, Spectrometers, Detectors and associated Equipment*, vol. 490, 299-307, 2002.

A novel detection system using neutron/gamma pulse shape discrimination, for use  
in active interrogation environments

7. M.D. Aspinall, "Real time digital assay of mixed radiation fields" Doctoral Thesis, Lancaster University, (2008)

## 5 Angular Orientation of Liquid Scintillators

The first set of experiments undertaken within this research investigated the quality of the PSD with regard to liquid scintillators and the orientation in which they are set up.

Organic liquid scintillation detectors have long been used for fast neutron detection ever since the late F. D. Brooks discovered that the difference in scintillation decay times between heavily-ionizing particles and photons could be exploited to discriminate fast neutrons from  $\gamma$  rays [1]. However for a long period of time, their use was confined to experimental laboratories and physics research installations due to them being highly flammable and potentially hazardous to use in industrial environments such as the liquid scintillator EJ-301, NE213, BC501 etc. As mentioned in section 3.3.1, low-hazard variants such as EJ-309 are available and more recently, solid forms of organic materials that offer similar pulse-shape discrimination (PSD) properties to those of liquids, such as EJ-299-33 have been discovered [2]. These developments, along with the advent of real-time digital electronic PSD processing [3], have stimulated a great deal of research interest in the use of organic scintillation materials for industrial applications associated with, for example, nuclear safeguards and security [4, 5].

With these capabilities, it is feasible to realize fast-neutron multiplicity assay with very low accidentals rates and a relatively small number of detectors. Often, to account for the  $1/r^2$  spatial dependence from measurements that come from positioning of detectors equidistant from a source or sample under scrutiny, it is

desirable to arrange detectors comprising an array throughout the range of  $4\pi$ . In this case, some cells in such a system can be required to operate consistently with one another despite being at contrasting angles of orientation. Similar demands are made of portable systems where the orientation of detectors can vary from one measurement to another. Whilst solid scintillators are not expected to be affected by orientation on account of the material stiffness of the scintillator, in the case of liquids, there is an obvious settling of the fluid that in some circumstances, has the potential to influence the amount of liquid in contact with the photomultiplier tube (PMT), and thus might affect the light transport to the photocathode. The premise behind this has come from the presence of the nitrogen bubble within the device to accommodate expansion of the liquid due to changes in operation temperature and the presence of light guides in some variants and not others. Any movement of the scintillator results in the nitrogen bubble changing position and in theory, certain angles affect the light yield from the scintillator to the PMT. The experiments carried out in this section also explore the throughput characteristics and the dependency that that has. For these tests two different-shaped detectors both filled with EJ-309 were chosen and are fully described above section 3.3.1. These are both coupled to 3" diameter photomultiplier tubes. One consideration however is that the top coupling face of the cylindrical detector has a bigger surface area than the cubic. This means that at the extreme angle, when the entire nitrogen bubble is between the liquid scintillator and the PMT, the effects will be constrained to a smaller depth in the cylindrical detector, due to the extra overhang area it possess on the PMT. However the cubic-shaped scintillator cell also incorporates a light guide within the cell. This light guide covers the area of the PMT

A novel detection system using neutron/gamma pulse shape discrimination, for use in active interrogation environments

photocathode area and allows the nitrogen bubble to sit around the bubble where the scintillator cell overhangs the PMT. This should prevent the nitrogen bubble from being directly in front of the PMT when the detector is facing vertically down, limiting potential effects to the acute angles only.

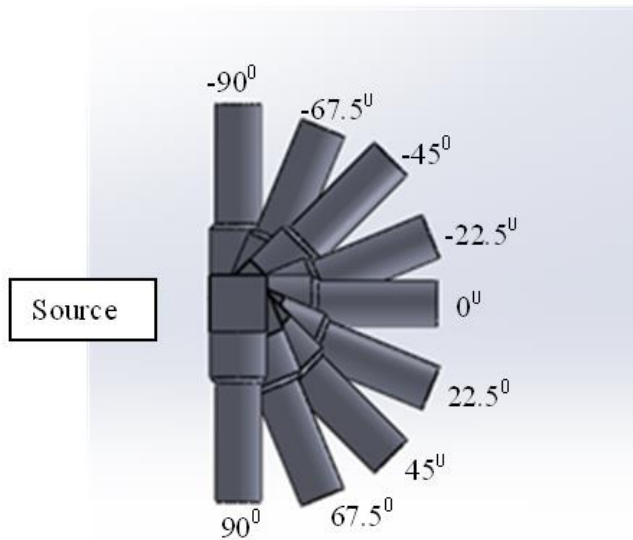


Figure 31. The different arrangements of the detector explored in this work relative to the position of the source situated at  $0^\circ$ , shown in the vertical plane.

In Figure 31, a detector is depicted schematically in nine different orientations with respect to a source located at  $0^\circ$ . Note the distance between the source and the detector was 150 mm and is not shown to scale in the schematic. In each of these orientations it is anticipated that the expansion volume inside the cell will be in a different location within the detector. When the detector is at  $-90^\circ$ , it is anticipated that the bubble will settle above the liquid scintillator, but below the optical window of the PMT, thus offering maximum influence on the light transport of the detector through to the PMT. As the angle is increased towards the horizontal position at  $0^\circ$ , the effect of the bubble is expected to decrease until it has no influence on the light transport to

the PMT through the scintillator. This is the origin of the anticipated effect on the response of an individual detector.

The pioneering research in this regard of late is that of Naeem et al. [6] who explored the dependence of pulse height spectra (PHS) on the angle of orientation of organic liquid scintillation detectors. In this work, two contrasting detector volumes were explored both with simulations and with exposure to a  $\gamma$ -ray source. For the larger detector without a light guide, the position of the Compton edge in the PHS was observed to undergo a significant change as a result of positioning, whilst the smaller detector with a light guide did not exhibit such a dependence.

The experiments in the present research with regards to angular orientation were carried out using the 75 MBq  $^{252}\text{Cf}$  source at Lancaster described in section 3.1. The source is moved to the side of the inner hull during exposure, with the apparatus set up outside the vessel as shown in Figure 32 a and b, such that the source is a distance of approximately 150 mm away from the front face of the detector. In this research the first set of experiments used the VS-1105-21 detector (Scionix, Netherlands) that contains the EJ-309 scintillator within a cubic cell. This was connected to a single channel of a 4-channel MFA out of a stack of four MFAs, as shown in Figure 32. These units perform PSD processing in real-time, with an event throughput of  $3 \times 10^6$  events per second and 6 ns time jitter [7]. The PSD operation is based on the pulse-gradient analysis method as mentioned earlier [8], in which samples of the pulse at the peak and in the falling edge of the pulse are compared following processing with the moving-average filter.

A novel detection system using neutron/gamma pulse shape discrimination, for use in active interrogation environments

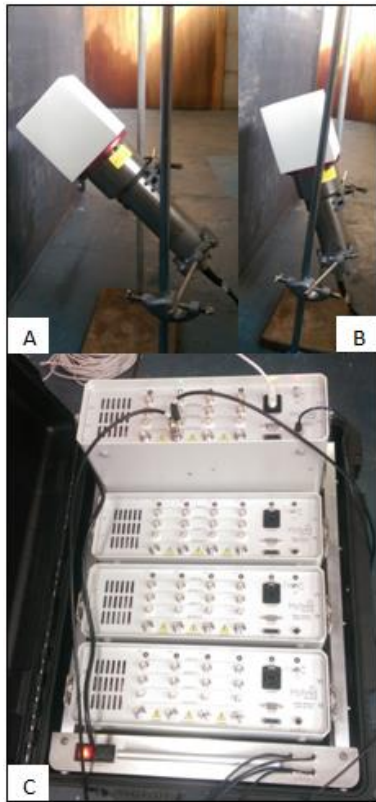


Figure 32. Detector set up at (a)  $45^{\circ}$ , (b)  $67.5^{\circ}$  and (c) the 4-channel MFA used to process the data.

To observe whether there would be any gain shifts requiring a change in HV between different angles, runs at  $0^{\circ}$  (horizontal),  $+45^{\circ}$ ,  $-45^{\circ}$  and  $+90^{\circ}$  were performed with a  $^{137}\text{Cs}$  sources. These were carried out to match the gains on the detector and thus ensure they were consistent with each other at each of the different positions and did not require different settings. The duration of these runs were set to be sufficient to collect several thousand events. The PHD obtained via this approach were all observed to be consistent in shape and in terms of the position of the Compton edge, indicating that the detector would not need further calibration between changing the angles when under investigation. Two example MCA plots are shown in Figure 33.

A novel detection system using neutron/gamma pulse shape discrimination, for use in active interrogation environments

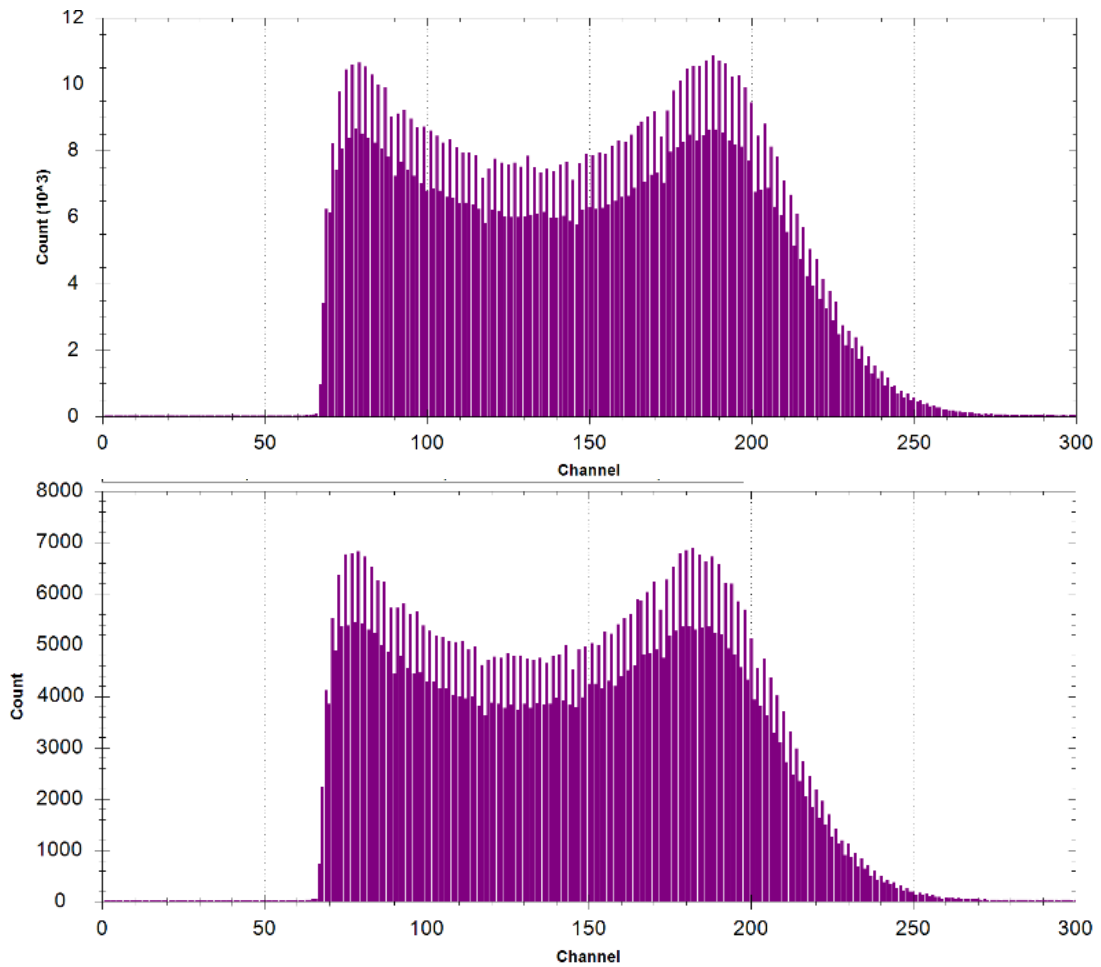


Figure 33. MCA plots for cubic EJ-309 exposed to a gamma sources at 0 degrees (upper), and +45 degrees (lower).

After gain matching measurements were taken, the setup was changed to the  $^{252}\text{Cf}$  source previously described. A scatter plot of first versus second integral was then collected in order to set the PSD threshold settings. To obtain the data necessary for this, the detector was exposed to the source for 100100 pulses, due to the analyser automatically recording an extra 0.1% of counts required, with the detector at  $0^\circ$ . This produced the PSD plot in Figure 34. Two distinct plumes are visible, with the upper being attributed to  $\gamma$  rays and the lower to neutrons.

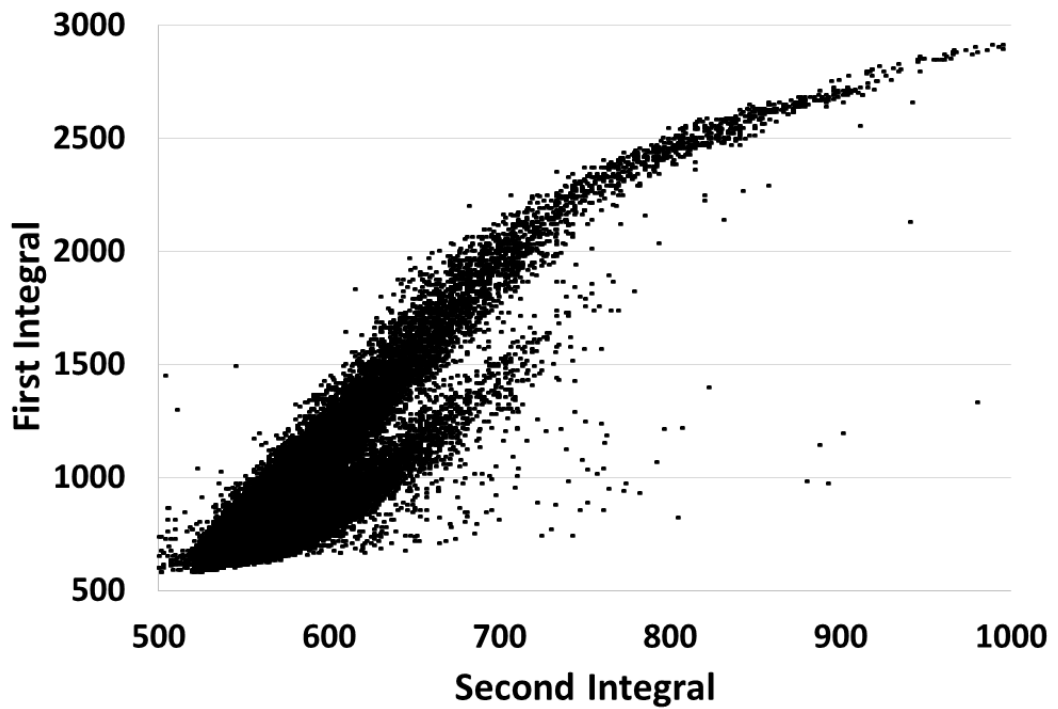


Figure 34. Scatter plot obtained from the cubic detector exposed to the  $^{252}\text{Cf}$  source at  $0^\circ$  for 100100 counts. The upper plume is attributed to  $\gamma$  rays and the lower plume to neutrons.

After the calibration run, the detector was set at each angle with respect to the source using a clamp stand and a magnetic elevation meter, a device for measuring elevations, accurate to  $\pm 0.5^\circ$ . The system was run for 5 minutes at each angle to allow the system to stabilize at that angle before the source was exposed. A run was made for 100100 counts at each position. Four of the plots can be seen below in Figure 35.

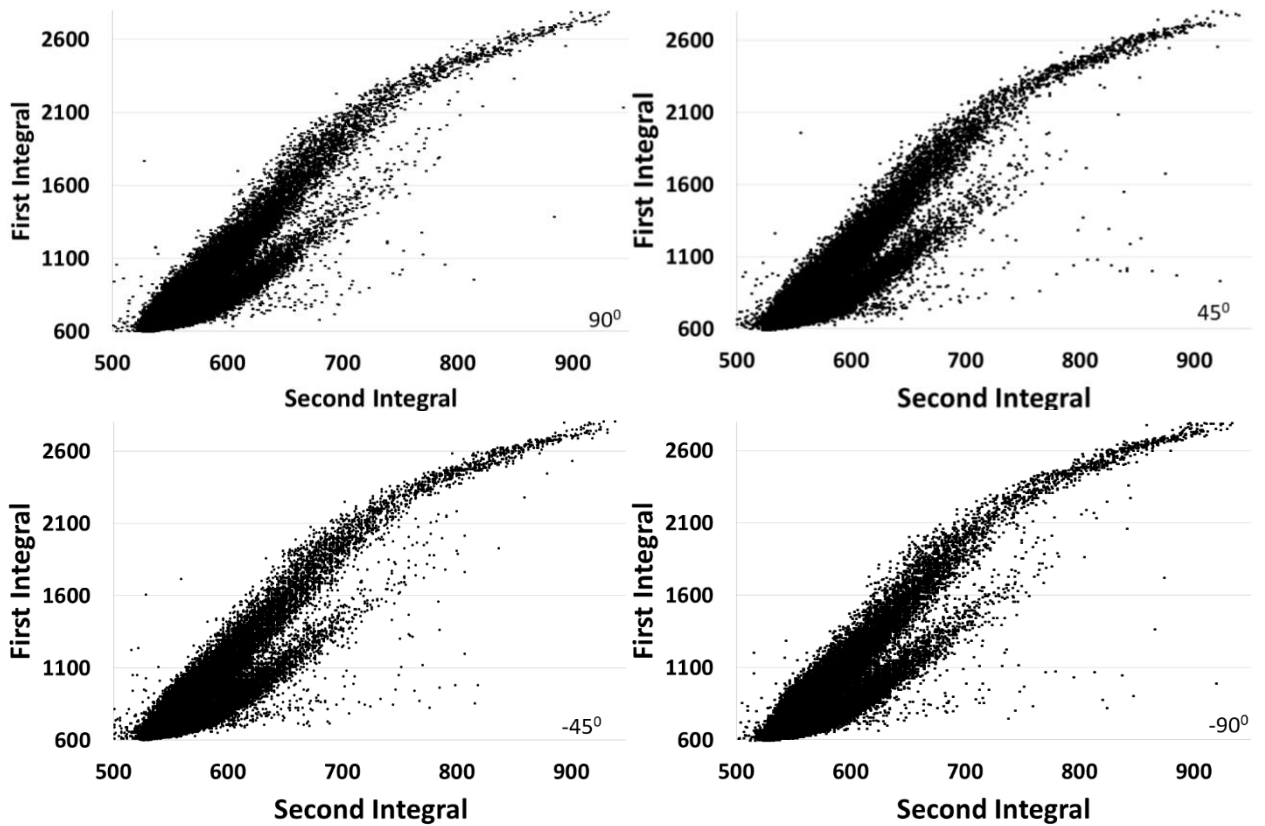


Figure 35. Scatter plots obtained from the cubic detector at a variety of angles during exposure to the  $^{252}\text{Cf}$  source for 100100 counts, angles denoted bottom right corners.

The  $\gamma$ -ray and neutron counts are provided as a function of angle in Table IV. As would be expected the ratio of  $\gamma$  ray to neutrons is consistent throughout, although it was observed that the time taken to reach the desired counts required was greater at some positions than others. To quantify this effect, each run at each orientation was repeated for a set exposure time of 2 minutes, and the number of counts observed in each case compared. These results are shown in Table V.

Table IV.  $\gamma$ -ray and neutron composition of 100100 events with  $^{252}\text{Cf}$  as a function of angle for the cubic cell.

Angle / $^{\circ}$	$\gamma$ -ray events	Neutron events	$\gamma$ -ray / neutron ratio
90.0	82302 $\pm$ 287	17798 $\pm$ 133	4.624 $\pm$ 0.038
67.5	82320 $\pm$ 287	17780 $\pm$ 133	4.630 $\pm$ 0.038
45.0	82267 $\pm$ 287	17833 $\pm$ 134	4.613 $\pm$ 0.038
22.5	82390 $\pm$ 287	17710 $\pm$ 133	4.652 $\pm$ 0.039
0.0	82187 $\pm$ 287	17913 $\pm$ 134	4.588 $\pm$ 0.038
-22.5	82282 $\pm$ 287	17818 $\pm$ 133	4.618 $\pm$ 0.038
-45.0	82226 $\pm$ 287	17874 $\pm$ 134	4.600 $\pm$ 0.038
-67.5	82161 $\pm$ 287	17939 $\pm$ 134	4.580 $\pm$ 0.038
-90.0	82316 $\pm$ 287	17784 $\pm$ 133	4.629 $\pm$ 0.038

Table V.  $\gamma$ -ray and neutron composition for 2 minutes exposure with  $^{252}\text{Cf}$  as a function of angle for the cubic cell.

Angle / $^{\circ}$	$\gamma$ -ray events	Neutron events	$\gamma$ / neutron ratio	Total Events
90.0	194970 $\pm$ 442	41530 $\pm$ 204	4.695 $\pm$ 0.025	236500 $\pm$ 486
67.5	262231 $\pm$ 512	56969 $\pm$ 239	4.603 $\pm$ 0.021	319200 $\pm$ 565
45.0	329524 $\pm$ 574	71576 $\pm$ 268	4.604 $\pm$ 0.019	401100 $\pm$ 633
22.5	380668 $\pm$ 617	82832 $\pm$ 288	4.596 $\pm$ 0.018	463500 $\pm$ 681
0.0	392768 $\pm$ 627	85732 $\pm$ 293	4.581 $\pm$ 0.017	478500 $\pm$ 692
-22.5	313248 $\pm$ 560	69452 $\pm$ 264	4.510 $\pm$ 0.019	382700 $\pm$ 619
-45.0	271227 $\pm$ 521	59773 $\pm$ 244	4.538 $\pm$ 0.021	331000 $\pm$ 575
-67.5	213214 $\pm$ 462	46186 $\pm$ 215	4.616 $\pm$ 0.024	259400 $\pm$ 509
-90.0	172920 $\pm$ 416	36980 $\pm$ 192	4.676 $\pm$ 0.027	209900 $\pm$ 458

Using the same scintillator material EJ-309 the next stage of the experiment was to carry out the tests with the second detector of a different cell shape, specifically a 130 mm diameter cell of type R127 A 76/3 M and an approximate cell volume of 1 litre. This allows comparison between the two shapes and an assessment of the impact a light guide has with respect to the effect of orientation on discrimination performance. This was carried out in exactly the same way as described above, with a cylindrical detector cell as opposed to a cubic cell as in the first instance. The detector HV was calibrated as before with a  $^{137}\text{Cs}$  source, but in this case, analysis of the MCA plot showed that it had shifted when at the  $-90^\circ$  position. The detector, at  $0^\circ$  (horizontal), was then calibrated with the  $^{252}\text{Cf}$  source to determine the PSD thresholds, and the resulting scatter plot can be seen in Figure 36.

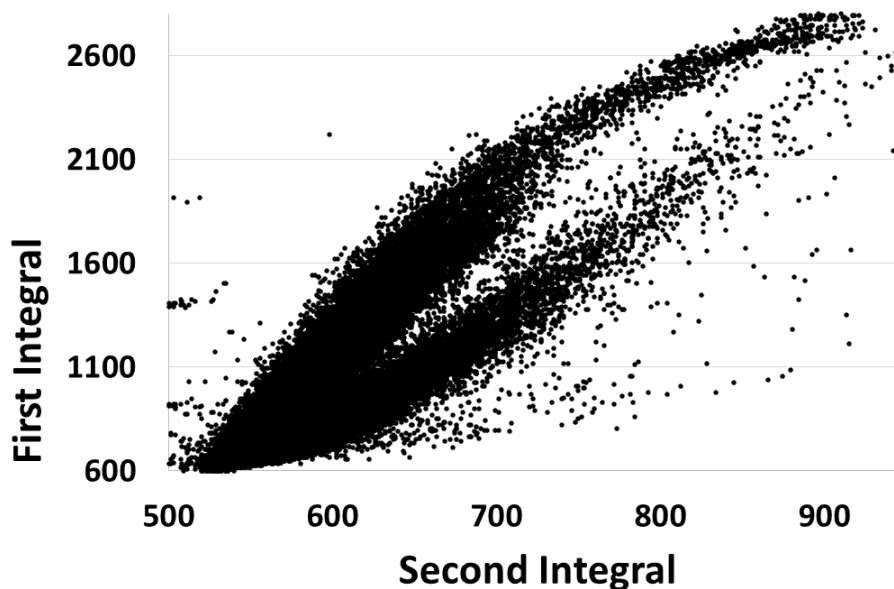


Figure 36. Scatter plot obtained from the cylindrical detector exposed to the  $^{252}\text{Cf}$  source at  $0^\circ$  for 100100 counts. The upper plume is attributed to  $\gamma$  rays and the lower plume to neutrons.

Following the calibration run as described previously, the detector was set to each angle and run for 100100 counts. Four plots can be seen below in Figure 37. In general, the separation with the cylindrical cell is not as distinct, meaning that the discrimination will be less accurate. This could be attributed to the effect of the shape of the cell.

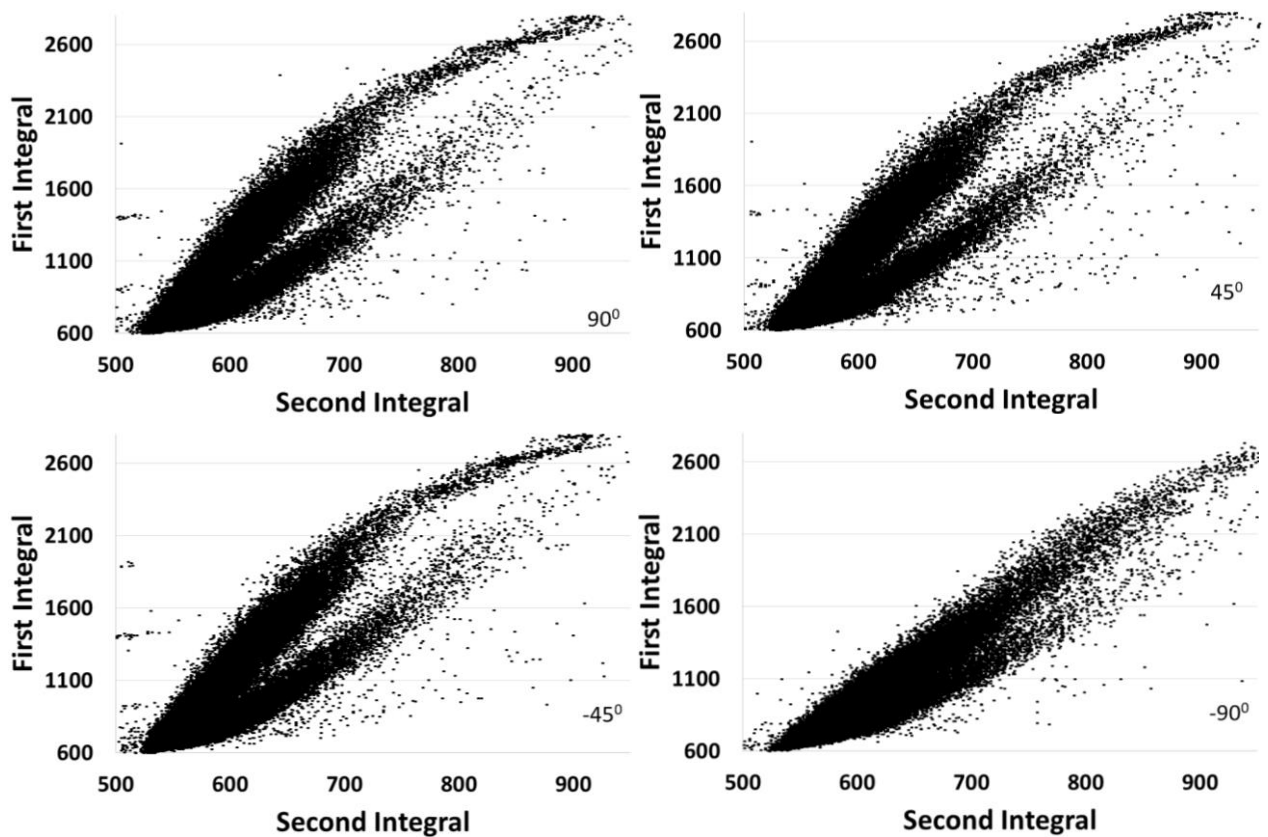


Figure 37. Scatter plots obtained from the cylindrical detector at a variety of angles during exposure to the  $^{252}\text{Cf}$  source for 100100 counts, angles denoted bottom right corners.

The number of counts of each radiation type for each angle with the cylindrical cell is shown in Table VI. As can be seen, at  $-90^\circ$ , the ratio is almost lost. The scatter plot corresponding to the  $-90^\circ$  measurement, Figure 37, shows a significant variation in the position of the neutron and  $\gamma$ -ray distributions at this angle. This shift was also

observed in the MCA plot consistent with that previously reported [9]. The PSD thresholds therefore needed to be adjusted for this specific case of  $-90^0$ , as a result of the influence on the detector at this orientation. Following adjustment, the measurement at this angle was repeated with the revised PSD thresholds and the results are given in Table VII.

Table VI.  $\gamma$ -ray and neutron composition with  $^{252}\text{Cf}$  as a function of angle for 100100 counts for the cylindrical cell.

Angle / $^{\circ}$	$\gamma$ -ray events	Neutron events	$\gamma$ -ray / neutron ratio
90.0	67051 $\pm$ 259	33049 $\pm$ 182	2.029 $\pm$ 0.014
67.5	66947 $\pm$ 259	33153 $\pm$ 182	2.019 $\pm$ 0.014
45.0	66758 $\pm$ 258	33342 $\pm$ 183	2.002 $\pm$ 0.013
22.5	66487 $\pm$ 258	33613 $\pm$ 183	1.978 $\pm$ 0.013
0.0	66146 $\pm$ 257	33954 $\pm$ 184	1.948 $\pm$ 0.013
-22.5	66378 $\pm$ 258	33722 $\pm$ 184	1.968 $\pm$ 0.013
-45.0	66464 $\pm$ 258	33636 $\pm$ 183	1.976 $\pm$ 0.013
-67.5	64813 $\pm$ 255	35287 $\pm$ 188	1.837 $\pm$ 0.012
-90.0	22041 $\pm$ 148	78059 $\pm$ 279	0.282 $\pm$ 0.002

Table VII.  $\gamma$ -ray and neutron composition with  $^{252}\text{Cf}$  at  $-90^0$  for 100100 counts for the cylindrical cell.

Measurement	$\gamma$ -ray events	Neutron events	$\gamma$ -ray / neutron ratio
1 <sup>st</sup>	88631 $\pm$ 298	11469 $\pm$ 107	7.73 $\pm$ 0.008
2 <sup>nd</sup>	88471 $\pm$ 297	11629 $\pm$ 108	7.61 $\pm$ 0.008
3 <sup>rd</sup>	88751 $\pm$ 298	11349 $\pm$ 107	7.82 $\pm$ 0.008

## A novel detection system using neutron/gamma pulse shape discrimination, for use in active interrogation environments

The recalibration of the thresholds was performed three times to check consistency and a comparison of scatter plots for  $0^\circ$  and  $-90^\circ$  is shown in Figure 38. From Figure 38c, the plot following recalibration can clearly be seen to have two distinct regions, although the data exhibits less separation than is evident in all other plots for the angles investigated in this research. Reduced separation between neutron and  $\gamma$ -ray plumes increases the uncertainty in PSD reducing the level of confidence with which one radiation type can be successfully discriminated from the other, reflected in the way the ratio has increased.

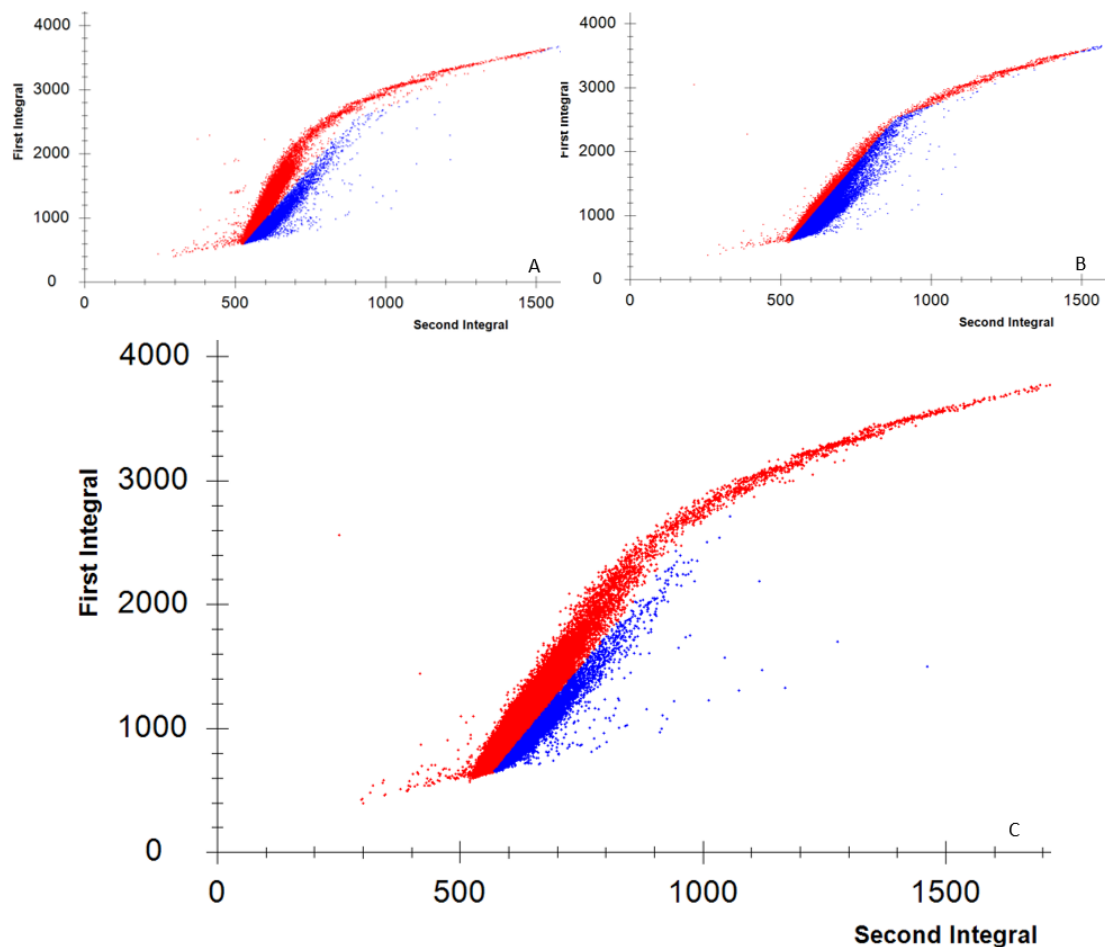


Figure 38. Scatter plots for the cylindrical cell (a)  $0^\circ$ , (b)  $-90^\circ$ , (c)  $-90^\circ$  with revised PSD threshold, red points (upper) corresponds to gammas, blue points (lower) to neutrons.

As with the cubic cell, it was observed with the cylindrical cell that the acquisition time for some positions varied with orientation. Table VIII provides the counts observed for a set exposure time of 2 minutes with the cylindrical cell. With this second set of tests, the PSD threshold for  $-90^\circ$  was set to the new PSD threshold depicted in Figure 38c which produced the data in Table VII.

Table VIII.  $\gamma$ -ray and neutron composition with  $^{252}\text{Cf}$  as a function of angle for 2-minute exposure for the cylindrical cell.

Angle / $^\circ$	$\gamma$ -ray events	Neutron events	$\gamma$ -ray / neutron ratio	Total Events
90.0	402935 $\pm$ 635	131965 $\pm$ 363	3.053 $\pm$ 0.010	534900 $\pm$ 731
67.5	492799 $\pm$ 702	164101 $\pm$ 405	3.003 $\pm$ 0.009	656900 $\pm$ 810
45.0	586236 $\pm$ 766	203564 $\pm$ 451	2.880 $\pm$ 0.007	789800 $\pm$ 889
22.5	625133 $\pm$ 791	219367 $\pm$ 468	2.850 $\pm$ 0.007	844500 $\pm$ 919
0.0	696869 $\pm$ 835	246531 $\pm$ 497	2.827 $\pm$ 0.007	943400 $\pm$ 971
-22.5	591757 $\pm$ 769	209143 $\pm$ 457	2.829 $\pm$ 0.007	800900 $\pm$ 895
-45.0	455139 $\pm$ 675	159761 $\pm$ 400	2.849 $\pm$ 0.008	614900 $\pm$ 784
-67.5	352793 $\pm$ 594	124507 $\pm$ 353	2.834 $\pm$ 0.009	477300 $\pm$ 691
-90.0	245707 $\pm$ 496	31993 $\pm$ 179	7.680 $\pm$ 0.046	277700 $\pm$ 527

The results from these experiments have shown that the throughput varies at different detector orientations as well variations can be observed in the quality of the separation of radiation plumes and consequently the PSD ability of the device.

## 5.1 Analysis

The results from the first set of experiments with regards to the angular orientation are based on the cubic-shaped scintillator cell being exposed to a  $^{252}\text{Cf}$  source. The total

counts for a 2-minute period can be seen in section 5, Table V, and the scatter plots of 4 different angular positions in Figure 35. As mentioned above, the scatter plots have the baselines removed and are normalised to give a linearised plot. An example is shown in Figure 39.

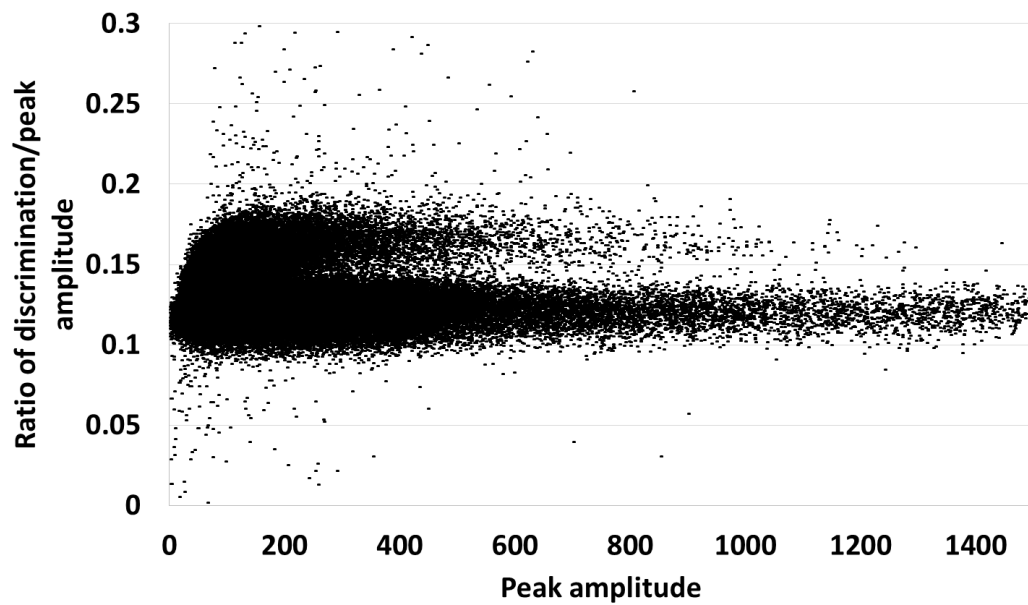


Figure 39. Example normalised plot for the cubic EJ-309 exposed to  $^{252}\text{Cf}$ .

The 4 different scatter plots shown in Figure 35 translate to the following four normalised plots in Figure 40.

A novel detection system using neutron/gamma pulse shape discrimination, for use in active interrogation environments

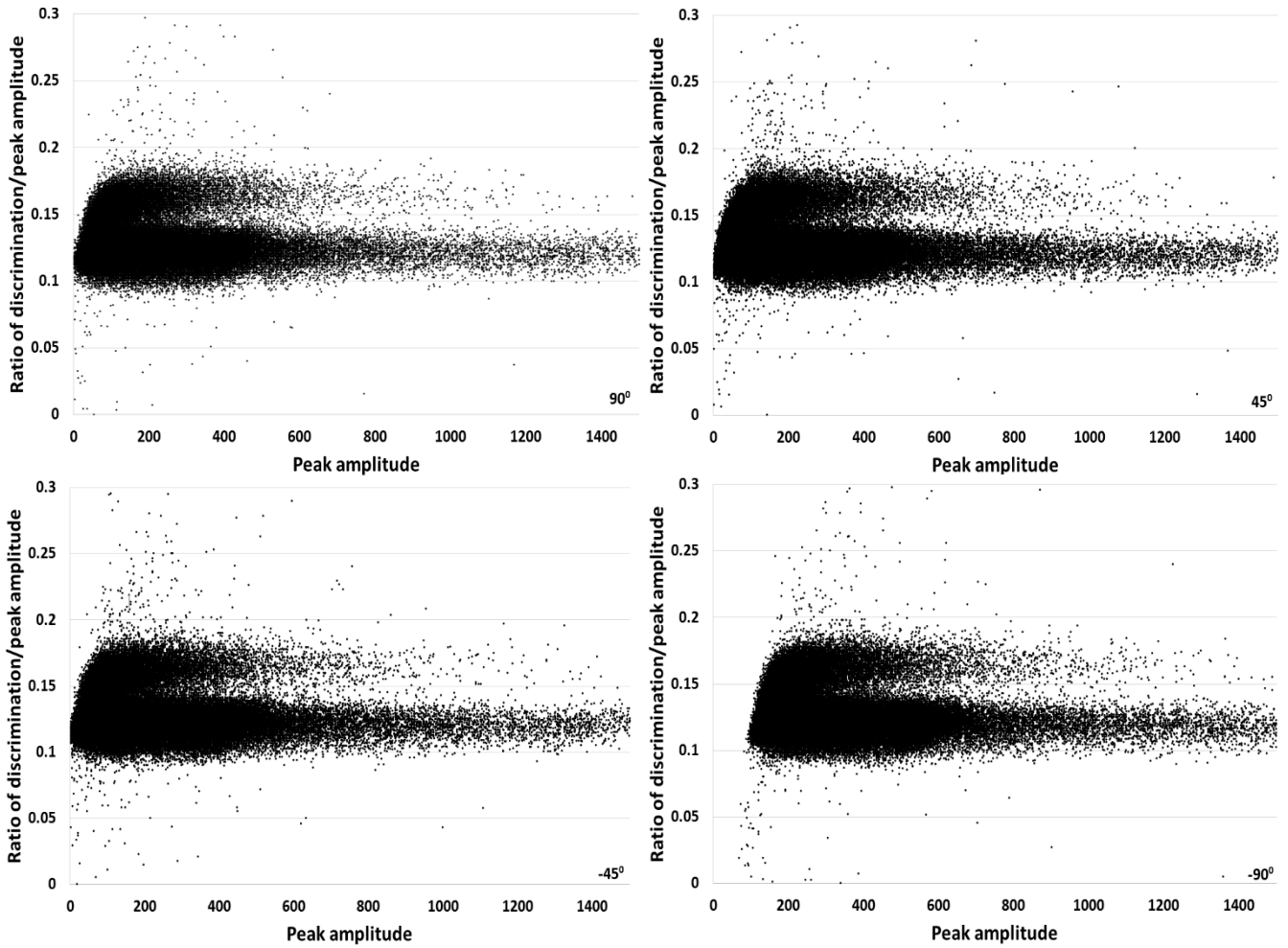


Figure 40. Four normalised plots corresponding to Figure 35 obtained using the cubic detector at a variety of angles during exposure to the  $^{252}\text{Cf}$  as denoted in the lower right.

Similarly the 4 different scatter plots for the cylindrical-shaped EJ-309 scintillator cell, Figure 37, translate to the four normalised plots in Figure 41. As mentioned previously the plot at  $-90^0$  has changed shape and shows no clear separation.

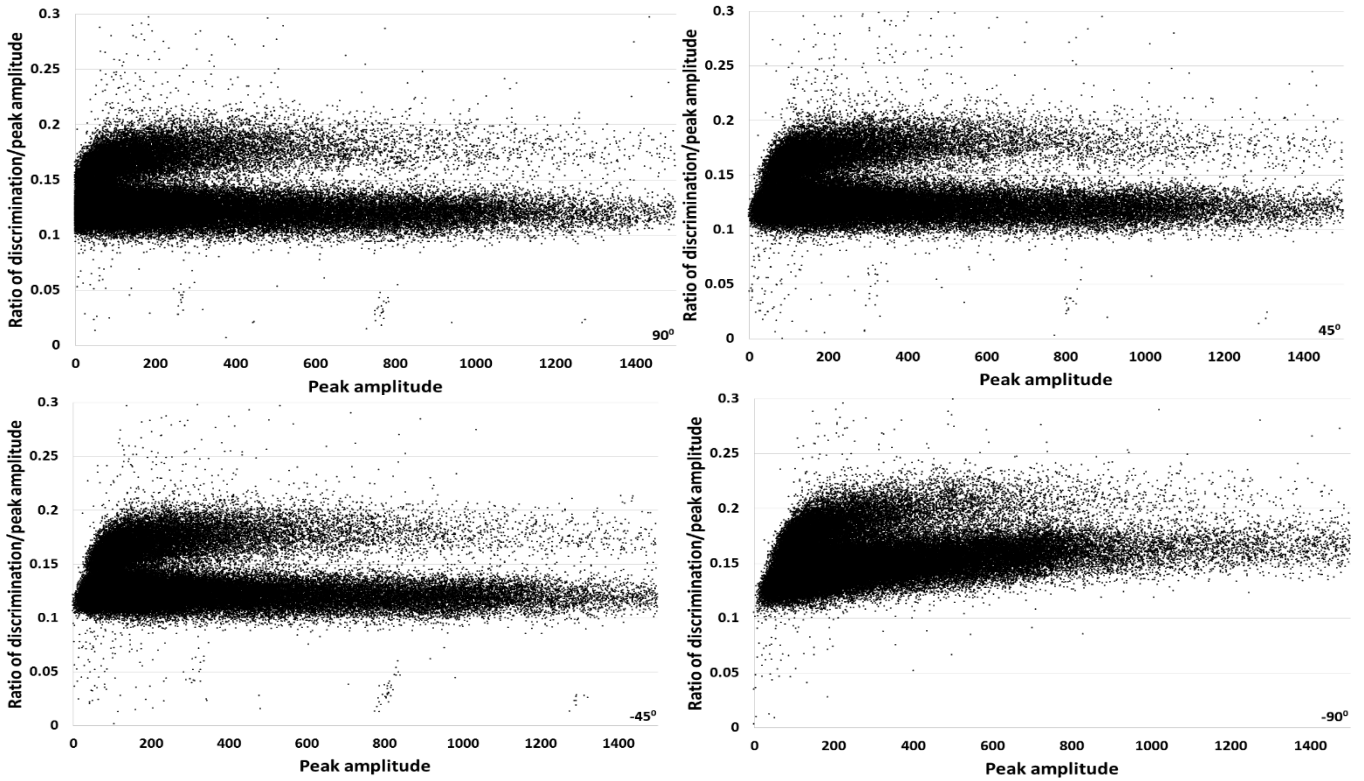


Figure 41. Four normalised plots corresponding to Figure 37 obtained using the cylindrical detector at a variety of angles during exposure to the  $^{252}\text{Cf}$ .

### 5.1.1 Figure-of-Merit calculations

Each linearised plot was then converted into a histogram allowing the FoM value for each case to be extracted. These histograms were produced by taking the number of counts versus channel from the normalized plots shown in Figure 40 & 41. An example double Gaussian fitted to these histograms is shown in Figure 42. The double Gaussian plots for all the cubic and cylindrical detector tests can be seen in Figure 43 & 44 respectively. The values for the FWHM and the separation of the two peaks can then be taken and used to calculate the FoM values which are given in Table IX. In each case the consistency of the fit with the data was also calculated and the corresponding reduced chi-squared  $\chi^2_\nu$  values are included in Table IX.

A novel detection system using neutron/gamma pulse shape discrimination, for use in active interrogation environments

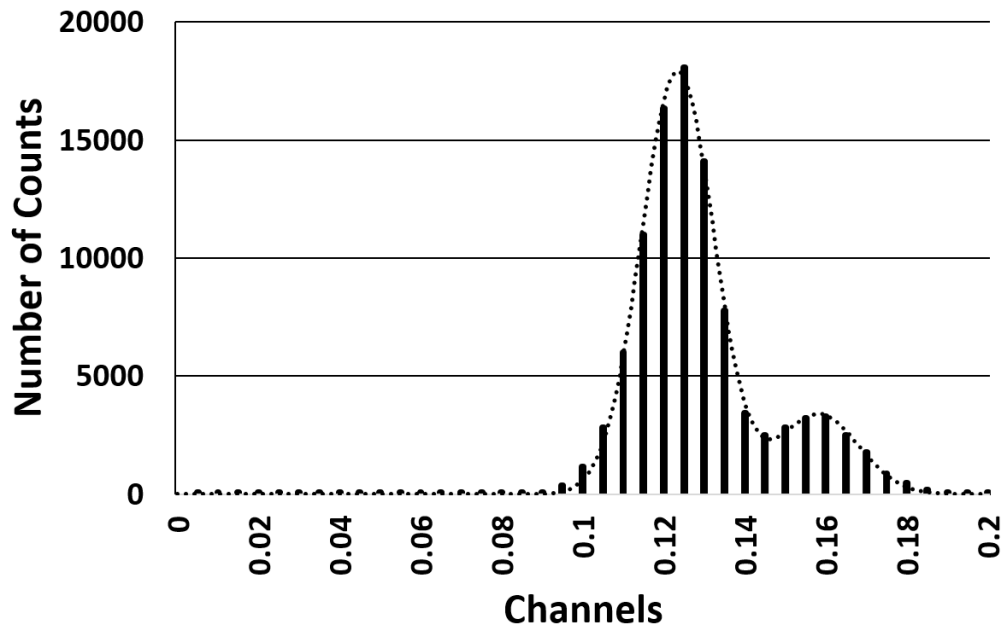


Figure 42. A histogram of the number of counts for the cubic detector for the full energy range exposed for 100100 counts at  $0^\circ$ , with the model fit over the top.

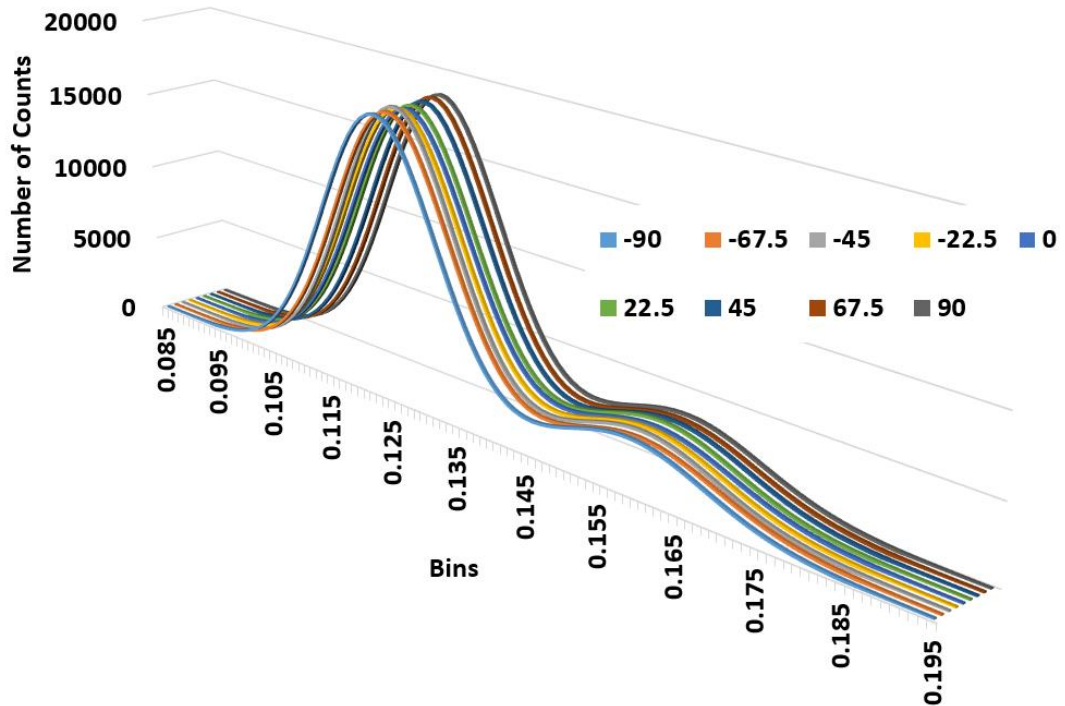


Figure 43 Double Gaussian fits for each angle tested using the cubic detector exposed to  $^{252}\text{Cf}$ .

A novel detection system using neutron/gamma pulse shape discrimination, for use in active interrogation environments

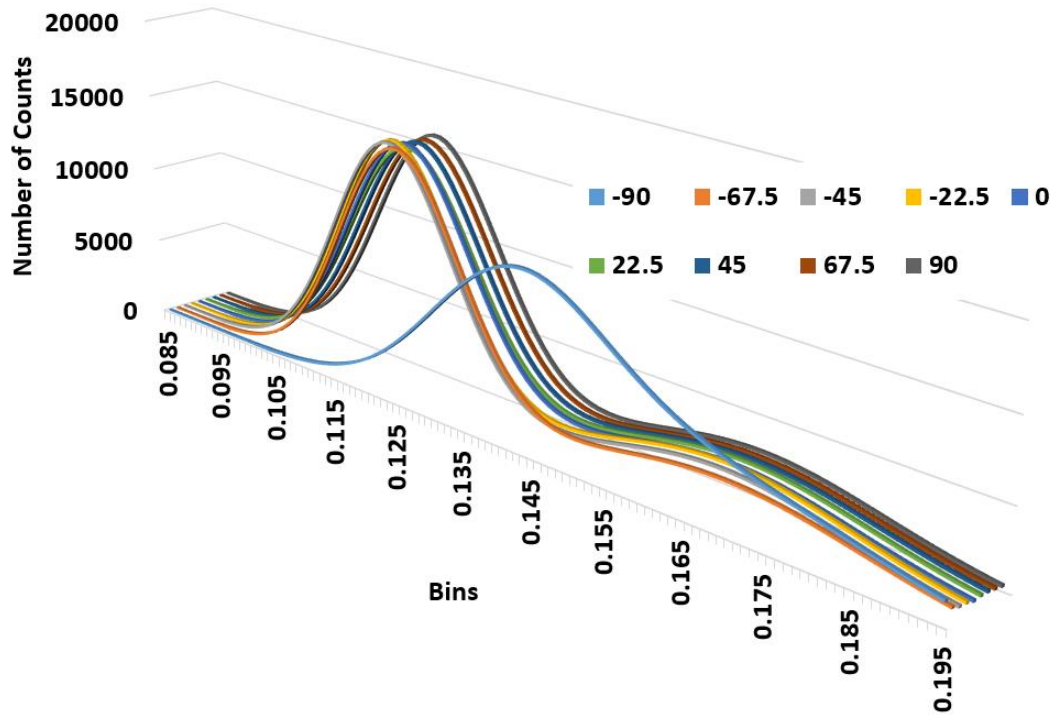


Figure 44 Double Gaussian fits for each angle tested using the cylindrical detector exposed to  $^{252}\text{Cf}$ .

Table IX. FoM as a function of angle exposed to  $^{252}\text{Cf}$  for 100100 counts with the cubic and cylindrical detectors.

Angle / °	Figure-of-Merit Cubic	$\chi^2_{\nu}$	Figure-of-Merit Cylindrical	$\chi^2_{\nu}$
90.0	0.814±0.044	1.00	0.789±0.033	0.98
67.5	0.814±0.044	0.99	0.780±0.031	0.97
45.0	0.814±0.044	0.99	0.763±0.031	0.97
22.5	0.795±0.043	0.99	0.750±0.030	0.97
0.0	0.795±0.043	0.99	0.789±0.033	0.98
-22.5	0.773±0.042	0.99	0.763±0.031	0.97
-45.0	0.791±0.044	0.99	0.780±0.031	0.97
-67.5	0.795±0.043	0.99	0.776±0.032	0.97
-90.0	0.837±0.045	0.99	N/A	N/A

As can be seen in Figure 44 the cylindrical detector at  $-90^{\circ}$  no longer exhibits two peaks of radiation although the other angles seem to hold the ability to discriminate with reasonable consistency. To further explore the indication that the count rate might be dependent on the orientation of the detector, the results from the 2-minute exposure runs have been plotted against the angle in Figure 45.

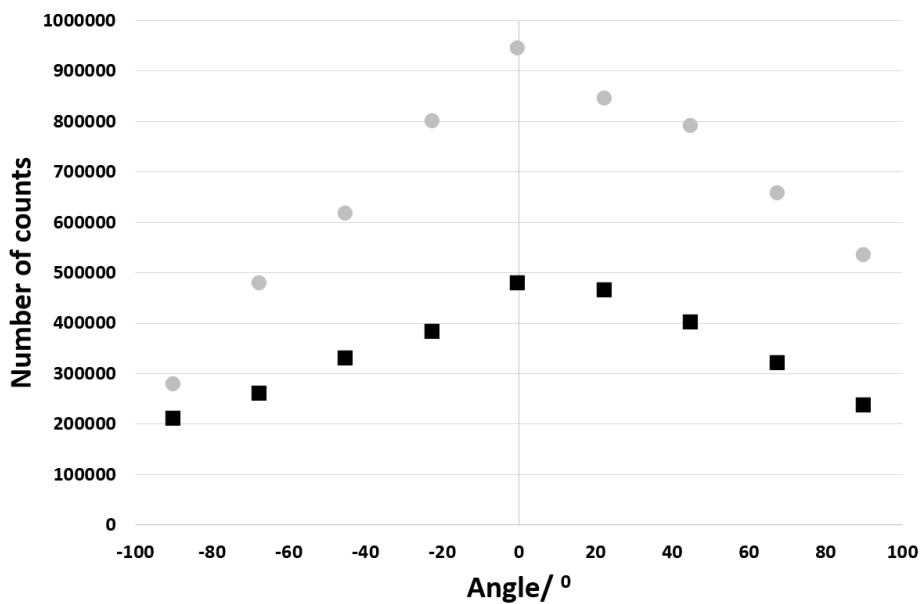


Figure 45. Total counts recorded for the 2-minute exposures of the cubic (black squares) and the cylindrical (grey circles) detector as a function of angle (uncertainties smaller than the size of the symbols in each case).

The discrimination performance is discussed in more detail later on in section 5.2 however the poorest values seem to occur at the two smallest angles away from the horizontal for the cylindrical detector. This was followed up by an investigation rotating the detector through the same angles but in the horizontal plane as opposed to the vertical as previously explored, these tests are to justify whether the conclusion of different rate affect can be attributed to the detectors front face not being in line with the source. The hypothesis is depicted in Figure 46 with a sphere representing a

A novel detection system using neutron/gamma pulse shape discrimination, for use in active interrogation environments

uniform radiation field from a point source and the cube representing the detector cell. The top two diagrams place the point source of radiation at a distance of 150 mm from the first receiving point of the detector, whilst the bottom two diagrams place the centre of the radiation field at a distance of 145mm. The bottom left diagram has the detector face on with the radiation source and half the scintillator cell is exposed at a distances of 145mm, whereas the bottom left diagram has the detector at an angle of  $45^{\circ}$  with the point source of radiation and less than half the scintillator cell is exposed at 145mm. This suggests that the reduction in solid angle between the source and the front face of the detector may be causing the effect responsible for the lower FoM values at small angles.

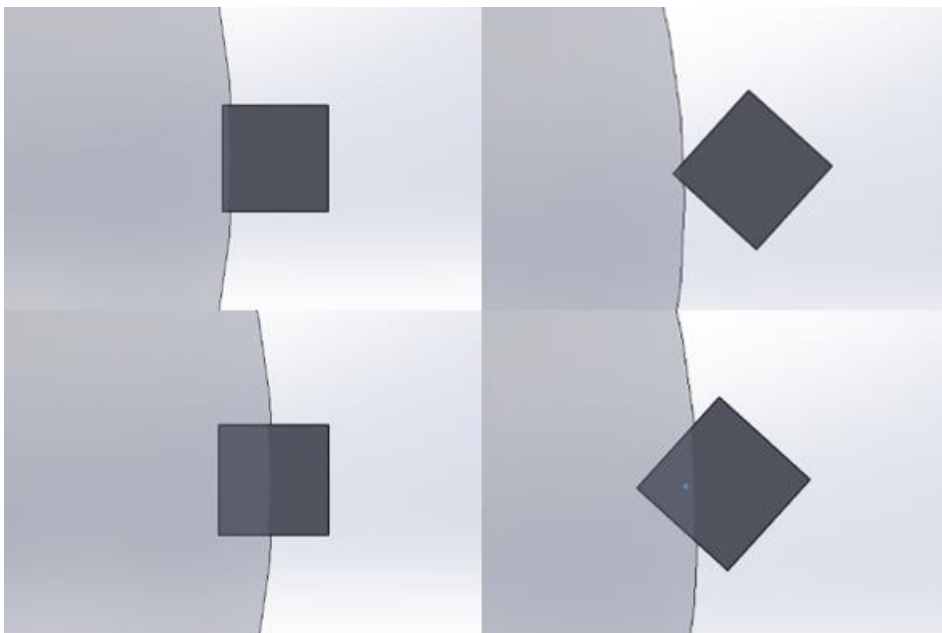


Figure 46. Pictorial representation of the uniform radiation field bisecting the detector cell.

To investigate this hypothesis, 2-minute tests were carried out with both detectors rotated whilst keeping parallel with the floor, starting perpendicular to the

source through to being face on and continuing to being perpendicular with the face of the source tank on the other side of the detector. The results from the 2-minute exposures using the cubic and cylindrical cell can be seen in Table X & XI respectively. The results are shown graphically in Figure 47.

Table X.  $\gamma$ -ray and neutron composition with  $^{252}\text{Cf}$  as a function of angle for 2-minute exposure for the cubic cell rotating away from the source.

Angle / °	$\gamma$ -ray events	Neutron events	Total	FoM
90.0	140774±375	30926±176	171700±414	0.850±0.005
67.5	143429±379	31671±178	175100±418	0.84±0.002
45.0	144327±380	32273±180	176600±420	0.83±0.002
22.5	149226±386	33074±182	182300±427	0.84±0.005
0.0	150998±389	32902±181	183900±429	0.86±0.005
-22.5	147343±384	32757±181	180100±424	0.86±0.005
-45.0	143426±379	32174±179	175600±419	0.84±0.002
-67.5	143473±379	31727±178	175200±419	0.830±.002
-90.0	140493±375	31307±177	171800±414	0.84±0.001

Table XI.  $\gamma$ -ray and neutron composition with  $^{252}\text{Cf}$  as a function of angle for 2-minute exposure for the cylindrical cell rotating away from the source.

Angle / °	$\gamma$ -ray events	Neutron events	Total	FoM
90.0	181330±426	45070±212	226400±476	0.89±0.002
67.5	190070±436	48230±220	238300±488	0.88±0.005
45.0	197790±445	50910±226	248700±499	0.87±0.002
22.5	216968±466	57832±240	274800±524	0.89±0.005
0.0	211458±460	56042±237	267500±517	0.88±0.004
-22.5	202684±450	53816±232	256500±506	0.87±0.002
-45.0	199656±447	51244±226	250900±501	0.86±0.004
-67.5	191502±438	47598±218	239100±489	0.86±0.001
-90.0	182114±427	45286±213	227400±477	0.87±0.003

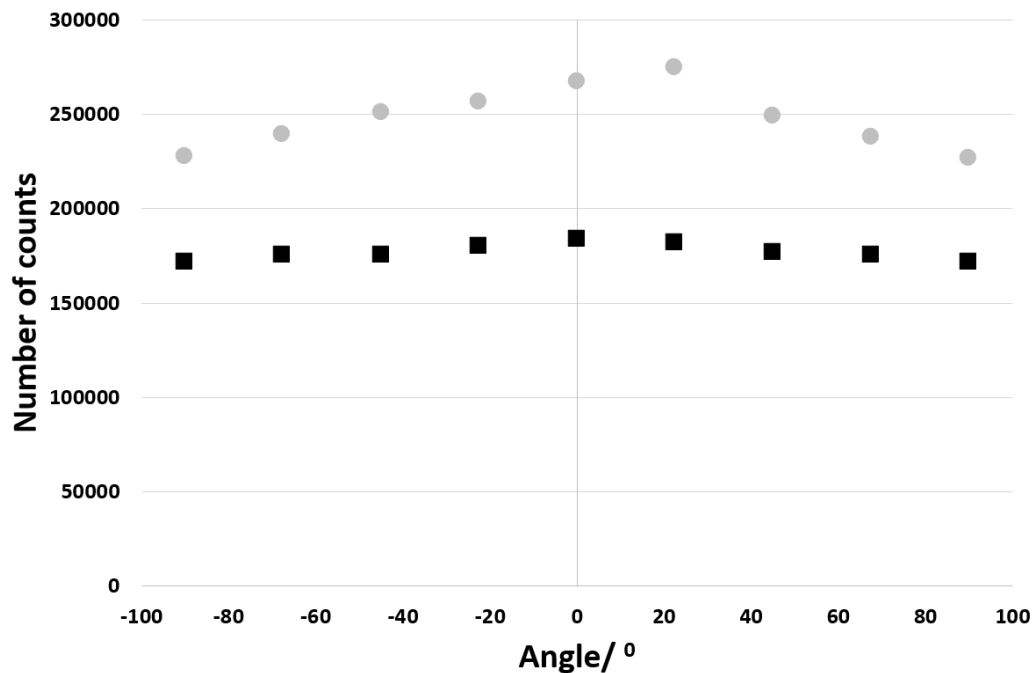


Figure 47. Total counts recorded for the 2-minute exposures of the cubic (black squares) and the cylindrical (grey circles) detector as a function of angle on the horizontal plane.

A novel detection system using neutron/gamma pulse shape discrimination, for use in active interrogation environments

For completeness of the rate dependence study, a last set of experiments was undertaken into face of the cubic cell of the detector which the source is direct towards. For these experiments involving the cubic EJ-309 detector and a  $^{137}\text{Cs}$  source the angle of the detector remained constant, but the detector was rotated by 90 degrees on its axis. Images of the four different positions with the cubic detector can be seen below in Figure 48. These tests were repeated three times for each side of the detector and the count rate averaged. The tests were carried out at two different distances away from the source, initially at 50 mm then with the source against the detector. The end count results are shown in Table XII & XIII.

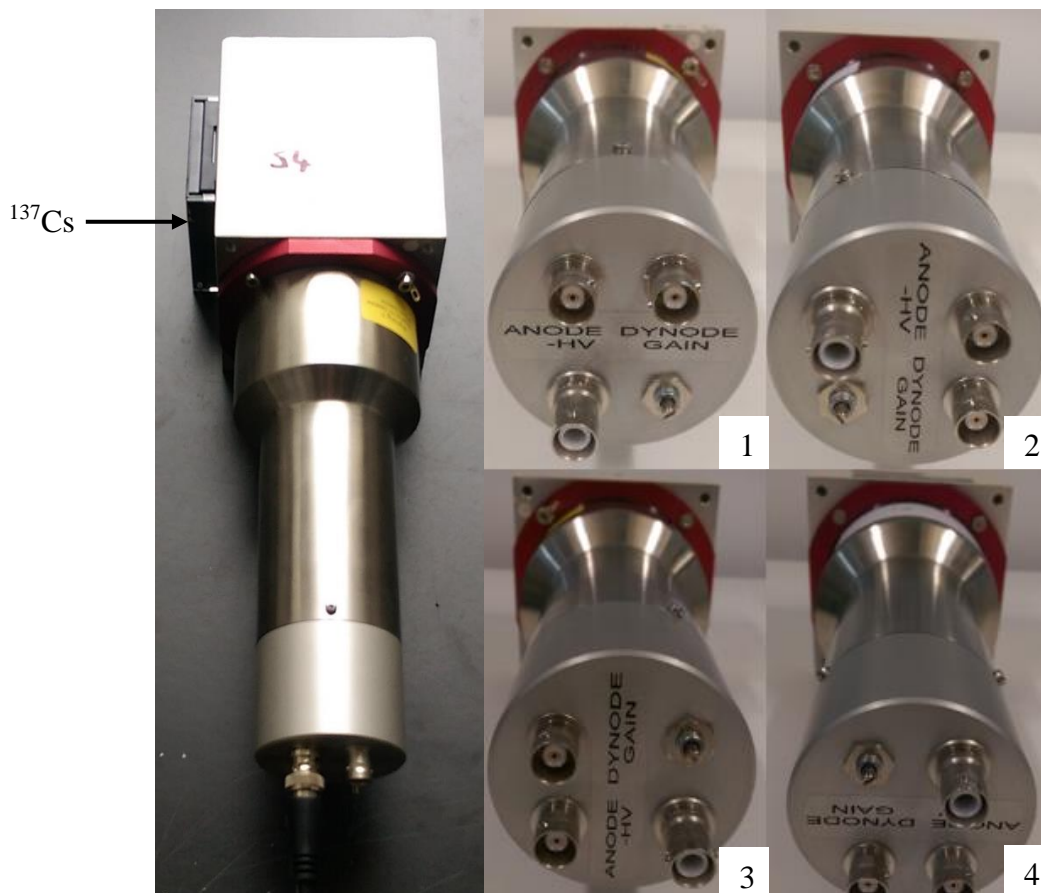


Figure 48 Cubic detector setup for surface of attack experiments.

Table XII.  $\gamma$ -ray count on different faces of the cubic EJ-309 with  $^{137}\text{Cs}$  source 50mm  
away.

Faces	Run 1	Run 2	Run 3	Average
1	662267 $\pm$ 814	663075 $\pm$ 814	660969 $\pm$ 813	662104
2	625870 $\pm$ 791	636767 $\pm$ 798	635066 $\pm$ 797	632568
3	640956 $\pm$ 801	642760 $\pm$ 802	643250 $\pm$ 802	642322
4	658320 $\pm$ 811	652449 $\pm$ 808	654457 $\pm$ 809	655075

Table XIII.  $\gamma$ -ray count on different faces of the cubic EJ-309 with  $^{137}\text{Cs}$  source  
against detector.

Faces	Run 1	Run 2	Run 3	Average
1	1121872 $\pm$ 1059	1101976 $\pm$ 1050	1107770 $\pm$ 1053	1110539
2	1111662 $\pm$ 1054	1124678 $\pm$ 1061	1120776 $\pm$ 1059	1119039
3	1108140 $\pm$ 1053	1114439 $\pm$ 1056	1119663 $\pm$ 1058	1114081
4	1144451 $\pm$ 1070	1129470 $\pm$ 1063	1127957 $\pm$ 1062	1133959

## 5.2 Conclusion

This aspect of the research has several important outcomes that can help utilising detection systems in the future. One of these is the effect of the orientation of liquid scintillators on pulse shape discrimination quality, efficiency and throughput.

In terms of the discrimination performance, Table IX shows that there are only minor fluctuations over the FoM values for both the cell shapes. The only exception to this, which has already been noted, is the  $-90^0$  experiment with the cylindrical detector, which is lacking an internal light guide. In this case there is no discrimination possible as the results produce a single radiation plume of data. Aside from this case

## A novel detection system using neutron/gamma pulse shape discrimination, for use in active interrogation environments

the cylindrical detector returns its poorest performance at small angles away from the horizontal.

From the measurements carried out and the analysis it is clear that when a liquid organic scintillator detector is horizontal the count rates are higher than at other angles. Additionally, the effect of the angle on the count rate is less severe when it is tilted in the positive direction i.e. when the nitrogen void is at the top of the cell, as opposed to the negative direction, where the void is at the interface between the scintillator and the photocathode of the PMT, this was evident with both cell shapes including the cell with the light guide. These observations indicate that these effects should be accounted for in large arrays of liquid scintillation detectors where the angles of the detectors comprising the array can contrast with one another particularly where such arrays might be used for spatial or angular assessment. This is qualitatively consistent with a previous report based on PHS analysis [6] and the hypothesis of restricted light transmission occurring as a result of the position of the expansion volume relative to the optical coupling inside a detector (in the absence of a light guide).

However, the change in count rate reported here has not been previously reported and is of a level of sufficient significance to warrant careful calibration of array systems based on liquids. The results given in Table X & XI, where the detectors are rotated on the horizontal plane parallel with the floor, show values for the total number of events hold less variation throughout the range of angles. The results suggest that the relative angle between the source and the detector does have some effect on the sensitivity of the detector, but does not account for the previously-

observed throughput changes. It also confirms that the poorest FoM results observed initially with the cylindrical detector at small angles away from the horizontal are not caused entirely by the solid angle of the detector facing the source as the FoM values are all consistent once uncertainties have been taken into account.

The final set of experiments involving the sensitivity of organic liquid scintillators investigated the side of the detector facing the source. This gave a good consistency through all the different faces exposed as observed in the average number of counts recorded. With the counts recorded being within 5% of each other when the source is 50 mm away and within 2% of each other when the source is against the detector. This would suggest that the face of the detector that is exposed has no effect on the throughput. The observations that this variable produces no influence and that only a slight contribution is seen from rotating the detector on a horizontal plane with respect to the source, both add weight to the reasoning that the sensitivity of the scintillator is affected due to the void in the cell learned from the initial experiments. The slight drop in the FoM values obtained with the cylindrical detector at very shallow angles is still unattributed to any major effect.

The observations show that to make the assumption that the pulse shape discrimination performance is independent of orientation could be erroneous. As demonstrated in this research, this is particularly evident when manipulating detectors into different positions between tests, as significant shifts in pulse shape can occur, thus requiring a recalibration of PSD threshold settings. It is clear that dramatic shifts in the PHS observed previously [6] can cause the entire discrimination plane to shift, thus requiring revision of PSD threshold settings in some positions, and yet not all, as

A novel detection system using neutron/gamma pulse shape discrimination, for use  
in active interrogation environments

observed in the case of the cylindrical detector at  $-90^{\circ}$ . Clearly, it remains best practice to check HV and PSD thresholds every time a detector is used, particularly when any positional adjustment or transport has occurred in between measurements. Where regular transportation is required, plastic scintillation media ought to be independent of these effects, although notwithstanding the need for a full angular sensitivity assessment of these media to confirm this.

Taken together, the data reported in all of these experiments indicate that where possible, low-hazard organic liquid scintillation detectors should be used in a horizontal arrangement to avoid the orientation dependency shedding a systematic influence on measurements made, particularly on those associated with count rate. In large arrays incorrect conclusions might be drawn from those detectors receiving a higher number of counts when this may purely be an effect of this intrinsic dependence. In best-practice scenarios the results presented in this thesis suggest that if possible liquid scintillators used within large arrays should be orientated in the same manner and where possible should have internal light guides in the scintillator cell. If it is impossible for the liquid scintillators to be placed in the same orientation, then a study to determine the relationship at the different angles should be devised to deduce the throughput between relative detectors rather than the assumption they will be equal. Where an array comprises detectors of different model types, the contrast in the severity of the effect needs to be an additional consideration; this has not been fully investigated in this research due to the extensive range that is available.

### 5.3 References

1. F.D. Brooks, "A scintillation counter with neutron and  $\gamma$ -ray discriminators", *Nucl. Inst. Meth.* (3) pp. 151-163 (1959)
2. N Zaitseva, et al., "Plastic scintillators with efficient neutron/gamma pulse shape discrimination" *Nucl. Instr. and Meth. A* 668 pp. 88-93 (2012).
3. M.J. Joyce, et al., "The design, build and test of a digital analyzer for mixed radiation fields", *IEEE Trans. Nuc. Sci.* 57 (5 pt. 2) 5603496 pp. 2625-2630 (2010).
4. M.J. Joyce, et al., "Real-time, pulse-shape discrimination in non-hazardous fast liquid scintillators: prospects for safety and security", *IEEE Trans. Nuc. Sci.* 59 (4 pt. 2) 6133314 pp. 1245-1251 (2012).
5. M. Flaska and S. A. Pozzi, "Identification of shielded neutron sources with the liquid scintillator BC-501A using a digital pulse shape discrimination method", *Nucl Inst. Meth A* 577 (3) pp. 654-663 (2007).
6. S. F. Naeem, et al., "Response of liquid scintillator assemblies as a function of angular orientation", *Nucl. Inst. Meth. Phys. Res. A* 749 pp. 35-41 (2014).
7. M.J. Joyce, et al., "A 16-channel real-time digital processor for pulse-shape discrimination in multiplicity assay", *IEEE Trans. Nuc. Sci.* 61 (4) pp. 2222-2227 (2014).
8. B. D'Mellow, et al., "Digital discrimination of neutrons and  $\gamma$ -rays in liquid scintillators using pulse gradient analysis" *Nucl. Instr. and Meth. A* 578 (1) pp. 191-197 (2007).
9. S. F. Naeem, et al., "Response of liquid scintillator assemblies as a function of angular orientation", *Nucl. Inst. Meth. Phys. Res. A* 749 pp. 35-41 (2014).

## 6 Radiation Hardness Tests & Trigger Tests

### 6.1 EJ-301 Radiation Hardness

A set of experiments was undertaken exploring the EJ-301 organic liquid scintillator in terms of the radiation hardness and tolerance of the detector. Information about the levels of radiation on liquid scintillators before damage occurs are desirable especially the saturation level when looking at active interrogation. The use of the EJ-301 detector was due to its size to fit within the irradiator chamber unlike the gated plastic or either of the different shaped liquid EJ-309 detectors. The irradiator facility used for the tests is located at the Dalton Cumbria Facility (DCF), Cumbria, United Kingdom. This facility houses a self-shielded model 812  $^{60}\text{Co}$  gamma irradiator that was developed and installed by Foss Therapy Services, Inc. shown in Figure 49. The irradiator is capable of supplying absorbed dose rates from 240 Gy/hr up to 27,000 Gy/hr. These dose rates can be attenuated and shielded to match desired experimental setups. The irradiator consists of three source rods that can be used simultaneously or individually depending on the desired dose. The irradiator chamber has two service ports of 19 mm diameter to accommodate cables for power supplies and signals.

A novel detection system using neutron/gamma pulse shape discrimination, for use in active interrogation environments



Figure 49.  $^{60}\text{Co}$  gamma irradiator, Foss Therapy Service, Inc.

The dose rate within the irradiator was measured using an ion chamber dose sensor model 10x6-0.18 supplied by Radcal. The ion chamber has a detection limit between 500 nGy/s to 6.31 Gy/s. This dose rate data is fed through a Radcal Accu-Dose+ digitizer module model ADDM+ to a desktop computer. The ion chamber was placed at the position in which the sensitive area of the detector would be positioned and the source exposed for a minute to gather a dose rate reading. It was expected to be able to observe degradation in either the pulse shape or throughput when radiation damage was starting to take place, at which point the exposure would be terminated.

The initial setup at DCF using the EJ-301 liquid scintillator was to expose this to roughly a 1000 Gy/hr  $\gamma$ -ray dose rate and observe the pulses produced as well as the

A novel detection system using neutron/gamma pulse shape discrimination, for use  
in active interrogation environments

throughput. The actual measured dose rate with the Radcal ion chamber was 942 Gy/hr  $\pm 2\%$ . The liquid scintillator was placed inside the irradiator as shown in Figure 50, with the power supply control box shielded further still behind a lead block as shown. The high voltage was supplied via a coaxial cable through the side of the irradiator chamber. The signal was fed back the same way.

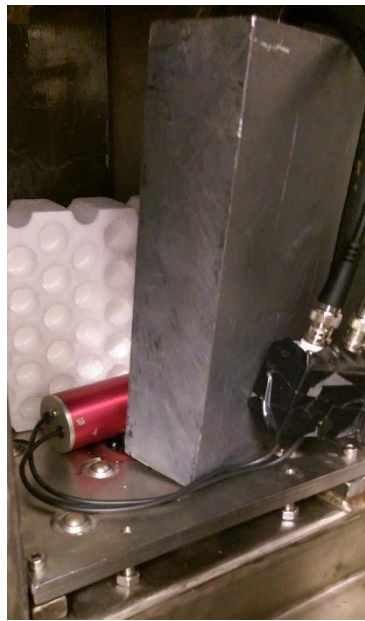


Figure 50. EJ-301 organic liquid scintillator inside the  $^{60}\text{Co}$  irradiator.

The polystyrene in front of the detector was used to prevent the detector from moving whilst being investigated and polystyrene was used due to its lack of attenuation. Once the setup was in place the irradiator was closed and the  $^{60}\text{Co}$  was raised into place for exposure. It was observed that the instant the sources were raised the detector went dead, producing no pulses or signal at all. Upon the detector going dead, the sources were retracted and the detector became instantly operational again. This instant recovery of the detector suggests that the problem the detector exhibited was not due to damage, as this would be expected to exhibit a gradual recovery if any

A novel detection system using neutron/gamma pulse shape discrimination, for use in active interrogation environments

at all. With this knowledge it was concluded that the detector must have become saturated due to the dose levels being used. To try and determine if there would be any radiation damage of the detector at this level of dose rate a long exposure was run, 50 minutes, giving a total dose of approximately 0.8 kGy, after this dose the detector was observed to still be operating as normal.

To try and corroborate this idea the dose rate was progressively reduced to try and find the point at which it saturated. Initially the dose rate was halved to 420 Gy/hr  $\pm 2\%$ , this exhibited the same result as previously with the detector instantaneously producing no pulses or signal output and hitting its saturation point. To find a dose rate that the detector could withstand more attenuation was added inside the irradiator. The final setup in which the detector was operational is shown below in Figure 51.



Figure 51. EJ-301 organic liquid scintillator inside the  $^{60}\text{Co}$  irradiator.

## A novel detection system using neutron/gamma pulse shape discrimination, for use in active interrogation environments

The dose rate was reduced to the minimum obtainable within the irradiator which was 9.9 Gy/hr  $\pm 2\%$ , at this dose rate the detector remained operational for the first few seconds of exposure, with intermittent count readings and producing some miss-shaped pulses. It is presumed that this dose rate is just above the upper saturation limit of the detector. The test was repeated three times and each resulted in a prominent plume of gamma counts as well as noise for these first few seconds. This is suggestive that the detector is on the verge of saturation at 9.9 Gy/hr for these first few seconds, before becoming fully saturated. This study was intended to give some idea of region that would saturate the PMT's coupled in the scintillator detectors described for this work, however due to the lack of space within the irradiator chamber the EJ-301 liquid scintillator was the only detector to fit. Meaning that only an idea on the saturation limit of the older smaller PMT could be established. Also due to the limitation on the smallest dose rate that can be provided by the irradiator an exact figure was unable to be determined. This does however give an upper limit onto the rate of saturation that can be expected.

### 6.2 Trigger tests

The next set of experiments utilised the recent development in plastic scintillators exhibiting PSD. This detector consisted of an integrated gating circuit on the PMT. This set of experiments investigated the ability to control when the PMT (and consequently, when the detector is active) by stimulating the trigger circuit using a strobe light. This allows for a user to control when the device will be active remotely.

## A novel detection system using neutron/gamma pulse shape discrimination, for use in active interrogation environments

The ability to interrogate objects non-destructively is a very attractive way of detecting special nuclear materials and, in particular active interrogation may hold the key to detecting highly enriched uranium when concealed intentionally [1]. Perhaps the most popular active interrogation method is that where the object or target in question is bombarded with neutrons [2] or photons [3, 4]. The use of neutrons as the interrogating medium is more widely associated with NDA due to their use in reactors to initialise the fission process in the power sector. However, the use of photons as the interrogating media, classed as photofission, is being considered increasingly for the identification of materials from both delayed radiation emissions [5, 6] and prompt emission [7, 8]. The active interrogation techniques are used to produce a mixed radiation field (i.e. comprising both  $\gamma$  rays and neutrons). This field can then be detected using a scintillation detector, converting the radiation into light. In this form the pulses corresponding to the radiation are converted relatively easily into an electrical signal by a photocathode and amplified with a photomultiplier tube (PMT). The amplified pulses can then be analysed to characterize the material in question.

Such a mixed radiation field can be separated into its  $\gamma$ -ray and neutron constituents by pulse-shape discrimination (PSD) [9]. Several different discrimination techniques have been developed [10]. The technique used in this research that allows for real-time analysis is pulse gradient analysis (PGA) [11]. PGA exploits the difference between the decay of  $\gamma$ -ray and neutron pulses and is based on a bit-shifting comparison of the normalized amplitudes of samples in this time dependence.

Interrogative neutron and photon procedures produce inevitably an associated prompt  $\gamma$ -ray emission, hereafter referred to as the  $\gamma$  flash. This arises due to the

A novel detection system using neutron/gamma pulse shape discrimination, for use  
in active interrogation environments

interrogation beam itself as well as the very short-lived nuclear states that contribute to the  $\gamma$ -ray continuum for the nuclei in the sample. This can be of an intensity sufficient to saturate the PMTs and thus, where a pulsed stimulus is used, a period of time is required for the system to recover before useful neutron-related data can be obtained. To alleviate this effect, some passive methods have been explored, for example such as, trying to shield the instrumentation from the effects of the  $\gamma$  flash with high-Z materials such as lead [12]. An immediate consequence of this is that the shielding reduces the effect of the  $\gamma$  flash as desired, but also reduces the intensity of the neutrons that constitute the assay. This introduces a perturbation to the measurement and, for intense interrogative procedures, it is likely that cumbersome quantities of high-Z material would be necessary.

An alternative approach to isolate the system from the deleterious effects of the  $\gamma$  flash is to record data exclusively after the intense transients have diminished to a level at which the detector is sensitive again. This requires that the detection system is held in a quiescent state until the prompt  $\gamma$  emission has passed. The research described concerns a prototype system designed to trigger the PMT of a low-hazard, solid organic scintillator detector. The approach explored in this research is relevant to applications where it is desirable for the PMT to be switched off for the  $\gamma$  flash and switched on to capture the delayed radiation (neutron and gamma) data at some point afterwards. Hypothetically, this would allow the use of real-time, high-intensity interrogation of objects without detector saturation problems, leading to a very effective system for security and safeguards applications.

## A novel detection system using neutron/gamma pulse shape discrimination, for use in active interrogation environments

Relatively little research has been reported concerning the remote triggering of organic scintillation detectors, allowing both neutrons and  $\gamma$  rays to be detected simultaneously via PSD at a synchronized point in time. It is not apparent that any other research has addressed this problem, particularly with real-time digital PSD and solid organic scintillators, as described here. Neither are there any prior reports of the specific gated detector unit investigated in this research. Previously, a PMT has been triggered using a signal generator and delay circuitry using a lanthanum bromide scintillator [13]. This research demonstrated triggering of a PMT for indirect measurements of fast neutrons, by virtue of associated capture  $\gamma$ -ray emissions, in the presence of an intense  $\gamma$  flash. It also demonstrated that the gating technique suppressed the saturation of the PMT, with the restoration time of the PMT gain after being gated calculated to be 0.5  $\mu$ s. However, a critical distinction of that from this research is that it was the capture  $\gamma$ -rays that were detected in the metal halide scintillator, i.e. those stimulated by the neutrons rather than a direct detection of the neutrons themselves. A further distinction of the system described in this research is that it is also triggered by a stimulus from a separate detector rather than a feed from the source of interrogation.

In this research the DC input signal to the gating unit is provided by a trigger circuit specifically designed in this research. The term trigger circuit refers to this separate circuit that has been designed and is external to the detector unit, as opposed to the gating circuit which is the gating board integrated within the detector unit. This trigger circuit uses a silicon PIN photodiode (Hamamatsu S1223-01) [14] as its sensor device. A photon-based stimulus causes a change in the output of the photodiode which

## A novel detection system using neutron/gamma pulse shape discrimination, for use in active interrogation environments

is then passed through an operational amplifier to constitute the trigger signal. A schematic of the circuit is shown in Figure 52.

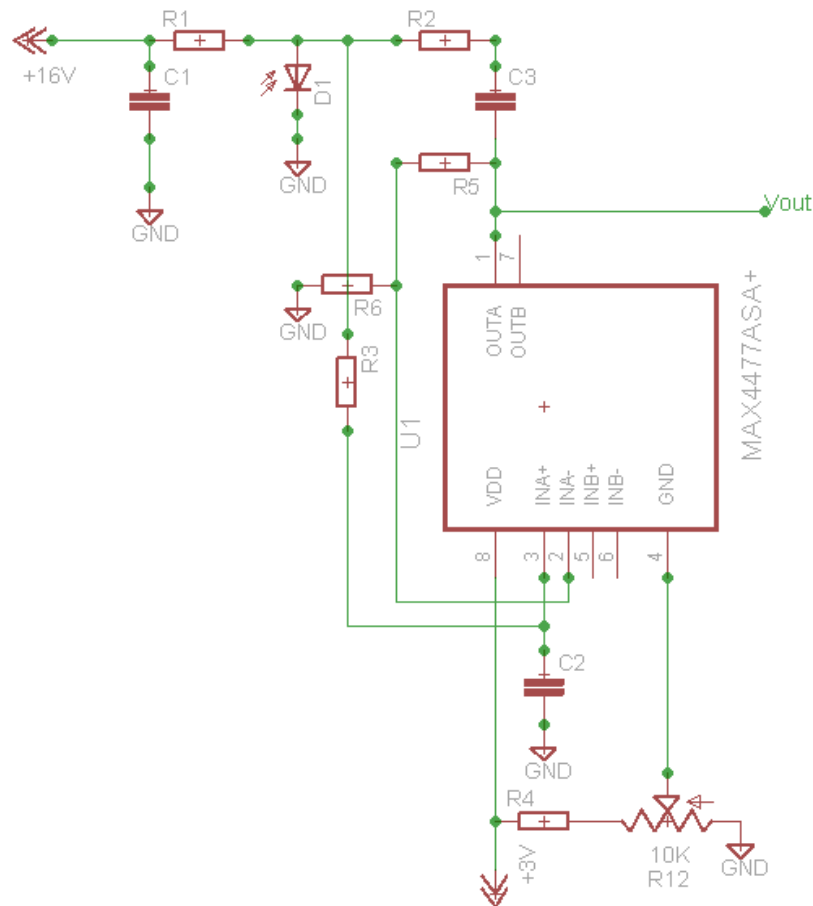


Figure 52. The circuit diagram of the trigger-signal circuit utilizing a silicon PIN diode developed in this work.

In the absence of a trigger pulse, the signal output from the VS1173-30 detector unit is passed to a 4-channel MFA [15]. Whilst only one channel is used in this research, the 4-channel device has been selected as the full prototype system is likely to be used as part of an array of detectors to ascertain directional information.

The adopted approach was to use a separate detector to provide the trigger signal to the gating unit, allowing for the system to be independent of an interrogating

## A novel detection system using neutron/gamma pulse shape discrimination, for use in active interrogation environments

feed signal or any pulse generator. It was also to make use of radiation of a different type to that central to the assay to constitute the trigger stimulus.

In these tests the trigger circuit was tested in response to a strobed light source. This was used since the photons produced by the light source stimulate the response of the PIN photodiode without the need for repeated use of an intense, pulsed  $\gamma$ -ray source and the associated, necessary precautions and logistical issues. This enabled an experimental campaign to prove the concept in the first instance prior to active tests, and to demonstrate light-based triggering of a fast neutron detector system, as might be desirable for some industrial applications such as nuclear decommissioning. The light source had limited settings and was set to run at a frequency of 20 Hz, with a 50% duty cycle. Under ideal circumstances of full illumination and darkness with zero switching time, 50% of the events would be anticipated from the plastic scintillator detector from the strobe light source. Due to the response time of the trigger circuit and the PMT, it is expected intuitively to observe slightly less than 50% of the counts. The output of the trigger circuit when exposed to the light source was observed with an oscilloscope to check that the signal supplied to the gating unit within the detector was satisfactory to switch the detector between states. The time-versus voltage trace for the response of the silicon PIN photodiode as well as the output from the complete trigger circuit are shown in Figure 53.

A novel detection system using neutron/gamma pulse shape discrimination, for use in active interrogation environments

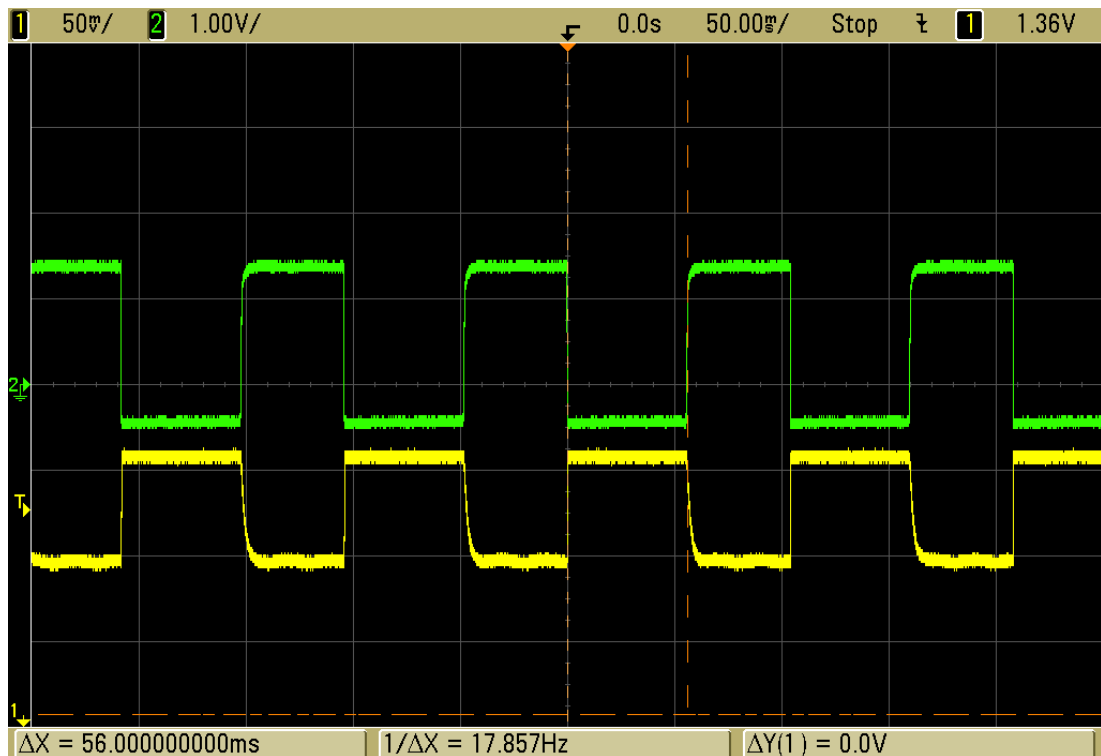


Figure 53. Oscilloscope traces of the PIN photodiode response under exposure to the strobed light (20 Hz) green trace (top) and the output from the trigger circuit (with voltage offset for clarity), yellow trace (bottom). Each square represents 50ms in the x axis and 1 V in the y axis.

As can be seen with the markers above, the PIN photodiode is operating as sensing light (negative going) for 56 ms out of every 100 ms. The trigger circuit produces a high signal (turning the PMT on the gated detector off) for this full 56 ms. The switching time for the trigger circuit from a high signal to a low signal (so to switch the PMT back to an operational state) is shown in Figure 54.

A novel detection system using neutron/gamma pulse shape discrimination, for use in active interrogation environments

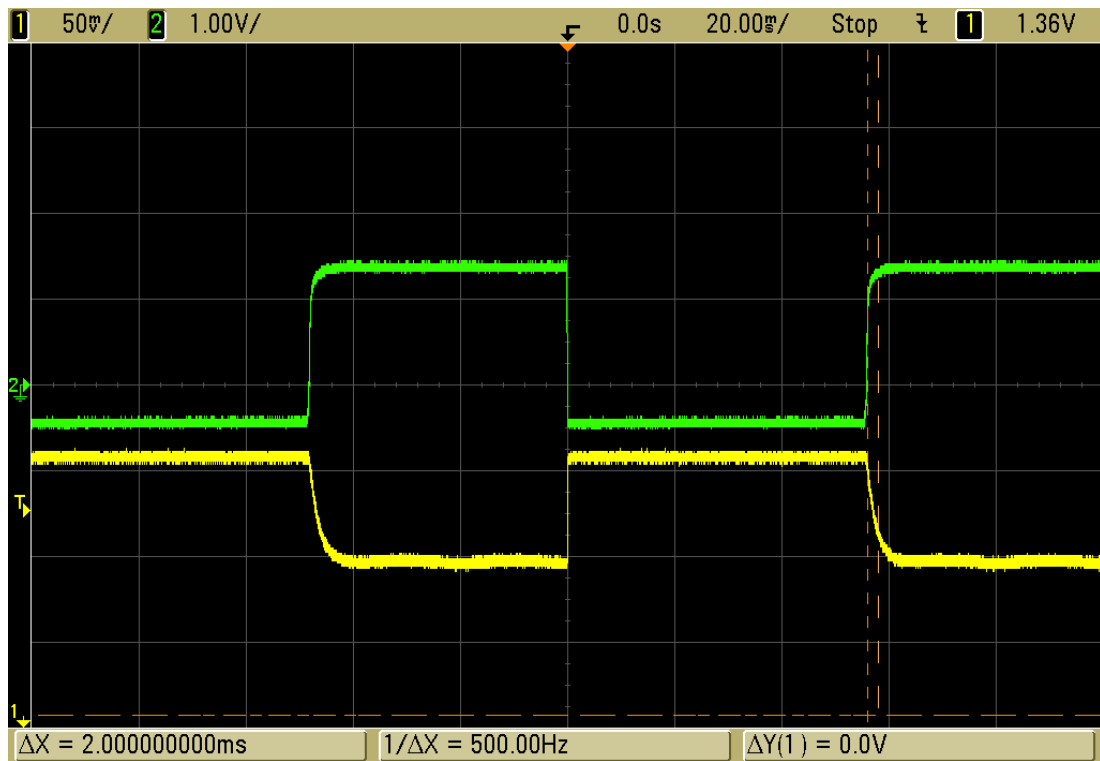


Figure 54. Switching time for the trigger circuit from a high signal (PMT off), to a low signal (PMT on), the PIN photodiode response under exposure to the strobe light (20 Hz) green trace (top) and the output from the trigger circuit (with voltage offset for clarity) yellow trace (bottom). Each square represents 20ms in the x axis and 1 V in the y axis.

The oscilloscope trace in Figure 54, shows that the time for the signal to switch within the trigger circuit is 2ms. Along with the shorter period due to the response of the silicon PIN photodiode, the gated detector is expected to be operational for 46 ms out of every 100 ms, i.e. ~46% of the time. This is depicted in Figure 55.

A novel detection system using neutron/gamma pulse shape discrimination, for use in active interrogation environments

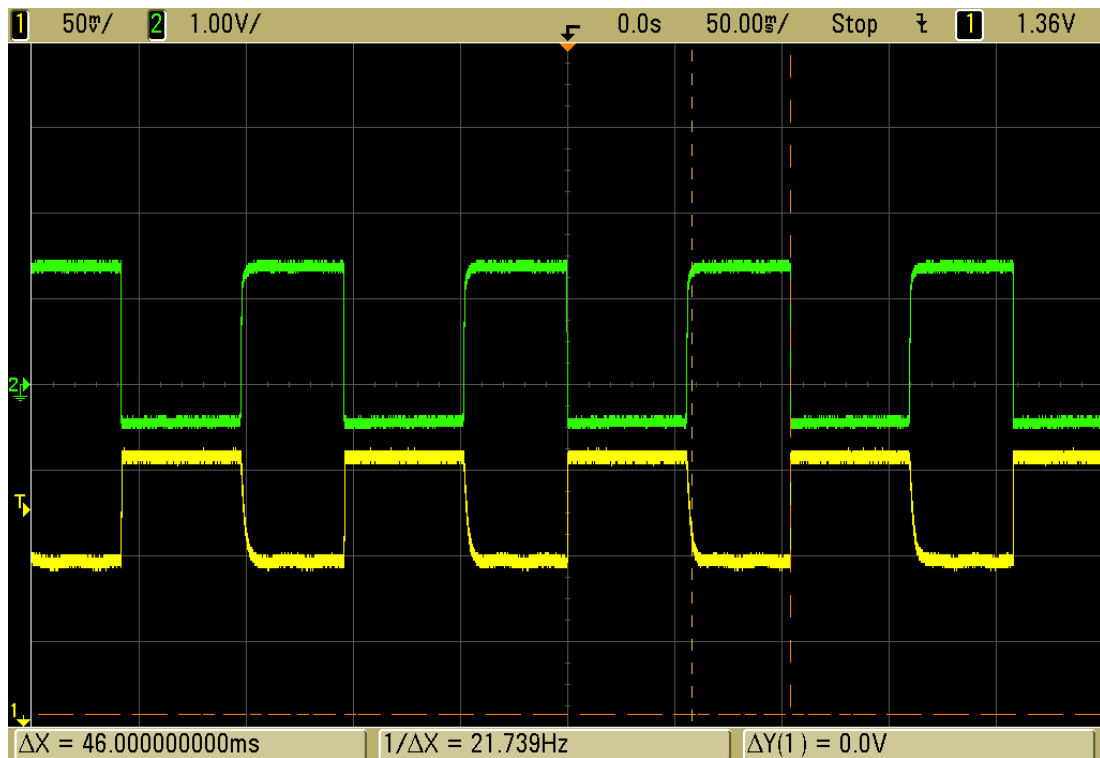


Figure 55. Low signal output from the trigger circuit, meaning gated detector is active, the PIN photodiode response under exposure to the strobed light (20 Hz) green trace (top) and the output from the trigger circuit (with voltage offset for clarity) yellow trace (bottom). Each square represents 50ms in the x axis and 1 V in the y axis.

The next part of the experimental programme was to assess the operation of the detector without the gating unit in order to both provide a basis for the normal response of the detector system, and to obtain a base count rate for comparison purposes for the triggered tests. The background tests were made with a 400 kBq  $^{137}\text{Cs}$  source placed 10 cm away from the face of the detector, and exposed for a 20-minute period. The MFA was placed into MCA mode (in which pulse-height distributions (PHD) are provided for calibration purposes as opposed to PSD mode). The detector settings were adjusted until a satisfactory calibration was achieved based on the position of the Compton edge. The detector was then connected to the trigger circuit

A novel detection system using neutron/gamma pulse shape discrimination, for use in active interrogation environments

and the strobe light switched on to serve as the trigger stimulus. The external trigger circuit was then placed in a sealed box with the strobe light source. A schematic diagram of the experimental setup for this part of the research is given in Figure 56. The PHD for the detector with and without triggering is shown in Figure 57. It is worthy of note that the acquisition times for this part of the research were not common. The objective was to obtain MCA plots with sufficient data to confirm that the shapes of the PHD with/without triggering were qualitatively consistent with one another, rather than quantitatively equivalent. Hence there are many more counts in the un-triggered case compared to that under triggering even accounting for the effect the triggering has.

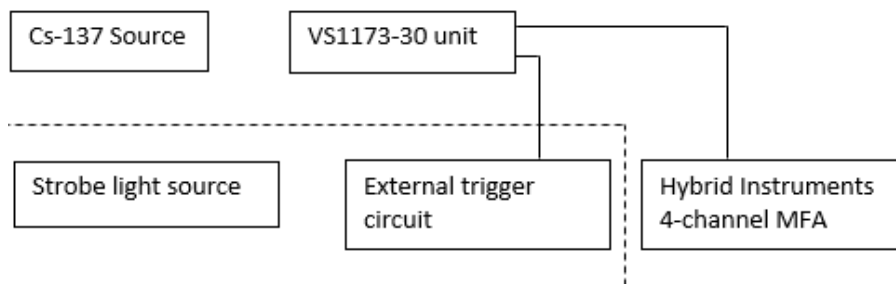


Figure 56. A schematic diagram of the experimental setup prepared for the trigger experiments described in this research.

A novel detection system using neutron/gamma pulse shape discrimination, for use in active interrogation environments

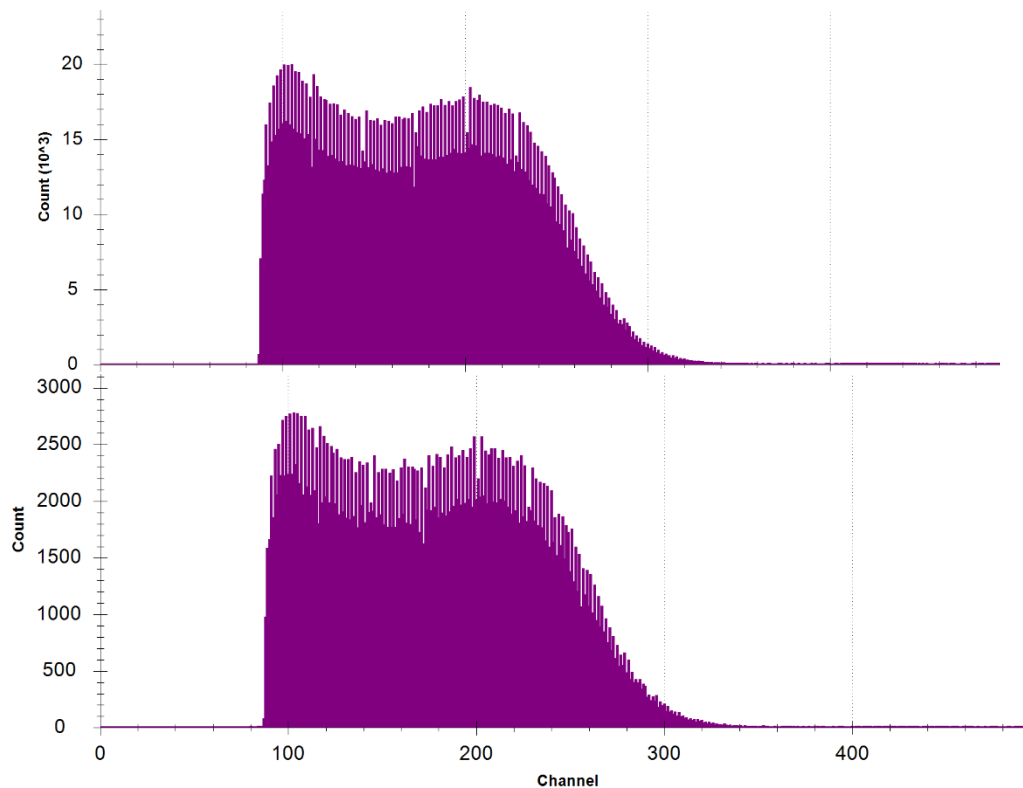


Figure 57. Pulse-height spectra (PHS) from the MFA operating in MCA mode of counts versus channel number with the VS1173-30 system exposed to  $^{137}\text{Cs}$ , without triggered (top), with triggering (bottom). Data were acquired to ensure qualitative consistency of PHS shape only; hence the acquisition periods were not the same for both plots.

Once the PHD measurements had been completed multiple 20-minute runs were carried out, again with  $^{137}\text{Cs}$  to obtain an average number of counts from the detector in both triggered and un-triggered arrangements. Two example scatter plots from these runs are shown in Figure 58, for each of the triggered and un-triggered cases. The average number of counts is shown below for each scenario in Table XIV.

A novel detection system using neutron/gamma pulse shape discrimination, for use in active interrogation environments

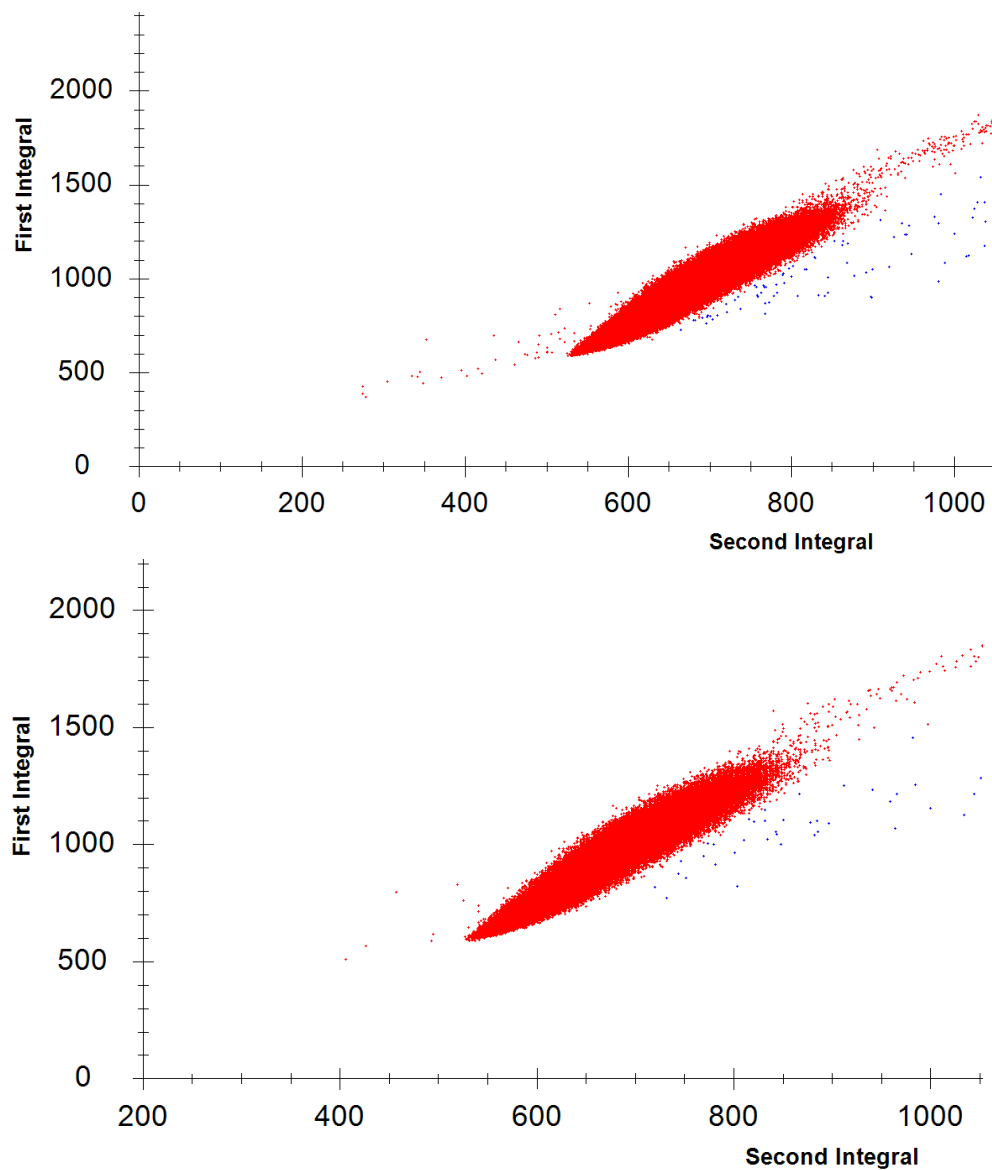


Figure 58. Scatter plots of first integral versus second integral for the system developed in this research exposed to  $^{137}\text{Cs}$  for 20 minutes, without triggering (top) and whilst being triggered by a strobe light source at 20 Hz, 50% duty cycle (bottom).

To demonstrate the robustness of the system the tests were repeated with the source closer to the detector to see if the gated system exhibited any degree of dependence on the counting rate. These second set of tests were conducted with the

A novel detection system using neutron/gamma pulse shape discrimination, for use  
in active interrogation environments

source as close as possible to the detector, resulting in roughly a 20% increase in counts. The corresponding results are given in Table XV.

Table XIV. The Average Number of Total Counts During 20-minute Exposure to  $^{137}\text{Cs}$ .

	Without triggering	With triggering
Total counts	748895±865	344131±587
Percentage / %	100	45.95±0.10

Table XV. The Average Number of Total Counts During 20-minute Exposure to  $^{137}\text{Cs}$  with Closer Proximity.

	Without triggering	With triggering
Total counts	906716±952	416395±645
Percentage / %	100	45.92±0.08

From Figures 57 & 58, it is clear that the MCA and the PSD scatter plots are virtually indistinguishable from each other for the triggered / no trigger scenarios by eye. This confirms that the gating system on the detector is not influencing the throughput of radiation information significantly and, perhaps more importantly, is not influencing the real-time PSD functionality of the instrument chain.

In both sets of experiments the percentage of the total counts with the trigger has dropped to 46%, which is what is expected from looking at the oscilloscope traces from the photodiode and trigger circuit. With both tests producing the same percentage drop in counts when under different intensities, this confirms that from these two

A novel detection system using neutron/gamma pulse shape discrimination, for use in active interrogation environments

setups, there is no evidence for any dependence on count rate and the effect of the gating element on the device for a ~20% increase in rate.

The next stage in the experimental process was to follow the same approach, but in a mixed-field to simulate the environment the system will eventually be used in. For all experiments, standard exposure tests run without the trigger being applied to the system were used as a base to work from prior to running the tests with the system being triggered. The mixed-field tests were conducted using the  $^{252}\text{Cf}$  source previously described. The source was moved to the side of the inner hull during exposure such that it is a distance of approximately 150 mm away from the front face of the detector. The results from these measurement are provided in Table XVI and the PSD scatter plots are shown in Figure 59.

Table XVI. The Average Number of Total Counts During 20-minute Exposure to  $^{252}\text{Cf}$ .

	Without triggering	With triggering
Count rate / $\text{s}^{-1}$	418932±647	198867±446
Percentage / %	100	47.5±0.1

A novel detection system using neutron/gamma pulse shape discrimination, for use in active interrogation environments

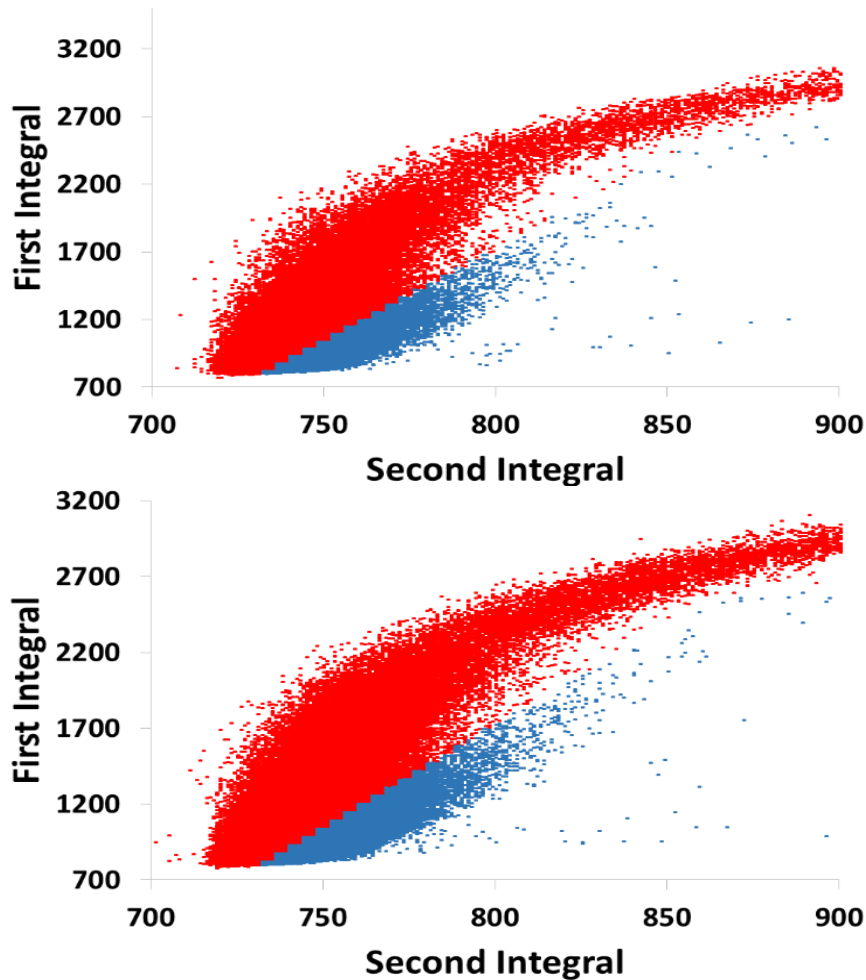


Figure 59. PSD scatter plots of first integral versus second integral for the system developed in this research exposed to  $^{252}\text{Cf}$  for 20 minutes, without triggering (top) and whilst being triggered by a strobe light source at 20 Hz, 50% duty cycle (bottom). Aside from triggering all other aspects of the measurements were unchanged.  $\gamma$ -ray events are denoted in red (upper) and neutrons in blue (lower).

The results from the experiment produced 47.5% of counts compared to the tests with the  $^{252}\text{Cf}$  without triggering. This is a slightly higher percentage than when the triggering was measured being exposed to the  $\gamma$ -ray source and, although the difference is small in absolute terms, it is outside of the uncertainties in the measurements. This was not realised until after the experiments, and the output of the trigger circuit was not observed through an oscilloscope during the  $^{252}\text{Cf}$  tests, as it

was presumed to be the same. However, possible explanations for this higher percentage of counts could be because the PIN diode was illuminated more effectively by the strobed source in the  $^{252}\text{Cf}$  source room than for the  $^{137}\text{Cs}$  tests. This could have been down to the lower light levels in the room and the strobe light being a closer proximity to the diode. More effective illumination by the light source due to the confined space could have yielded a greater intensity of illumination on the photodiode, and thus a higher voltage yield. The falling edge of the diode response with time when a strobe pulse ends is, to first order, one of exponential decay. Thus, in this case, the photodiode takes longer to return to the baseline and switch the detector back on than for the more distant case when the illumination is reduced. As is observed, the photodiode being on for longer results in a closer correlation to the strobed duty cycle, resulting in a greater proportion of acquisition compared to the case when the strobe is further away. Notwithstanding these effects, the difference observed appears unlikely to hold any significance in terms of the application of the technique, it is likely that the effectiveness of the triggering lies with the response of the detector (i.e. the silicon PIN photodiode), rather than anything else.

### 6.3 Analysis

The experiments with the  $^{252}\text{Cf}$  exhibit a poorer discrimination performance than expected when used with the water-based  $^{252}\text{Cf}$  source. In the literature it has been noted that plastic scintillators give a poorer performance than liquid scintillators in general use [16], although it is also reported that the plastic lacks specifically

A novel detection system using neutron/gamma pulse shape discrimination, for use  
in active interrogation environments

performance in the low-energy regions for neutrons below the 1 MeV level. The neutron energy spectrum from the  $^{252}\text{Cf}$  source has a most probable neutron energy of 0.7 MeV. It is hypothesised that this, alongside the moderation effect of the water tank in which the source is located, is the contributing reason for why the discrimination plot is not comparable to what was expected when compared to the liquids.

Due to the poor performance of the detector system in separating the radiations into two distinct regions, confirmation that the two regions that were being seen were associated with neutrons and  $\gamma$  rays respectively was required. These regions were verified by adding in different types of shielding. Four runs were carried out, all without any gating being applied to the detector: a background run in-situ, a run with no shielding and the source exposed, a run with lead shielding whilst the source was exposed and finally a run with polyethylene shielding whilst the source was exposed. The scatter plots from these runs can be seen in Figure 60 with the count rates and the FoM calculated in Table XVII.

A novel detection system using neutron/gamma pulse shape discrimination, for use in active interrogation environments

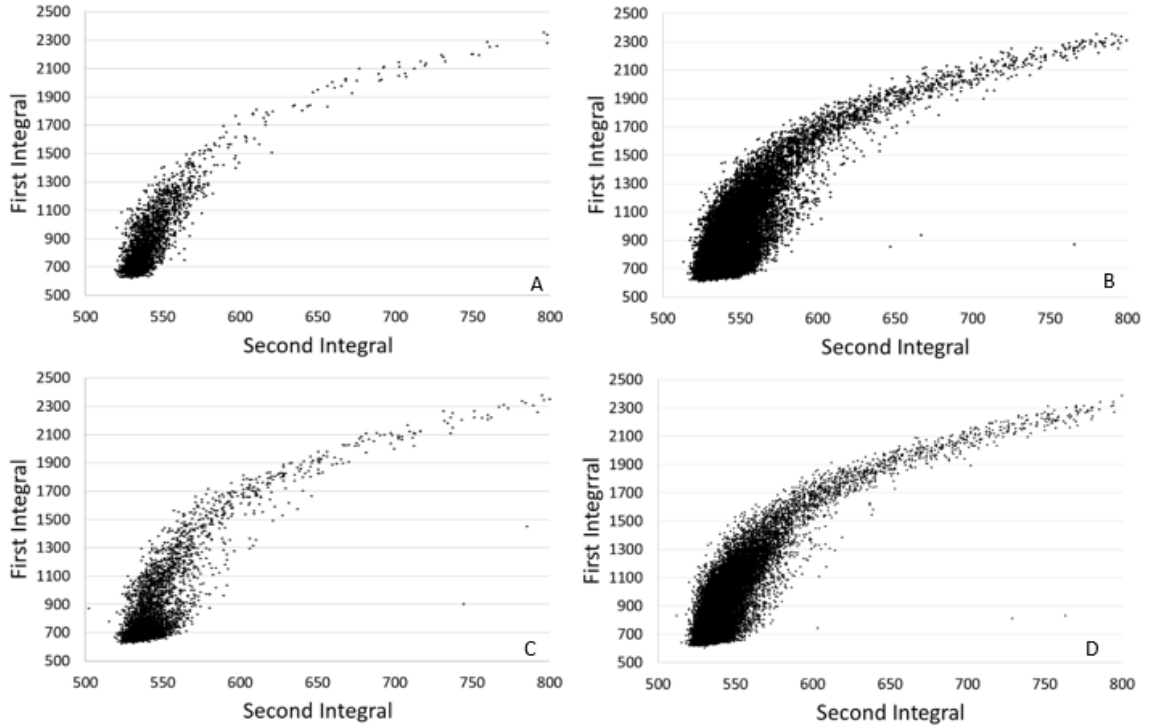


Figure 60. Individual runs of 5 minutes, A. Background run in-situ, B.  $^{252}\text{Cf}$  exposed with no shielding, C.  $^{252}\text{Cf}$  exposed with lead shielding, D.  $^{252}\text{Cf}$  exposed with polyethylene shielding.

Table XVII. Total number of counts for each run (relating to Figure 65).

Run	Gamma Count	Neutron Count	Gamma/Neutron ratio	Total Counts	FoM
A				3095±56	N/A
B	35807±189	2693±52	13.30	38500±196	0.37±0.002
C	3082±56	462±21	6.67	3544±60	0.41±0.005
D	29495±172	1005±32	29.35	30500±175	0.36±0.004

For run C the amount of lead used for shielding was 20cm thick and for run D the amount of polyethylene was 10cm thick, these values can be used to work out the

A novel detection system using neutron/gamma pulse shape discrimination, for use  
in active interrogation environments

relative intensity of gamma rays that are being seen by the detector by using the equation,

$$I_x = I_0 e^{-\mu x} \quad \text{[Equation 20]}$$

where  $I_x$  is the intensity at a set distance,  $I_0$  is the initial intensity,  $\mu$  is the linear absorption coefficient and  $x$  is the distance. This can be rearranged to work out the relative intensity of radiation after a block of shielding compared to before. For lead the linear absorption coefficient for 1 MeV gamma rays is 0.8 [16] which gives the relative intensity to be very small when used 20cm of lead at 0.00001%.

The polyethylene that was used measured 10 cm thick with a linear absorption coefficient for 1 MeV gamma rays of 0.070 [17]. This gives an intensity after the polyethylene shielding of half the intensity before the shielding.

As can be seen from the scatter plots comparing B to C, the lead shielded case shows an expected reduction in the observed gamma portion but retains most of the limited neutron portion that is observed. Unlike the polyethylene shielded case, as seen comparing B to D, the gamma portion is still evident whilst the bottom right of the plot which was the previously visible neutron plume is reduced. This verifies that what is actually being seen in the bottom right of the plume is associated with neutrons from the source, and that lead shielding is required to discern the two regions with more accuracy. The total number of counts shown in Table XVII for each run also adds validity to the experiment, with the highest counts being observed when there is no shielding present, and the polyethylene shielded case exhibiting a slightly lower number of counts as the shielding reduces the already low number of neutrons. The lead shielding has the greatest effect, significantly reducing the high number of

gammas the greatest source of radiation. The best results for the FoM values are obtained when lead shielding is present, illustrated by the increased clarity of the scatter plot as a result of the lower statistics being dealt with. To try and determine whether the moderation of the water surrounding the source had any impact on the performance and the quality of the separation produced, experiments were scheduled with two bare sources at another facility for comparison, see chapter 7.

## 6.4 Conclusion

The purpose of the trigger experiments was to demonstrate whether the gating unit would be suitable for holding the detector dormant when required. The experiments were designed to trigger when the detector was active by using an external stimulus; a strobe light. Initial experiments were concerned with whether the incorporation of a gating unit would negatively impact the quality of pulses that are produced and subsequently affect the scatter plots produced by the digitiser system. The scatter plots that are shown earlier in section 6.2 Figure 57, 58 & 59 give satisfactory evidence that the gating unit does not have an effect on the quality of the information obtained when compared to the gating not being in use.

The trigger circuit shown in Figure 52 has a theoretical duty cycle from the strobe light of 50%. The output from the trigger circuit showed that this theoretical duty cycle of 50% had already dropped to 46% active period by the time it reached the output of the circuit. The gamma source experiments showed that the number of counts observed at two different proximities from the source was at a rate of 46% for the

triggered runs relative to the runs without triggering. The experiments with the mixed field source gave better results in relation to the count rate, with a 47.5% count rate observed as measurements from the PIN diode and complete trigger circuit supplying the gated PMT were not observed through the oscilloscope at the time a maximum detector relative count percentage could not be calculated. However, it is reasonable to assume that as before the detector is likely to be operating to the same frequency as the trigger circuit and the losses are associated with the silicon PIN photodiode rather than the gating board or detector. These tests have proved in principle the working operation of the gating unit to hold the detector in a dormant state whilst a trigger signal is being provided but to recover and be operational when there is no signal.

## 6.4 References

1. R.C. Runkle, D.L. Chichester, S.J. Thompson, “Rattling nucleons: New developments in active interrogation of special nuclear material”, *Nucl Inst. Meth A* 663 (1) pp. 75-95 (2012)
2. C.D. Clemett et al., “Neutrons for active detection of special nuclear material: An intense pulsed  ${}^7\text{Li}(p,n){}^7\text{Be}$  source”, Nuclear Science Symposium and Medical Imaging Conference, IEEE, NSS/MIC’12
3. C. Hill et al., “Photofission for active SNM detection I: intense pulse 8MeV Bremsstrahlung source” Nuclear Science Symposium Conference Record, IEEE, NSS’12
4. P. Mistry et al., “Photofission for active SNM detection II: intense pulsed  ${}^{19}\text{F}(p,\alpha\gamma){}^{16}\text{O}$  characteristic  $\gamma$  source” Nuclear Science Symposium Conference Record, IEEE, NSS’12
5. M. Agelou, et al., “Detecting special nuclear materials inside cargo containers using photofission” Nuclear Science Symposium Conference Record, IEEE, NSS’09

6. J. Kavouras et al., "Pulsed photofission delayed gamma ray detection for nuclear material identification" Nuclear Science Symposium and Medical Imaging Conference Record, IEEE, NSS/MIC'12
7. J.M. Mueller, M.W. Ahmed, H.R. Weller, "A novel method to assay special nuclear materials by measuring prompt neutrons from polarized photofission", *Nucl Inst. Meth A* 754 (1) pp. 57-62 (2014)
8. J.M. Mueller et al., "Tests of a novel method to assay SNM using polarized photofission and its sensitivity in the presence of shielding", *Nucl Inst. Meth A* 776 (1) pp.107-113 (2015)
9. F.D. Brooks, "A scintillation counter with neutron and  $\gamma$ -ray discriminators", *Nucl. Inst. Meth.* (3) pp. 151-163 (1959)
10. K.A.A. Gamage, M. J. Joyce and N. P. Hawkes, "A comparison of four different digital algorithms for pulse-shape discrimination in fast scintillators" *Nucl. Instr. and Meth. A* 642 (1) pp. 78-83 (2011).
11. B. D'Mellow, et al., "Digital discrimination of neutrons and  $\gamma$ -rays in liquid scintillators using pulse gradient analysis" *Nucl. Instr. and Meth. A* 578 (1) pp. 191-197 (2007).
12. A. Laptev, et al., "Baseline distortion effect on gamma-ray pulse-height spectra in neutron capture experiments" *Nucl. Instr. and Meth. A* 543 (2-3) pp. 502-508 (2005).
13. K.Y. Hara, et al., " $\gamma$ -Flash suppression using a gated photomultiplier assembled with an LaBr<sub>3</sub>(Ce) detector to measure fast neutron capture reactions" *Nucl. Instr. and Meth. A* 723 pp. 121-127 (2013).
14. Hamamatsu Si PIN photodiodes S1223 series Datasheet, Accessed 29/06/2016 ([http://www.hamamatsu.com/resources/pdf/ssd/s1223\\_series\\_kpin1050e.pdf](http://www.hamamatsu.com/resources/pdf/ssd/s1223_series_kpin1050e.pdf))
15. Hybrid Instruments 4 Channel MFA Datasheet, Accessed 29/06/2016 (<http://hybridinstruments.com/products/mfax4.3.html>)
16. S.A. Pozzi, M.M. Bourne, S.D. Clarke, "Pulse shape discrimination in the plastic scintillator EJ-399-33", *Nucl Inst. Meth A* 723, pp. 19-23, (2013)

A novel detection system using neutron/gamma pulse shape discrimination, for use  
in active interrogation environments

17. NIST Physical Measurement Laboratory X-Ray mass attenuation coefficients  
data sheet, Accessed 29-06-2016  
<http://physics.nist.gov/physrefdata/xraymasscoef/tab3.html>

## 7 Plastic Scintillator Performance Improvements

The next set of experiments were undertaken at Sheffield University using bare  $^{252}\text{Cf}$  and bare Am-Be sources, and the plastic EJ-299-33 both in an un-triggered and triggered state. The motivation behind this set of experiments was to attempt to get a better response from the plastic detector for discriminating in mixed fields due to the higher energy neutrons that are observed from an Am-Be source, as the quality of separation observed in the Lancaster experiments were of lesser quality than has been observed in the literature [1, 2]. The research from these sources highlights that the ability of the plastic to discern neutron radiation below 1 MeV rapidly decreased with energy, due to the pulse shapes becoming more difficult to discern, thus leading to poor discrimination. This means that the tests carried out earlier using the water based  $^{252}\text{Cf}$  source, compound the difficulty with discrimination in this pulse height region, as the most probable neutron energy from the source is 0.7 MeV, for example [3]. Two sources were utilised at Sheffield so that there was a direct comparison between two bare sources allowing the conclusion to be made into whether the Lancaster source results could have been attributed to the moderation effect of the aqueous environment. The setup of the experiments carried out with the Am-Be and  $^{252}\text{Cf}$  source can be seen in the image below. In Figure 61, the source is not shown in the image, but when in use, is rested across the two clamp stands as indicated.

A novel detection system using neutron/gamma pulse shape discrimination, for use in active interrogation environments

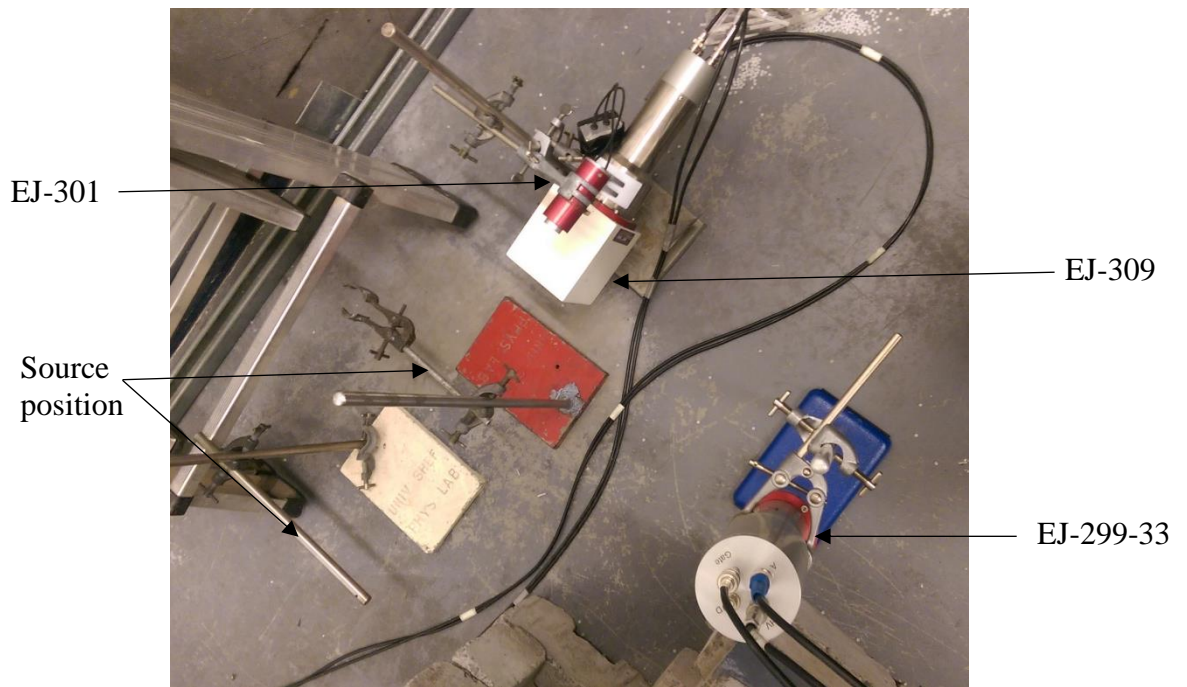


Figure 61. Detector and source arrangement.

The Am-Be experiments were carried out with an extensive range of settings to try and find the optimum placement of the second integral (discrimination sample) in terms of discrimination performance. The PSD scatter plots for three of these tests can be seen below in Figure 62.

A novel detection system using neutron/gamma pulse shape discrimination, for use in active interrogation environments

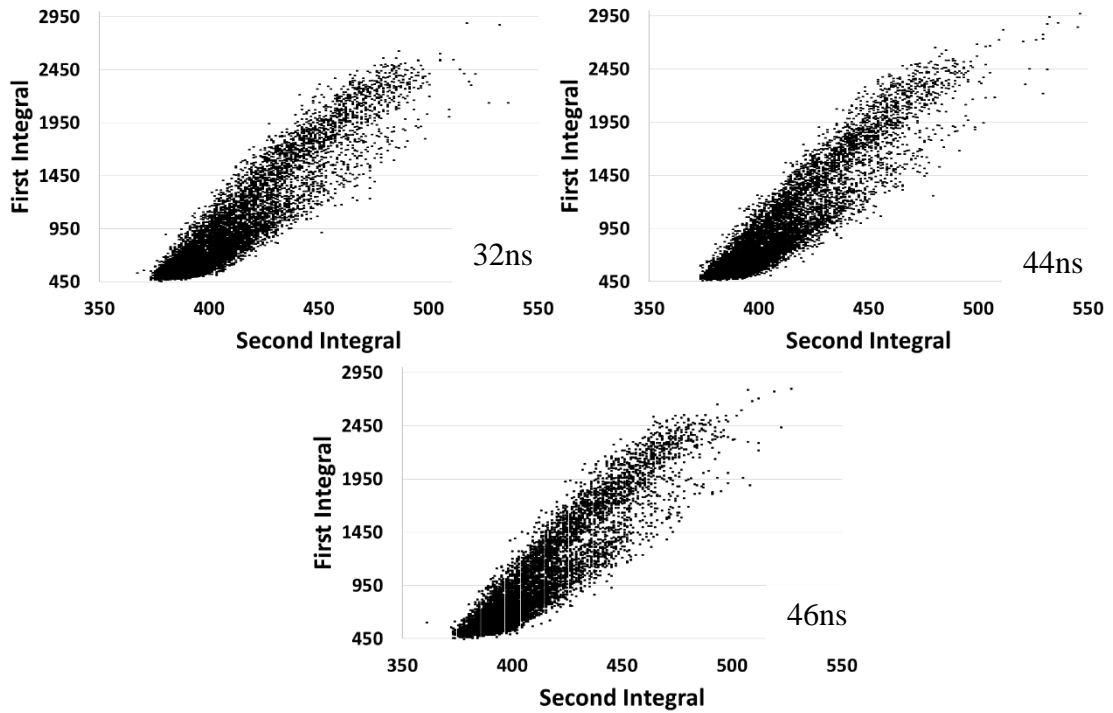


Figure 62. Three different second integral settings using the EJ-299-33 exposed to an Am-Be source, sample position denoted lower right.

These scatter plots highlight some separation at a high second integral point that is more distinct than for the Lancaster  $^{252}\text{Cf}$  tests, but this is still not as evident as has been reported elsewhere. Using the optimum settings from the above Am-Be tests, the next tests were carried out for both the bare Am-Be and  $^{252}\text{Cf}$  without being triggered, and then being triggered using the strobe light. This cross comparison was motivated to rule out the possibility that the improvement in quality is from the source situation being bare rather than water-based, as the water is a moderator reducing the neutron energies. A scatter plot from a 5 minute exposure to each source individually can be seen in Figure 63.

A novel detection system using neutron/gamma pulse shape discrimination, for use in active interrogation environments

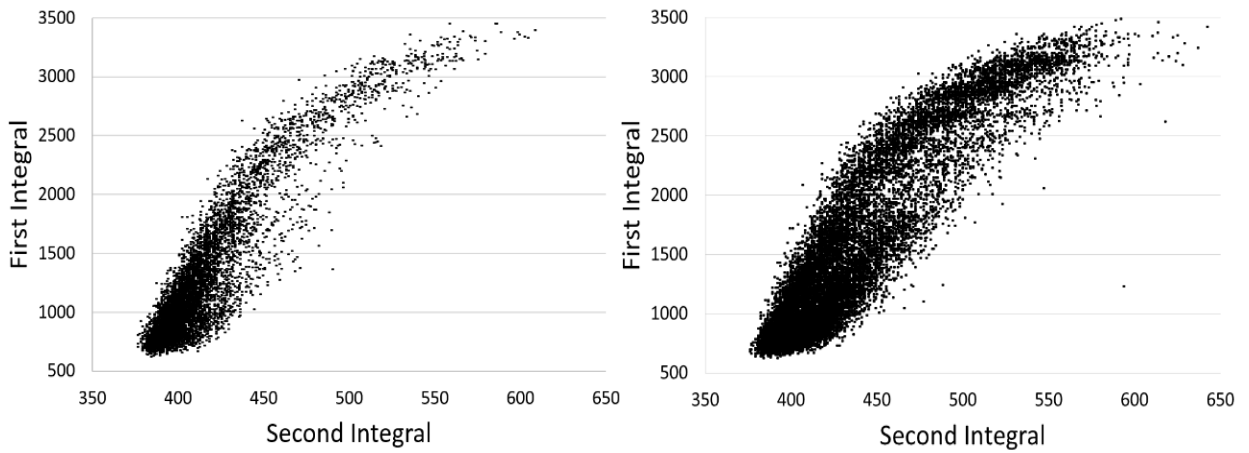


Figure 63. Scatter plots of EJ-299-33 exposed to  $^{252}\text{Cf}$  (left), and Am-Be (right).

Although the  $^{252}\text{Cf}$  plot is not as densely populated due to the lower activity of this source and the number of counts observed, it does show a poorer performance of separation than that of the Am-Be, verifying the initial hypothesis. To quantify the separation, the detector was then investigated with the triggering in use for both sources. The resulting scatter plots can be seen below in Figure 64, and the number of counts and FoM are given in Table XVIII.

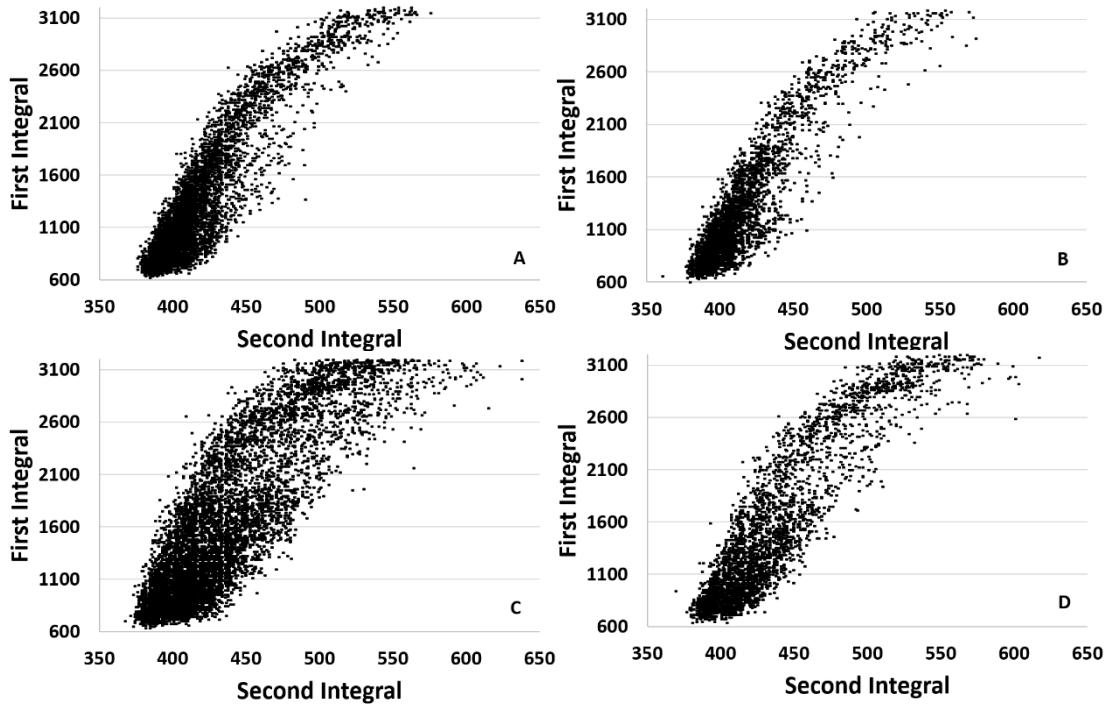


Figure 64. Scatter plots using the EJ-299-33 detector, A. Un-triggered exposed to  $^{252}\text{Cf}$  for 5 minutes, B. Triggered exposed to  $^{252}\text{Cf}$  for 5 minutes, C. Un-triggered exposed to Am-Be for 1 minute, D. Triggered exposed to Am-Be for 1 minute.

As can be seen from the scatter plots, the exposure time to each of the sources was different, 5 minutes for the  $^{252}\text{Cf}$  and 1 minute for the Am-Be. Different exposure times were used due to the different activities of the sources.

## 7.1 Analysis

The aim of these experiments was to determine if the PSD quality of the plastic scintillator detector was of a greater quality using a source producing a different spectrum of radiation, an Am-Be source. Some of the scatter plots finding the optimum placement of the second integral delay are shown in Chapter 7 Figure 62, with the corresponding normalised plots shown in Figure 65. The FoM results showing the

A novel detection system using neutron/gamma pulse shape discrimination, for use in active interrogation environments

quality of separation calculated for second integral delays of 44, 46 and 48 ns are shown in Table XVIII.

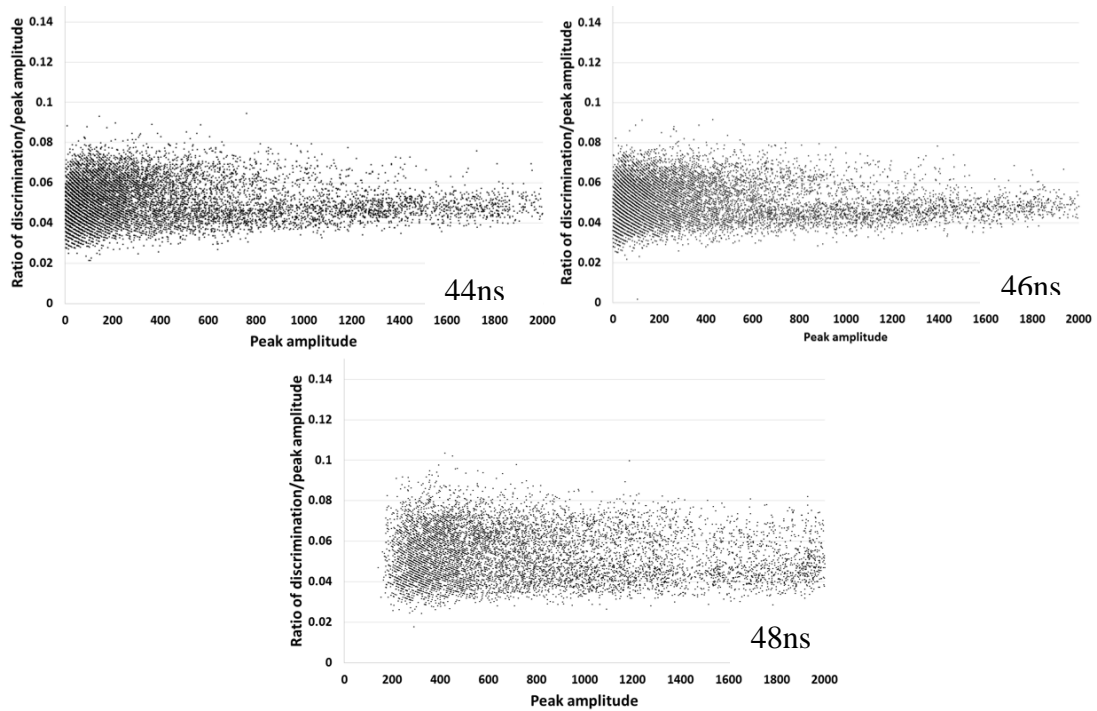


Figure 65. Normalised plots for the EJ-299-33 exposed to an Am-Be source with different second integral delays.

Table XVIII. FoM values for different 2nd integral delay times.

2 <sup>nd</sup> integral delay (ns)	FoM
44	0.52±0.005
46	0.56±0.001
48	0.54±0.001

The next setup, using the Am-Be and <sup>252</sup>Cf sources individually for both triggered and non-triggered tests, produced the normalised plots shown in Figure 66. The number of counts and FoM can be seen in Table XIX.

A novel detection system using neutron/gamma pulse shape discrimination, for use in active interrogation environments

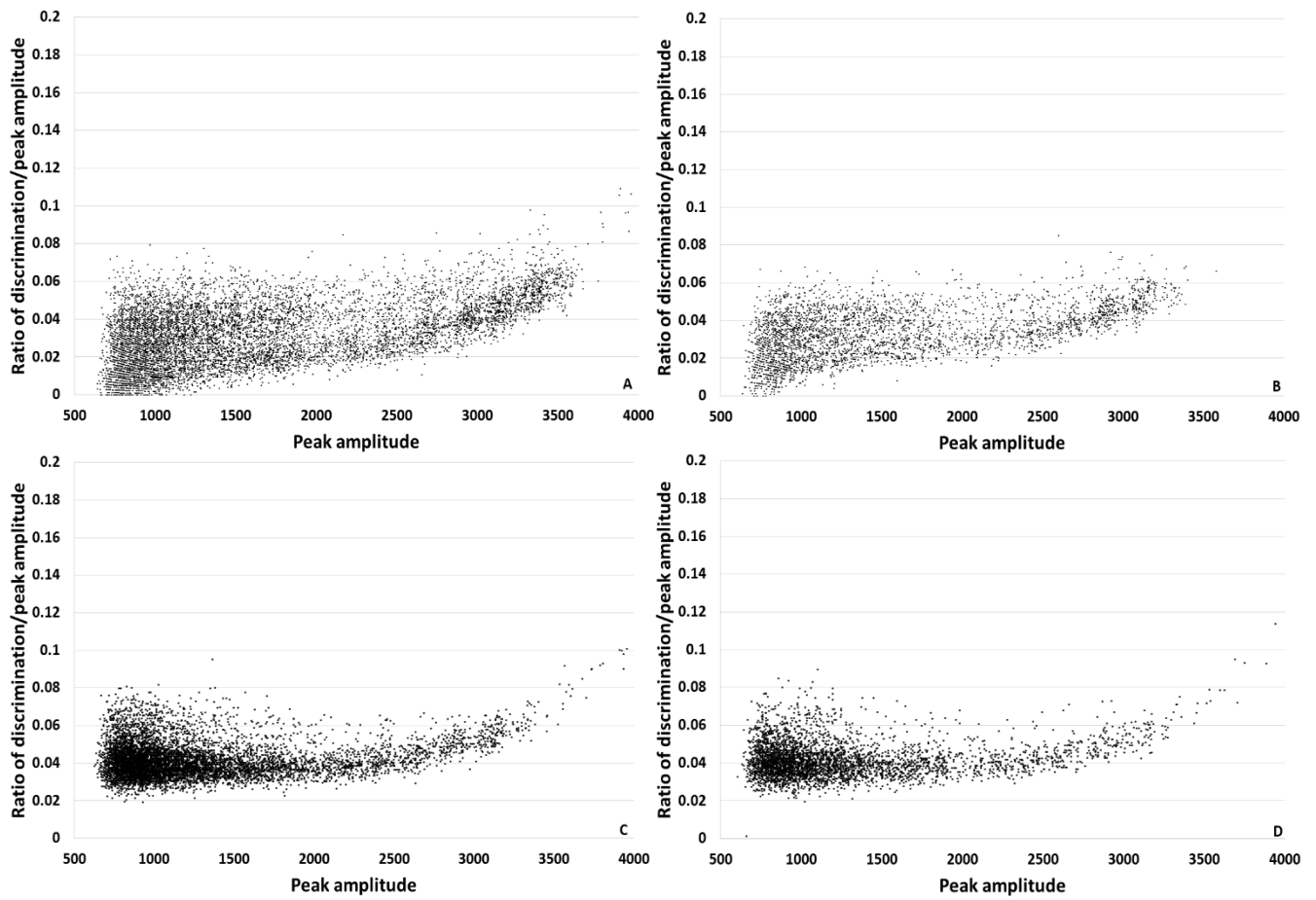


Figure 66. Normalised scatter plots for the EJ-299-33 A. Un-triggered exposed to  $^{252}\text{Cf}$  for 5 minutes, B. Triggered exposed to  $^{252}\text{Cf}$  for 5 minutes, C. Un-triggered exposed to Am-Be for 1 minute, D. Triggered exposed to Am-Be for 1 minute.

A novel detection system using neutron/gamma pulse shape discrimination, for use  
in active interrogation environments

Table XIX. Count data and FoM values for un-triggered and triggered cases for 1 minute  
Am-Be exposures and 5 minute <sup>252</sup>Cf exposures.

	Neutron Counts	Gamma Counts	Total Counts	Ratio	Percentage	FoM
Am-Be Un- triggered	3302	5398	8700±93	1.63		0.49±0.003
Am-Be triggered	1553	2546	4099±64	1.64	47.1%	0.47±0.001
<sup>252</sup> Cf Un- triggered	1757	6120	7877±89	3.48		0.32±0.005
<sup>252</sup> Cf triggered	836	2911	3747±61	3.48	47.5%	0.32±0.001

## 7.2 Conclusion

As shown the trigger circuit appears to work reliably with two different sources, still giving between 47-47.5% of the count rate as expected. The ratio of gamma rays to neutrons seen by the plastic detector for the <sup>252</sup>Cf source is also comparable to that with the liquid scintillator detector used in the earlier angular orientation experiments, adding confidence to the measurements even though the FoM value is low. As hypothesised the FoM value for the bare Am-Be source at Sheffield is higher than that for the water-based <sup>252</sup>Cf source at Lancaster. The FoM values obtained from the earlier tests finding the optimum second delay time gave higher results than in these trigger tests, this has been associated with the length of the run being greater, giving more statistics and allowing for smaller sample ranges for the histogram resulting in a more accurate value. Even with this greater degree of separation in comparison to other

published research carried out using plastic scintillators, it still is not as prominent as reported using the charge comparison method [4].

## 7.2 References

1. N Zaitseva, et al., “Plastic scintillators with efficient neutron/gamma pulse shape discrimination” *Nucl. Instr. and Meth. A* 668 pp. 88-93 (2012).
2. Q. Nishada “Characterisation of a new type of solid organic scintillator for neutron-gamma discrimination using pulse-shape discrimination techniques”
3. R.C. Martin, J.B. Knauer, P.A. Balo, “Production, Distribution, and Applications of Californium-252 Neutron Sources.” (1999)
4. S.A. Pozzi, M.M. Bourne, S.D. Clarke, “Pulse shape discrimination in the plastic scintillator EJ-399-33”, *Nucl Inst. Meth A* 723, pp. 19-23, (2013)

## 8 Chopped Gamma Triggering System

For the gated detector, once the concept had been proved using a strobe light source, it was required to show that a radiation sensitive detector would be able to be used in place of the PIN photodiode. The adopted approach was to replace the strobed light source with a chopped radiation source as the proof for this. A  $^{137}\text{Cs}$  source was used in conjunction with a system to modulate the radiation intensity on the detector, and thus produce a signal similar to that of the strobe light source. The only other research that has been reported in this area was a similar experiment at low frequencies, with a resonating tuning fork driven by a controller [1], similarly this was being used to strobe a light source. The same tuning fork device was considered but for chopping a gamma source over a light source. This would have required replacing the vanes on the tuning fork, this consists of 0.35mm metal and would be required to be lead so as to have sufficient shielding to block the gamma source when the vanes were closed. The highest frequency that these current devices can run at is 6 kHz, and this is before increasing the mass by changing the vanes to lead. Other drawbacks to this system include; the requirement for it to be pre-programmed to one set frequency, and the requirement for a control unit to operate the tuning fork.

Instead it was decided to design and manufacture a system with a rotating lead window. The advantages to tackling the problem this way meant that in spinning the device, this could have varying speed capabilities up to the maximum of the system. It was decided to use a Dremel 4000 series motor to spin the lead window, due to the

A novel detection system using neutron/gamma pulse shape discrimination, for use  
in active interrogation environments

variability in the speed settings and the ability of the Dremel unit to reach a maximum of 35,000 rpm. This is faster than any other system that could be sourced. For each rotation the window will be open for two periods of radiation and closed for two periods. The design for the experiments can be seen in Figure 67. The design consists of two support poles that hold two cross beams. These cross beams have slots that have been cut out to hold the lead screen and are held at a set height using wing nuts. The lead screen has a small opening with which a small offset piece of lead is aligned with. The small piece of lead window was soldered to the spindle of the Dremel motor and rotates to close or open the window, and allow the radiation to reach the detector on the opposite side. The whole design is enclosed in a Perspex box that has been added as a safety precaution in relation to spinning lead at such speeds. The lead window itself was made relatively small measuring 20 mm x 20 mm. This was to reduce the size of the object being rotated to minimise any slowing effect from the air or distortion of the window itself due to the malleable nature of lead. This system was fully designed and manufactured as part of this research for this thesis.

A novel detection system using neutron/gamma pulse shape discrimination, for use in active interrogation environments

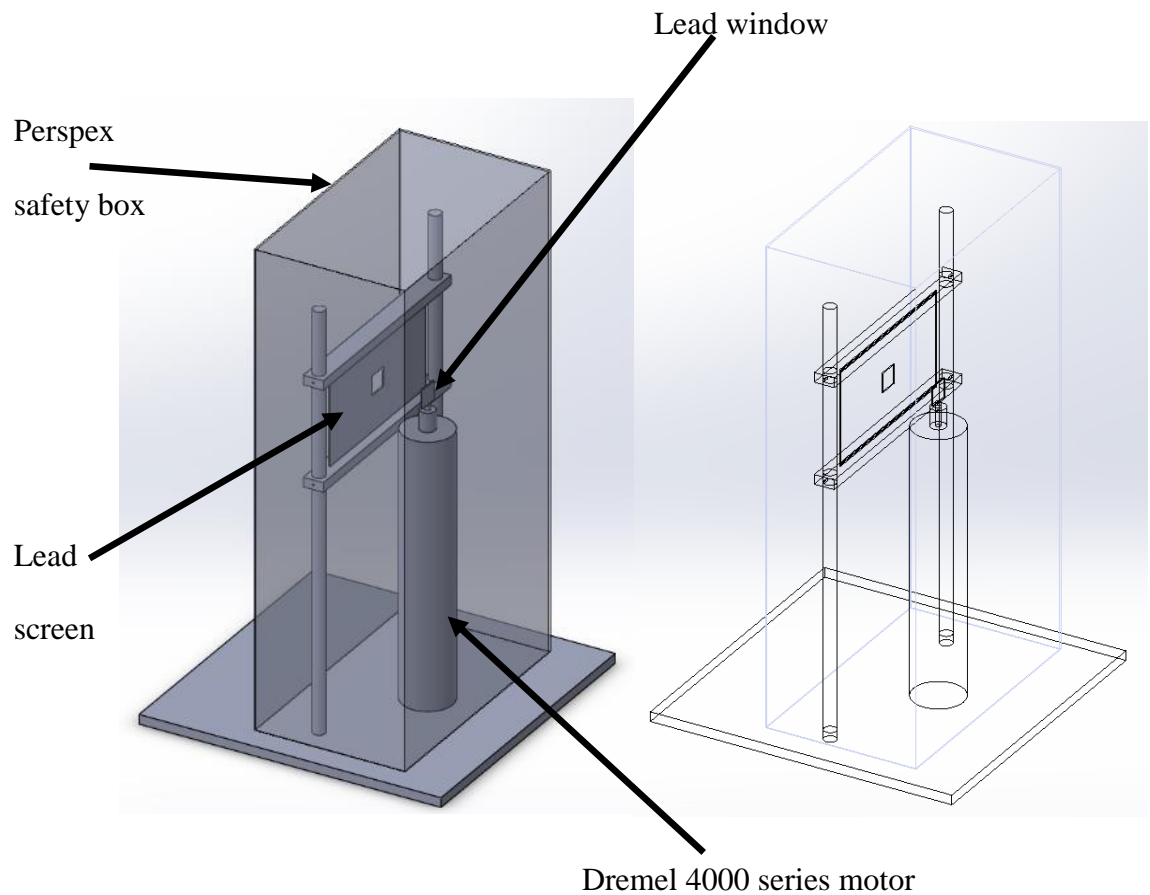


Figure 67. Design for chopped gamma experiments.

The detector chosen to act as the trigger was the EJ-301 liquid scintillator due to its availability, good PSD qualities and fast response. This was coupled to a single channel Hybrid Instruments MFA. The TTL output for the gamma constituents would be used as the signal to stimulate the trigger circuit in placement of the previously used silicon PIN photodiode. Tests were carried out to make sure that the lead chopper worked and chopped the radiation source to a satisfactory standard, as the trigger circuit and subsequently the gated detector had already been proved satisfactory.

Testing used a  $^{137}\text{Cs}$  source placed directly behind the lead screen positioned in line with the spinning window, and with the EJ-301 detector being held 100 mm

A novel detection system using neutron/gamma pulse shape discrimination, for use in active interrogation environments

away from the spinning window on the opposite side. These first tests kept the rotation of the window at 5,000 rpm. The tests were run with a source for 10 minutes and the number of counts were recorded, with each run repeated multiple times and the data averaged. Table XX shows the difference between when the window was left open, left closed, and rotating at 5,000 rpm.

Table XX. Count rates for chopped gamma field tests.

	Window open	Window closed	Window rotating at 5,000 rpm
Total average counts	36525±191	31860±178	37570±194

Due to the number of counts increasing when the device was switched on the next step was to look at the background counts with no source and investigate the origin of the increased number of counts. The results for the background count rate when no source was present are shown in Table XXI.

Table XXI. Background count rates for chopped gamma tests.

	Window open	Window closed	Window rotating at 5,000 rpm
Total background counts	622±25	616±25	4127±64

This shows that when the lead window is rotating and the Dremel unit is switched on, there seems to be an increased amount of background counts. This increase in background counts was attributed to electromagnetic compatibility problems between the detector and the Dremel unit. If the background counts were

A novel detection system using neutron/gamma pulse shape discrimination, for use in active interrogation environments

deducted from each initial count respectively, then the results are what would have been expected. This is shown in Table XXII.

Table XXII. Count rates using the gamma source with background counts deducted for chopped gamma tests.

	Window open	Window closed	Window rotating at 5,000 rpm
Total average counts with background deducted	35903±189	31244±177	33443±183

This shows that when rotating the source is being chopped with a 50% duty cycle as the count rate is in the middle of the closed and open window states. This result adds promise to the ability of the device to chop the gamma signal, however there are still counts that are being received even when the window is closed, meaning that the gated detector would be held in a dormant state.

The next set of experiments incorporated increasing the thickness of the lead sheet and lead window, so that when the window is closed the count rate is reduced to nothing, whilst still detecting the source when the window is open. The window itself was increased by three times, whereas another 4 sheets of lead were added in front of the detector. With the new lead setup each run was carried out the same as before but for 5 minutes each time, the background count without the window spinning was 235±15 counts. With the window spinning the background counts again increased but this time to only 338±18 counts. The results for when the <sup>137</sup>Cs source was introduced (deducting the background counts) are below in Table XXIII.

A novel detection system using neutron/gamma pulse shape discrimination, for use in active interrogation environments

Table XXIII. Count rates using the gamma source with background counts deducted for chopped gamma tests.

	Window open	Window closed	Window rotating at 5,000 rpm
Total average counts with background deducted	262±16	204±14	227±15

Again as before the rotating count rate, taking into account the errors on the counts, is in the middle of the count rates whilst not rotating as expected. There are still counts evident when the window is closed but drastically reduced from the previous experiment. It is suggested for a successful run that the opening in the lead screen needs to be reduced and the lead window itself extended as well as made thicker. Also when the system is operating at a higher speed the count rate tended to increase towards what is observed when the window is open, the possible solution to resolve this would involve having a bigger area of window. This solution however seems impractical to implement due to the aforementioned malleable nature of the lead causing a larger window to deform whilst rotating at such high speeds.

For the proof of principle the EJ-301 was connected to operate the trigger circuit, without any chopping device. The liquid scintillator was put in place of the silicon PIN photodiode. This setup was effective at holding the gated detector in a quiescent state whilst radiation was upon it, and had no effect when there was no radiation present. This is not useful for active interrogation purposes as any radiation count seen by the liquid scintillator would switch the gated detector off, but it does prove the concept of being able to replace the silicon PIN photodiode with a radiation sensitive detector, and still operate as required. A threshold will eventually need to be applied for switching the detector when only above a certain intensity level.

## 8.1 Conclusion

The chopped gamma triggering system was an idea to prove the possibility of replacing the silicon PIN photodiode with a radiation sensitive detector. The radiation-sensitive detector was to be used alongside a MFA with the signal being used from the TTL line. The TTL data line has been used to feed a signal to the trigger circuit in place of the PIN diode but only whilst constantly sending radiation signals meaning the gated detector was constantly switched off. The triggering system devised and presented earlier had limited success.

This system exhibited high background signals whilst the window was closed which prevented the system from being fully tested to a duty cycle as with the strobe light source. However, if deducting the background counts observed the counts when the lead window is spinning was in the middle of the counts when it was open and closed. This was observed with different thickness of lead shielding which shows in principle the concept of cutting the gamma source works. The difficulty as mentioned arises with limiting the count rate to zero when the window is closed as the radiation detector was always sensitive to the source even when the window was closed.

If the system is implemented with thresholds for the radiation levels to protect the gated detector it should alleviate the problems with these background events that have been occurring due to the low nature of them.

## 8.2 References

1. Q. Li, P.K. Dasgupta, H. Temkin, "A time-gated fluorescence detector using a tuning fork chopper", *Analytica Chimica Acta*, 616, pp. 63-68 (2008)

## 9 Conclusions & Recommendation

### 9.1 Overall Conclusions

Overall the research that has been carried out has had several important conclusions that have previously been discussed. The first of these conclusions came from looking into the feasibility of separating different types of radiation pulses based on the rising edge of the pulse. The results of this are that the concept is very desirable, and it may be possible to state that certain pulses are gamma signatures, although at present the classification of pulses as neutrons using the rising edge as proposed is not currently possible.

The ability of liquid organic scintillators has been investigated in terms of orientation effects on pulse shape discrimination quality, efficiency and throughput of pulses. Minor fluctuations are shown in the FoM values for both cell shapes, and the liquid cell lacking an internal light guide produces no discrimination at  $-90^{\circ}$  to the source. Additionally the throughput of the detector is affected by the orientation with the highest count rate being when the detector is horizontal with respect to the source of radiation. This would need to be accounted for in large arrays of liquid scintillators where special constraints force the angles of the detectors to be contrasting.

These tests produced the next important outcome which has been the ability to remotely trigger a detector using a light source. The system can have numerous applications and allows the user to control and protect the detector being used. In terms of the radiation pulses that are being outputted by the detector the gating has been shown to have no impact on either the shapes or quality of the scatter plots, or the

## A novel detection system using neutron/gamma pulse shape discrimination, for use in active interrogation environments

ability to discern the radiation types relative to the detector when it is not being gated. The system has been proven to hold the detector in a dormant state and then recover back to being operational in the presence of a variety of different sources. This satisfies the requirement that the gating aspect of the PMT is operational and able to keep the detector inactive when needed without any negative ramifications which are applicable to one of the aims initially set out in this research to be able to stop the radiation ‘flash’ from saturating the PMT. The weakness in the system is down to the trigger circuit providing the signal to the gating board within the detector. The current setup has shown that the gating board has been fully responsive to the same period of the trigger circuit. From this it is not possible to characterise the limitations of the gating board performance, but only to say that it operates at an equivalent or a quicker speed than the trigger circuit (the silicon PIN diode) devised and used in this research.

The results here have taken the research in [1] further in having the detector suppressed under the signal of a separate trigger rather than taking a signal from the interrogating medium and incorporating a set delay time. The separate trigger signal is the intermediate step onto a system that can detect high levels of radiation and protect itself. This as yet ideal system would have the advantage of being compatible to any setup and experiment without having to undergo calibration and adjustments on timings. This intelligent system would allow autonomy alleviating any user input with maximum output of data whenever available by replacing the photodetector used in this research with a radiation sensitive detector. The system in its current state however, does not utilise a radiation detector for the triggering of the device when the flux gets to a point that will saturate the detector. Also, in these tests the rate of

switching is still at a low frequency while repetitive switching is not required for the foreseeable applications for active interrogation, it would need to be investigated more thoroughly if this requirement changed or for other applications that may require it.

Another important outcome has been the discovery of the difficulties that are experienced when utilising an organic plastic scintillator with a real-time PSD system. The averaged pulse shapes for  $\gamma$  rays and neutrons have been plotted [2] in Figure 68. The separation between the pulses for neutrons and gammas is observed to be limited, which is the reason for the more difficult discrimination than with the organic liquid scintillators. This was shown in the results as the plastic scintillator that was set out to be used in the gated detector due to its inherent stability compared to its liquid counterparts produced poorer discrimination results.

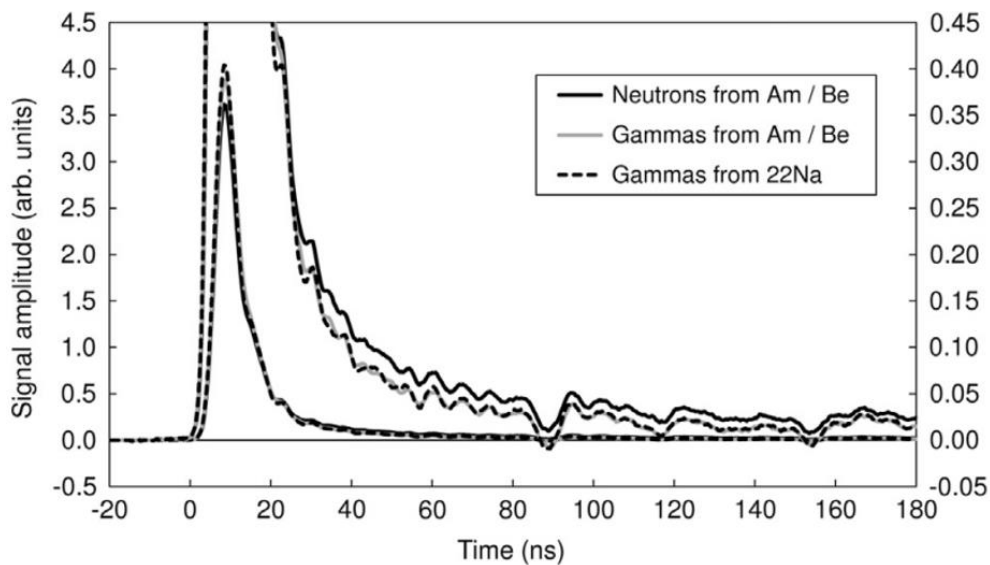


Figure 68. Average measured pulse shapes for neutrons and gammas. Each shape is plotted twice, once showing the entire trace and again at a magnification factor of 10 (see right-hand scale) so as to show the pulse tail in detail. Reprinted from Nuclear Instruments and Methods in Physics Research Section A: Accelerators, Spectrometers, Detectors and Associated Equipment, 729. N.P. Hawkes, G.C. Taylor, 'Analysis of the pulse shape mechanism in a plastic scintillator with efficient neutron/.gamma pulse shape discrimination', 522-526, 2013, with permission from Elsevier [2].

## A novel detection system using neutron/gamma pulse shape discrimination, for use in active interrogation environments

Verification experiments have been carried out using the organic plastic scintillator with different sources and with different shielding combinations to try and optimise the results. In the literature FoM values have been reported of 0.82 with the plastic exposed to  $^{252}\text{Cf}$  [3] using the charge comparison method. Despite producing poorer separation the PGA technique has the advantage of being a real time system with higher throughput and with instant population of the scatter plots and MCA this allows for quicker calibration and visual feedback whilst the system is in operation. The advantage of the CC method is the ability to process pulses with a gate width of hundreds of nanoseconds, this ability to look at longer pulses is the key to why CC can distinguish the radiation more readily producing a higher FoM value. Despite this limitation of the PGA technique the system can still be used to discern radiation types to an acceptable limit, and the inclusion of shielding may improve the value further as was the case with the water based  $^{252}\text{Cf}$  source at Lancaster.

In terms of initial requirements set out for this research, the plastic is still feasible for use with the PGA technique if the setup includes sufficient and appropriate shielding although confirmation of the correct shielding would be counterproductive to the faster nature of the investigation process being sought after. The alternative of using the CC technique is a viable option, however this would have a detrimental impact on the speed of the system which would be counterproductive to the initial specifications of the system unless post processing is feasible. In other operations where speed is not as important, the incorporation of another PSD technique utilised with the plastic may be desirable. For this particular application when speed is the

important factor the use of the plastic may not be the best choice for the detector as the quick distinction between radiation types it is more attainable with an organic liquid. Although the detector is not as inherently safe as the solid there is the newer low hazard version available.

## 9.2 Recommendations

The research that has been completed has addressed each of the desired aims in section 1.1 individually but does not present an entirely conclusive solution or a fully operating system. The recent breakthrough in organic plastic scintillators was utilised into a system with the ability to discriminate between radiation types. This system was controlled remotely by a trigger circuit that can hold the detector in a dormant state ensuring it is immune to a high flux fields that would normally cause saturation. The trigger circuit controlling the detector made use of a photon detector and a mixed neutron/gamma detector was shown to be able to also provide a signal capable of switching the system off. However the system is not autonomous, this still requires the information from the radiation based detector to be analysed and thresholds applied so to only provide a signal to the main system when the radiation fields will get to a point of saturation for the plastic detector. Therefore there are several recommendations for further work to improve the operation of the system and to complete a fully autonomous ideal system with the ability to shield itself from high flux situations.

### 9.2.1 Autonomous Detector

This research has shown that a detector can be switched off and on with good stability using a stimulated silicon PIN photodiode. These initial tests have shown the ability of the detector system to still operate whilst being triggered, as well as producing consistent results from the DAQ unit prove that there were no detrimental effects on the data collection side. The shape of the pulses have also been compared whilst the detector is being triggered and shown no detriment again has been observed in terms of the gating system clipping or cutting pulses compared to when it is not undergoing triggering. The relative count rate as a percentage is equal to the percent of time the triggering circuit is not making the gating PMT dormant, meaning the speed of switching for the gated detector is equal or faster than the triggering circuit. This silicon PIN photodiode has been replaced with an EJ-301 organic liquid scintillator which has also been able to hold the detector system dormant, although the sensitive nature of the liquid scintillator has made it difficult to switch between states as was possible with the photodiode and the strobe light source.

A chopping system has been designed and initially tested to incorporate the EJ-301 liquid scintillator. The lead window vane currently needs increasing in thickness and dimensions to fully block all the gamma counts being observed when the window is closed as described earlier. Once this has been implemented to a satisfactory standard the output from the MFA that the liquid scintillator is connected to can be sent to the trigger circuit and drive the gating board in the same manner that the photodiode was able to. In this setup the EJ-301 will have been used as a remote sensor whenever it sees any gamma radiation to switch the plastic detector off.

The last step is to develop a way of using the EJ-301 detector to control the gated detector only when the radiation levels are hitting a point that will saturate it. The developments that have yet to be dealt with are the ability to control the threshold level at which the EJ-301 would provide a signal to trigger the plastic scintillator detector. As the EJ-301 will provide a signal whenever radiation is present it is hypothesised that to make the system autonomous this would be used to provide the signal based on the count rate that is being produced from the detector. This would work by keeping track of the count rate and when this goes above a certain predetermined threshold that the gated detector would not be able to tolerate then the signal is produced. For a generalised solution capable of being compatible with varying scintillator materials and different amplification devices these thresholds would need to be adjustable within the system to allow for the different saturation levels. To find the saturation limit for any detector configuration desired tests similar to those carried out at DCF will need to be undertaken, although a facility that has a larger chamber may be required.

### 9.2.2 Gated Detector

In the wider sense of the field the developments of scintillators is progressing as shown by the development of the plastic organic scintillator with mixed field capabilities. The plastic used in this work gives an approach that is widely viewed as a stable solution to any toxicity and flammability issues. The discrimination ability of the plastic in relation to different radiation types being on the edge of what is required. Since this research began the state of the field of plastic scintillators has continually improved,

with more recent variants of the EJ-299 plastic being produced. As shown in this work and reported by others the energy range that the EJ-299-33 can be effective in are limited, with some energy levels experiencing a drop in efficiency as high as 40% compared to its liquid counterparts [4]. A full investigation into the more recently-developed plastics and the ability they have at certain lower energy ranges in comparison would be beneficial.

There has been research undertaken showing improved discrimination performance in the newer plastic material EJ-299-34 coupled to a silicon photomultiplier and exposed to an Am-Be source [5]. Investigations into the possibility of using different amplification devices could reduce the level of which the detector becomes saturated.

Alternatively the low-hazard liquid organic scintillator EJ-309 coupled to the gating board might be a more feasible option. This would have improved PSD results obtained when using the real-time PGA technique.

### 9.2.3 New Algorithms

Pulse shape discrimination is the term used to describe a number of techniques that distinguish between radiation types based on the shape of the pulses that are produced from scintillation media. This area comprises a variety of different approaches to carry out this analysis. Recently, several new techniques have been developed. The PGA technique utilised in this research holds the advantage of being a real-time technique. Recently two alternatives to charge-comparison that is working toward real-time pulse processing has been reported [6], one of these based on the current charge comparison

## A novel detection system using neutron/gamma pulse shape discrimination, for use in active interrogation environments

method called the charge-to-current ratio method. This method takes the amplitude of the PMT current pulse with the integral of the pulse. This method has also been used in solar neutrino experiments [7]. In comparison with the charge comparison method this technique avoids the use of a short integral, reducing the computations by ~ 40%, although not necessarily increasing the speed of the system to interrogate objects to discern the material in question.

Another technique that holds promise is principal component analysis (PCA) boasting the advantage of automatic extraction of pulse-shape characteristics. PCA has been used in different areas for investigation into patterns in datasets in image processing, neuroscience and other disciplines [8]. PCA eliminates the need for any adjustments of PSD parameters as the analysis of radiation type is carried out based on the data received during a pre-acquisition run. Recent research [9] suggests that it has superior performance to that of charge-comparison method whilst being computationally efficient. With the only comparison thus far being against charge-comparison, it is hard to say whether this would stand up against the PGA technique in terms of speed of performance which was the aim of the research presented here. A comparison of the two techniques would determine this and resolve this research question.

### 9.3 References

1. K.Y. Hara, et al., “ $\gamma$ -Flash suppression using a gated photomultiplier assembled with an LaBr<sub>3</sub>(Ce) detector to measure fast neutron capture reactions” *Nucl. Instr. and Meth. A* 723 pp. 121-127 (2013).
2. Reprinted from Nuclear Instruments and Methods in Physics Research Section A: Accelerators, Spectrometers, Detectors and Associated Equipment, 729. N.P. Hawkes, G.C. Taylor, ‘Analysis of the pulse shape mechanism in a plastic scintillator with efficient neutron/.gamma pulse shape discrimination’, 522-526, 2013, with permission from Elsevier
3. S.A. Pozzi, M.M. Bourne, S.D. Clarke, “Pulse shape discrimination in the plastic scintillator EJ-399-33”, *Nucl Inst. Meth A* 723, pp. 19-23, (2013)
4. R.S. Woolf, et al., “Comparing the response of the PSD-capable plastic scintillator to standard liquid scintillator”, *Nucl Inst. Meth A* 784, pp. 80-87, (2015)
5. R.M. Preston, J.E. Eberhardt, J.R. Tickner, “Neutron-gamma pulse shape discrimination using organic scintillators with silicon photomultiplier readout” *IEEE Trans on Nuclear Science*
6. T. Alharbi, “Simple algorithms for digital pulse shape discrimination with liquid scintillation detectors” *Radiation Physics and Chemistry* 106 pp. 50-55 (2015)
7. H.M. O’Keeffe, E. O’Sullivan, M.C. Chen “Scintillation decay time and pulse shape discrimination in oxygenated and deoxygenated solutions of linear alkylbenzene for the SNO+ experiment” *Nucl Inst. Meth A* 640 pp. 119-122 (2011)
8. I.T. Jolliffe, “Principal Component Analysis” Springer-Verlag, New York, 2002, second edition
9. T. Alharbi, “Principal component analysis for pulse-shape discrimination of scintillation radiation detectors” *Nucl Inst. Meth A* 806 pp. 240-243 (2016)

# Appendix A

The following is the paper that was part of the conference proceedings for ANIMMA 2013

## Pulse-shape Discrimination in Organic Scintillators Using the Rising Edge

Ashley Jones<sup>1</sup> and Malcolm J. Joyce, *Member IEEE*<sup>1</sup>

**Abstract**– The possibility of discriminating between neutrons and  $\gamma$  rays on the basis of differences in the rising edge of corresponding pulses from organic scintillation detectors is described. It has long been known that radiation type can be discerned on the basis of subtle differences in pulse shape from a variety of detection materials, but discrimination in fast organic scintillators has long been reliant on the separation in decay face of the pulse. This can constrain pulse-shape discrimination techniques to follow after the peak amplitude of the event and they can thus be more susceptible to the effects of pile up. Furthermore, discrimination in the decay face places a fundamental limit on the time relative to the evolution of the event when discrimination can be performed and thus this can be a significant constraint on the event processing rate for high pulse-rate applications. In this paper the correspondence between established mathematical models of organic pulse shape and real events in the rising edge part of the event is investigated, and the potential for rise-time based pulse-shape discrimination in mixed-field data from organic scintillators is explored. Special nuclear materials (SNM) are of particular interest to security surveillance and based on active interrogation. Active interrogation involves neutrons hitting a material that is fissile, and detecting the emitted  $\gamma$  rays and neutrons to try and classify materials. Faster, more efficient and more transportable devices are being sought to help in the prevention of illicit transport of nuclear materials. SNM are difficult to detect due to high-flux  $\gamma$  emissions, and very low neutron signatures.

### I. INTRODUCTION

The ability to be able to interrogate objects non-destructively is a very attractive way of classifying radioactive materials.

In active neutron methods, the object or target in question is bombarded with neutrons, to produce a mixed radiation field of both  $\gamma$  rays and neutrons. This radiation is often then detected by using a scintillator detector, which converts such radiation into light. The light pulses from the scintillator are then converted with a photocathode and enter a photomultiplier tube (PMT) to provide the primary stage of amplification. The pulses amplified by this PMT can then be analyzed to identify the material in question.

The most commonly-used method for pulse-shape discrimination with organic scintillators in a mixed radiation

field is based on the trailing edge of an acquired pulse due to a distinct difference between the pulses of  $\gamma$  rays and neutrons [1]. The problems that arise from this are it can be susceptible to pulse pile-up resulting in reduced detection rates and spurious pulse assignments whilst pile-up recovery can be a lengthy and data-intensive process. An ability to discriminate on the rising edge could reduce the processing intensity and the time required to carry out investigations on objects. Discrimination has previously been suggested based on the time it takes each pulse to reach its peak [2], but the advancement of technology has previously prevented practical application of this.

### II. MODELING

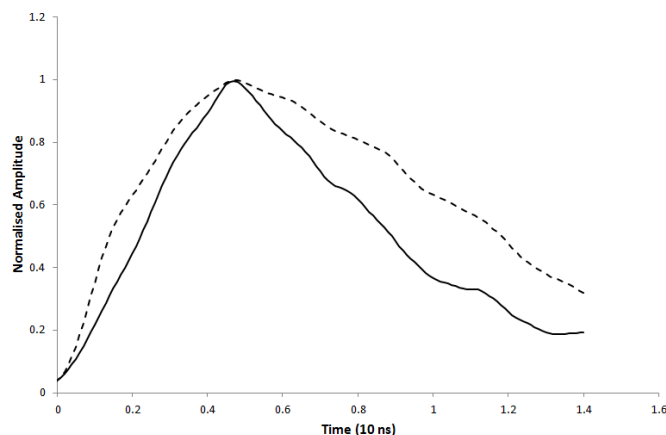


Figure 1: Averaged data for  $\gamma$ -ray (solid) & neutron (broken) pulses of voltage versus time arising from previous measurements [3].

To investigate the possibility of rising-edge discrimination, experimental data have been analyzed for this purpose from a data set collected as described in a previous publication [3]. The data set comprised of over 4000 pulses, which was truncated to a workable number of 250 for the purposes of this paper. These were then separated into  $\gamma$ -ray and neutron events and then averaged to give an average  $\gamma$ -ray pulse shape and an average neutron pulse shape from the mixture of 250 events as described in our earlier work [4]. The resulting average pulses shapes are shown below in Figure 1, exhibiting the potential for separation on the rising edge. With separation evident on the rising edge, the next stage was to determine if this was

Manuscript received May 31, 2013. This work was supported and sponsored by AWE plc.

A. Jones and M. J. Joyce are with the Engineering Department, Lancaster University, UK (telephone: +44 1524 593812, e-mail: m.joyce@lancaster.ac.uk).

consistent with numerical models, particularly that reported by Marrone *et al.* [5]. This model has long been used for modeling on pulse-shape analysis in organic scintillators, as given in Eqn. 1.

$$L(t) = A(e^{-\theta(t-t_0)} - e^{-\lambda_s(t-t_0)}) + B(e^{-\theta(t-t_0)} - e^{-\lambda_l(t-t_0)}) \quad (\text{Eqn. 1})$$

The usual application of the model for amplitude as a function of time  $L(t)$  in Eqn. 1 is focused on the trailing edge, the equation gives the case for a single decay time, where  $\theta$ ,  $\lambda_s$  and  $\lambda_l$  are exponential decay constants,  $t_0$  is the time reference and  $A$  and  $B$  are normalization parameters. By plotting the models it could be determined if they show if any discrimination was feasible between the rising edges of a neutron and  $\gamma$ -ray pulse, or whether the model was not robust enough. The resulting pulses, shown in Figure 2, demonstrate there are clear differences between the trailing edges as is well known. Furthermore, however, focus on the start of the pulses indicate that there is some separation on the rising edge within the first couple of nanoseconds also, as highlighted in an expanded portion of the model in Figure 3.

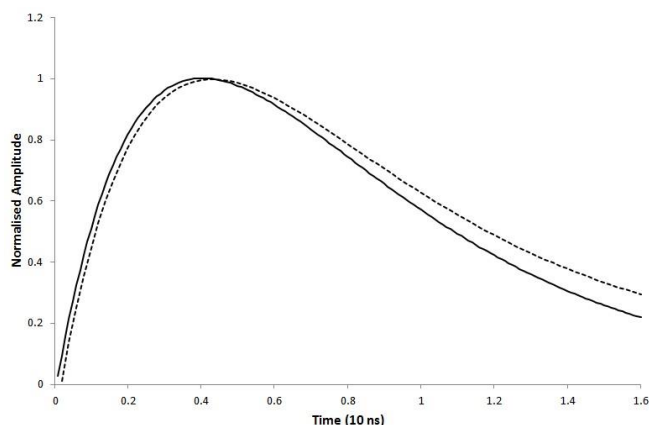


Figure 2: Neutron (broken) and  $\gamma$ -ray (solid) pulses from the model reported by Marrone *et al.* as a function of voltage a time, normalised to each other for clarity.

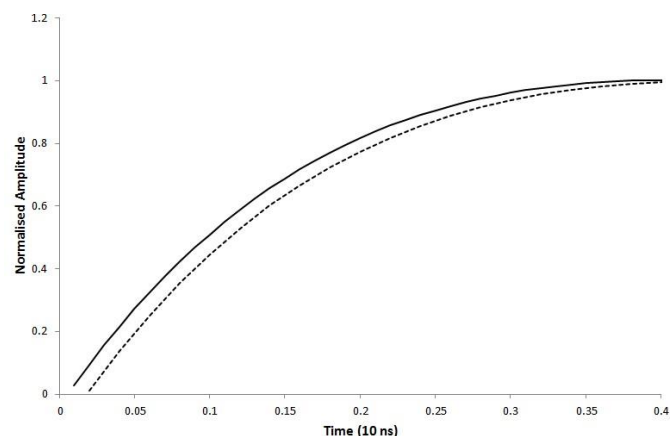


Figure 3: The first nanosecond of the neutron &  $\gamma$ -ray pulses based on the Marrone model.

The data however infers a much more significant degree of separation between the rising edges of the pulses. This suggests the possibility that a development of the Marrone

formalism might better describe a generalized form of early-stage, pre-peak amplitude PSD, and from these new models work towards a practical solution of rising-edge separation.

### III. RISING EDGE MODELING

To obtain a closer degree of consistency for the rising edge, a revised model has been developed. This model was initially based on a combination of several exponent terms and is entirely empirical. It was then tuned to fit the pulse shapes as effectively as possible. The resulting model is given as:

The resulting model tracks the data analyzed in this work very accurately, as shown in Figures 4 & 5. However, this model still needs to be tested against a wider selection of data ideally from a variety of organic scintillation compounds to determine how widely applicable it is.

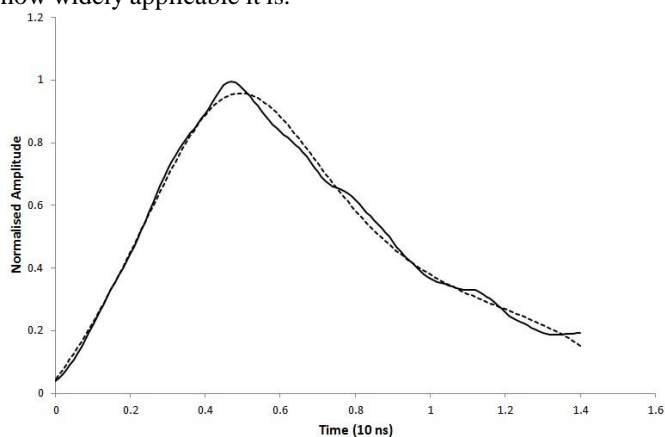


Figure 4: New  $\gamma$  model (broken) against averaged data (solid).

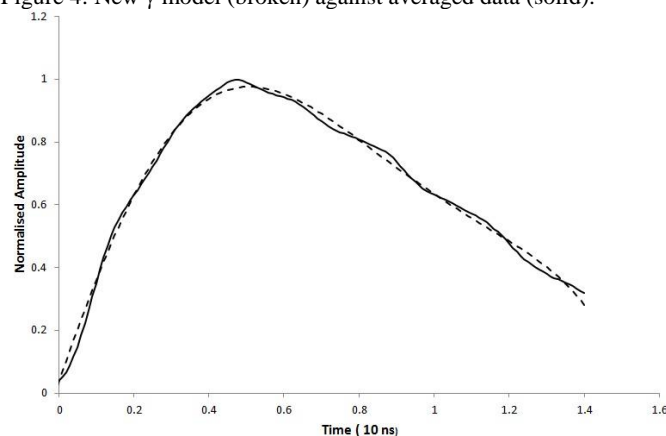


Figure 5: New neutron model (broken) against averaged data (solid).

### IV. FURTHER WORK

The implications of the modeling work carried out suggest that there is a possibility of rising-edge pulse-shape discrimination. The next stage is to see whether this is cross applicable to other detectors and scintillator materials, then to see whether the rising-edge discrimination is possible with current technology capability. Suggestions show that with recent advancements in the likes of MCP-PMT's and with ultra fast

DAQ systems, that this could already be a possibility. If so this will lead to ultra-fast mixed-field discrimination, constituting a significant step forward in neutron detection.

## V. ACKNOWLEDGEMENTS

The work in this paper was funded and supported by AWE plc. Aldermaston.

## VI. REFERENCES

- [1] F.D. Brooks "Development of Organic Scintillators", *Nuclear Instruments and Methods*, vol. 162 477-505, 1979.
- [2] A.J. Peurrung, R.R. Hansen, R.A. Craig, W.K. Hensley, C.W. Hubbard, P.E. Keller, P.L. Reeder, D.S. Sunberg, "Direct Fast Neutron Detection: A Status Report", 1997.
- [3] M.D. Aspinall, B. D'Mellow, R. Mackin and M.J. Joyce, "Verification of the digital discrimination of neutrons and gamma rays using pulse gradient analysis by digital measurement of time-of-flight", *Nuclear Instruments and Methods in Physics Research*, vol. A583 432-438, 2007.
- [4] M. D. Aspinall, B. D'Mellow and M. J. Joyce, "The empirical characterisation of organic liquid scintillation detectors by the normalized average of digitized pulse shapes", *Nuclear Instruments and Methods*, vol. 578 261- 266, 2007.
- [5] S. Marrone, D. Cano-Ott, N. Colonna, C. Domingo, F. Gramegna, E. Gonzalez, F. Gunsing, M. Heil, F. Kappeler, P. Mastinu, P. Milazzo, T. Papaevangelou, P. Pavlopoulos, R. Plag, R. Reifarh, G. Tagliente, J. Tain and K. Wisshak "Pulse shape analysis of liquid scintillators for neutron studies", *Nuclear Instruments and Methods in Physics Research Section A. Accelerators, Spectrometers, Detectors and Associated Equipment*, vol. 490, 299-307, 2002.

© British Crown Owned Copyright 2013/AWE "This document is of United Kingdom origin and contains proprietary information which is the property of the Secretary of State for Defence. It is furnished in confidence and may not be copied, used or disclosed in whole or in part without prior written consent of Defence Intellectual Property Rights DGDCDIPR-PL - Ministry of Defence, Abbey Wood, Bristol, BS34 8JH, England"

